

Electronic Thesis and Dissertation Repository

9-24-2012 12:00 AM

Wood Infill Walls in Reinforced Concrete Frame Structures: A Wood/concrete Construction Niche

Jeffrey R. L. Blaylock
The University of Western Ontario

Supervisor
Prof. F. M. Bartlett
The University of Western Ontario

Graduate Program in Civil and Environmental Engineering
A thesis submitted in partial fulfillment of the requirements for the degree in Master of Engineering Science
© Jeffrey R. L. Blaylock 2012

Follow this and additional works at: <https://ir.lib.uwo.ca/etd>

Recommended Citation

Blaylock, Jeffrey R. L., "Wood Infill Walls in Reinforced Concrete Frame Structures: A Wood/concrete Construction Niche" (2012). *Electronic Thesis and Dissertation Repository*. 888.
<https://ir.lib.uwo.ca/etd/888>

This Dissertation/Thesis is brought to you for free and open access by Scholarship@Western. It has been accepted for inclusion in Electronic Thesis and Dissertation Repository by an authorized administrator of Scholarship@Western. For more information, please contact wlsadmin@uwo.ca.

**WOOD INFILL WALLS IN
REINFORCED CONCRETE FRAME STRUCTURES:
A WOOD/CONCRETE CONSTRUCTION NICHE**

(Spine title: Wood Infill Walls in Reinforced Concrete Frame Structures)

(Thesis Format: Monograph)

By

Jeffrey R. L. Blaylock

Graduate Program in
Civil and Environmental Engineering

A thesis submitted in partial fulfillment
of the requirements for the degree of
Master of Engineering Science

The School of Graduate and Postdoctoral Studies
Western University
London, Ontario, Canada
September 2012

© Jeffrey R. L. Blaylock, 2012

WESTERN UNIVERSITY
SCHOOL OF GRADUATE AND POSTDOCTORAL STUDIES

CERTIFICATE OF EXAMINATION

Supervisor

Dr. F. Michael Bartlett

Examiners

Dr. Maged A. Youssef

Dr. George K. Knopf

Dr. Hanping Hong

The thesis by

Jeffrey R. L. Blaylock

entitled:

Wood Infill Walls in Reinforced Concrete Frame Structures: A Wood/concrete Hybrid
Construction Niche

is accepted in partial fulfilment of the
requirements for the degree of
Master of Engineering Science

Date _____

Chair of the Thesis Examination Board

ABSTRACT

This thesis investigated light-frame wood/concrete hybrid construction as part of the NSERC Strategic Network on Innovative Wood products and Building Systems (NEWBuildS). A review of eight wood/concrete niche areas identified three with potential to be used in mid- to high-rise structures. Light-frame wood structures of seven or more storeys with wood/concrete hybrid flooring seem to have little feasibility unless a concrete lateral-load-resisting system is provided and material incompatibilities are solved. Non-load-bearing light-frame wood infill walls in reinforced concrete frame structures were recognized to have potential feasibility in mid- to high-rise structures. A full-scale, single frame test apparatus was successfully designed and constructed at the Insurance Research Lab for Better Homes. The frame is statically loaded to accurately replicates realistic horizontal sway and vertical racking deformations of a typical eight storey reinforced concrete frame structure at SLS and ULS. A linear-elastic analysis of the test apparatus was generally able to predict the results during testing. The 2.4m x 4.8m (8 ft. x 16 ft.) infill wall specimen did not satisfy serviceability deflection limitations of $L/360$ when subjected to representative out-of-plane wind pressures of +1.44/-0.9 kPa. The out-of-plane response was not significantly affected by horizontal sway deflections of ± 7.2 mm or vertical racking deflections of +9.6mm. Although a nominal 20mm gap was provided to isolate the wall from the surrounding frame, insulation foam sprayed in the gap facilitated load transfer between them.

Keywords: *Wood/Concrete Hybrid, Light-frame Wood, Infill Wall, Reinforced Concrete Frame Structure.*

ACKNOWLEDGEMENTS

First and foremost, I would like to thank Prof. F. Mike Bartlett for his supervision. His guidance, expertise and insights have been invaluable throughout this project.

I would like to thank Andrew Klazinga for all his assistance during the construction and testing phase. I would also like to thank Wilbert Logan for his insights throughout the design and construction phase and Jared Harnish for his help during the final testing phase.

I would also like to recognize the people who participated in the various thesis-related discussions, both large and small, with special thanks to Daniel Grenier, Randy Van Straaten, and my colleagues in the Grad Addition.

I would also like to acknowledge the NSERC Strategic Network on Innovative Wood Products and Building Systems (NEWBuildS) for funding this research.

TABLE OF CONTENTS

	PAGE
Certificate of Examination.....	ii
Abstract and Keywords.....	iii
Acknowledgements.....	iv
Table of Contents.....	v
List of Figures	viii
List of Tables	xi
List of Appendices	xiii
Nomenclature.....	xiv
1 INTRODUCTION	1
1.1 Overview	1
1.1.1 Introduction.....	1
1.1.2 ComplEmentary Materials	2
1.1.3 Potential Benefit.....	4
1.2 NEWBuildS.....	6
1.3 Research Objectives	7
1.4 Outline of Thesis	8
2 NICHE AREAS FOR MID-RISE LIGHT-FRAME WOOD/CONCRETE HYBRID CONSTRUCTION.....	10
2.1 Introduction	10
2.1.1 Objective	10
2.1.2 Defining Terms	10
2.2 Evaluation of Niche Areas	11
2.2.1 Scope.....	11
2.2.2 Light-Frame Wood Structure.....	12
2.2.3 Wood Structure with Wood/Concrete Floor Systems.....	13
2.2.4 Wood Structure with Concrete Foundation and Lower Storeys	15

2.2.5	Wood Structure with Concrete Lateral-load-resisting System	16
2.2.6	Hybrid Structures with Compartmentalization	16
2.2.7	Reinforced Concrete Structures with Wood/Concrete Floor Systems.....	17
2.2.8	Reinforced Concrete Structure with a Wood Roof or Wood Upper Storeys..	18
2.2.9	Reinforced Concrete Structure with Interior Wood Partition Walls.....	19
2.2.10	Reinforced Concrete Structure with Exterior Light-frame Wood Infill Walls	19
2.3	Assessment of Potential Niches	20
2.3.1	Approach.....	20
2.3.2	Wood Structure with Wood/Concrete Floor System	21
2.3.3	Wood Structure with Concrete Lateral-Load-Resisting System.....	32
2.3.4	Reinforced Concrete Structure with Light-frame Wood Infill Walls	34
2.4	Summary and Conclusion	36
3	TEST DESIGN AND CONSTRUCTION	40
3.1	Objective	40
3.2	Prototype Structure.....	41
3.2.1	Idealization.....	42
3.2.2	Loading Assumptions	43
3.2.3	Principal In-plane Deflections	44
3.3	Test Apparatus.....	51
3.3.1	Objective and Constraints.....	51
3.3.2	Final Design	53
3.3.3	Design and Construction Challenges	61
3.4	Wood Infill Wall Specimen.....	66
3.4.1	Criteria	66
3.4.2	Connection Design Concept	69
3.4.3	Construction.....	76
3.4.4	Modelling.....	77
3.5	Summary and Conclusions	78

4 EXPERIMENTAL PROGRAM AND RESULTS	80
4.1 Overview	80
4.2 Out-of-plane Test 1	81
4.2.1 Procedure	81
4.2.2 Instrumentation	83
4.2.3 Performance of Specimen	85
4.2.4 Performance of Test Apparatus	94
4.3 Lateral Sway Tests	97
4.3.1 Instrumentation	97
4.3.2 Performance of Test Apparatus	98
4.3.3 Performance of Specimen	107
4.4 Vertical Racking Tests	111
4.4.1 Performance of Test Apparatus	112
4.4.2 Performance of Specimen	118
4.5 Out-of-plane Test 2 and 3.....	121
4.5.1 Effect of Vertical Racking Test	121
4.5.2 Effect of Lateral Sway Test	121
4.6 Summary and Conclusions	123
4.6.1 Out-of-Plane Pressure Test 1	123
4.6.2 Lateral Sway Test	124
4.6.3 Vertical Racking Test	125
4.6.4 Out-of-Plane Pressure Tests 2 and 3	126
5 SUMMARY AND CONCLUSIONS.....	127
5.1 Summary	127
5.2 Conclusions	128
5.3 Suggestions for Future Work	131
REFERENCES.....	133
CURRICULUM VITAE.....	171

LIST OF FIGURES

	PAGE
Figure 1-1 - Section of a Feasible Light-frame Wood/concrete Mid-rise Structure	5
Figure 2-1 - Spectrum of Potential Wood/concrete Hybrid Systems.....	12
Figure 2-2 - Conceptual 16 storey Wood/concrete Hybrid Building (Smith, 2008b).....	17
Figure 2-3 - Load Arrangement for Maximum Internal Reaction	22
Figure 2-4 - Tributary Area for a Wall	23
Figure 2-5 - Results for Case 1: Wood Structure under Residential Occupancy	29
Figure 2-6 - Results for Case 3: Wood Structure with Light-weight Concrete and Wood Composite Flooring under Residential Occupancy	29
Figure 3-1 - Summary of Prototype Structure	42
Figure 3-2 - Principal In-plane Deflections	45
Figure 3-3 - Sway Deformation of the Prototype Structure at SLS and ULS.....	46
Figure 3-4 - Sway Deflection Limits for Critical Frame	47
Figure 3-5 - Vertical Creep Deformation of Exterior and Interior Columns at SLS and ULS	48
Figure 3-6 - Vertical Creep Deformation Limits for Critical Frame	49
Figure 3-7 - Mid-span Deflection of Critical Beam.....	50
Figure 3-8 - Load Cases Investigated: a) In-plane; b) Out-of-plane.....	51
Figure 3-9 - Final Test Apparatus: a) As Designed; b) As Constructed at IRLBH	54
Figure 3-10 - General Layout of Test Apparatus with Instrumental Grid System.....	55
Figure 3-11 - Test Apparatus Details for SAP Model	56
Figure 3-12 - Prototype Deflections vs. Test Apparatus Deflections for Lateral Racking	58
Figure 3-13 - Prototype Deflections vs. Test Apparatus Deflections for Vertical Racking.....	60
Figure 3-14 - Out-of-Plane Pressure Loading System.....	61
Figure 3-15 - As-built Variation from Designed Concrete Frame Dimensions.....	62
Figure 3-16 - Corner Reinforcement Detailing: a) Top View; b) Front View; c) As Constructed	63

Figure 3-17 - Connection Detailing at Base of Concrete Frame: a) Front View; b) Side View During Lateral Sway Test; c) Side View During Vertical Racking Test	64
Figure 3-18 - Concrete Frame to Steel Frame Connection and Jack Locations.....	65
Figure 3-19 - As-built Concrete Frame with Airbag and Back Panel.....	66
Figure 3-20 - Degrees of Inset of an Infill Wall: a) Not Inset; b) Partially Inset; c) Fully Inset ...	67
Figure 3-21 - Type and Location of Connections for Infill Wall System.....	70
Figure 3-22 - Cross Sections of Top Connections: (a) Partially Prefabricated Wood Wall; (b) Light-gauge Steel Wall; (c) Fully Prefabricated Wood Wall.....	71
Figure 3-23 - Initial Bottom Connection Design: (a) Cross Section; (b) Deformed Shape for Positive Wind Pressure; (c) Deformed for Negative Wind Pressure.	73
Figure 3-24 - Modified Bottom Connection with Shim: (a) Cross Section; (b) Shim.	74
Figure 3-25 - Final Wall Design	75
Figure 3-26 - Final Gap Dimensions.....	77
Figure 4-1 - Pressure Loading Trace.....	82
Figure 4-2 - Details of Pre-pressure Phase.....	83
Figure 4-3 - Out-of-Plane LVDT Locations	84
Figure 4-4 - LVDT Location and Points of Rotation at Bottom Connection.....	86
Figure 4-5 - Deformation of Bottom Plate With Respect to Shim Deflections	89
Figure 4-6 - Midheight Deflection of Infill Wall.....	91
Figure 4-7 - Comparison of Tests 1.1, 1.2 and 1.3 at points a) T5; b) B5 and c)M5.....	93
Figure 4-8 - Net Deflections at: a) Mid-height of Column; b) Midspan of Beam	96
Figure 4-9 - In-plane Instrumentation Location and Test Apparatus Details	98
Figure 4-10 - Lateral Sway Response at SLS	99
Figure 4-11 - Lateral Sway Pull Test Response at SLS and ULS.....	101
Figure 4-12 - Steel Frame Displacement for Average Push Test 1 and 2 Results at SLS	102
Figure 4-13 - Steel Frame Displacement for Avg. Pull Test 1/2 at SLS and Test at ULS.....	103

Figure 4-14 - Deflected Shape of Concrete Frame under Lateral Sway Loading.....	104
Figure 4-15 - Notation for Gap Change and Wall Movement	108
Figure 4-16 - Change in Gap at Top Right Corner for Lateral Sway Loading at SLS	111
Figure 4-17- Observed and Predicted Response due to Vertical Racking at SLS and ULS	113
Figure 4-18 - Response of Steel Frame During Vertical Racking Test at ULS.....	115
Figure 4-19- Deflected Shape of Concrete Frame under Vertical Racking	117
Figure A-1 - Results for Case 2: Wood Structure with Light-weight Concrete Topping under Residential Loading.....	139
Figure A-2 - Results for Case 4: Wood Structure with Light-weight Concrete Slab under Residential Loading.....	139
Figure A-3 - Results for Case 5: Wood Structure with Normal-weight Concrete and Wood Composite Flooring under Residential Loading.....	140
Figure A-4 - Results for Case 6: Wood Structure with Light-weight Concrete and Wood Composite Flooring under Business Loading.....	140
Figure A-5 - Results for Case 7: Wood Structure with Normal-weight Concrete and Wood Composite Flooring under Business Loading.....	141
Figure B-1 - Pressure Cases for the Loading on Exterior Cladding.....	144
Figure E-1 - Predicted Applied Moments under Loading at ULS.....	151
Figure G-1 - In-plane Design Forces for Test Apparatus.....	160
Figure H-1 - Lifting Connection Attached to Infill Wall.....	162
Figure H-2 - Lifting of the Infill Wall.....	163
Figure I-1 - Out-of-plane Infill Wall Deflection: a) Original Position; b) Case 1; c) Case 2.....	166
Figure J-1 - Out-of-Plane Test LVDT.....	170
Figure J-2 - In-Plane Test LVDT.....	170

LIST OF TABLES

	PAGE
Table 1-1 - Material Properties for Wood and Concrete.....	3
Table 2-1 - Maximum Spans for Wood Joists	24
Table 2-2 - Parameter Ranges Investigated	25
Table 2-3 - Multi-Storey Wood Structures with Wood/concrete Flooring	27
Table 2-4 – Maximum Number of Storeys: Gravity Loading Only.....	30
Table 2-5 - Maximum Number of Storeys: Lateral Load Included	32
Table 2-6 - Maximum Number of Storeys: Gravity Loading with Lateral-load-resisting System	33
Table 3-1 - Final Deflection Limits of the Prototype Structure at SLS and ULS	50
Table 3-2 - Positive and Negative Test Pressures.....	52
Table 3-3A - Deflection of Concrete Frame under Lateral Sway Loading at SLS.....	58
Table 3-3B - Deflection of Concrete Frame under Lateral Sway Loading at ULS.....	58
Table 3-4A - Deflection of Concrete Frame under Vertical Racking at SLS	60
Table 3-3B - Deflection of Concrete Frame under Vertical Racking at ULS.....	60
Table 4-1 - Summary of Tests Performed.....	81
Table 4-2 - Out-of-plane Horizontal Deflections near the Top and Bottom Connections	86
Table 4-3- Displacement of the Bottom of the Wall with Respect to the Shims	89
Table 4-4 - Deflection of the Wall at Midheight	91
Table 4-5 - Out-of-Plane Test 1.1/1.2 compared to Test 1.1/1.2/1.3 under Positive Pressure.....	93
Table 4-6 - Out-of-plane Support Deflections for Test 1.1.....	94
Table 4-7 - Concrete Frame Deflections Between Supports.....	96
Table 4-8 - Concrete Frame Response During Lateral Sway Test at SLS.....	99
Table 4-9 - Steel Frame Response during Lateral Sway Tests	103
Table 4-10A - Concrete Frame Deformation for Lateral Sway (Push) Loading at SLS.....	105
Table 4-10B - Concrete Frame Deformation for Lateral Sway (Pull) Loading at SLS.....	105

Table 4-10C - Concrete Frame Deformation for Lateral Sway (Pull) Loading at ULS.....	105
Table 4-11A - Wall Rotation under Lateral Sway (Push) Loading at SLS.....	108
Table 4-11B - Wall Rotation under Lateral Sway (Pull) Loading at SLS.....	108
Table 4-12A - Change in Gap under Lateral Sway (Push) Loading at SLS	110
Table 4-12B - Change in Gap under Lateral Sway (Pull) Loading at SLS.....	110
Table 4-13 - Test Apparatus Response During Vertical Racking Test.....	113
Table 4-14 - Steel Frame Response During Vertical Racking Test.....	115
Table 4-15A - Displacement of Test Apparatus During Vertical Racking Tests at SLS.....	118
Table 4-15B - Displacement of Test Apparatus During Vertical Racking Tests at ULS.....	118
Table 4-16- Wall Rotation During Vertical Racking Tests at SLS.....	120
Table 4-17 - Change in Gap During Vertical Racking Tests at SLS	120
Table 4-18 - Comparison of Out-of-Plane Test 1.3 and 2.....	122
Table 4-19 - Comparison of Out-of-Plane Test 2 and 3.....	122
Table B-1 - Wind Loading Factors for the Prototype Structure.....	143
Table B-2 - Pressures Applied to Prototype Structure.....	143
Table B-3 - Wind Loading Factors for the Exterior Cladding Elements.....	144
Table C-1 - Axial Load in Columns at SLS and ULS.....	146
Table C-2 - Vertical Shortening Results.....	147
Table I-1 - Displacement of Infill wall under Negative Pressure.....	166
Table I-2 - Displacement of Infill wall under Positive Pressure.....	167
Table J-1 - Logbook Summary.....	169

LIST OF APPENDICES

APPENDIX A FEASIBILITY STUDY RESULTS FOR CASES 2, 4-7.....	138
APPENDIX B WIND LOADING.....	142
B.1 Prototype Structure.....	143
B.2 Test Apparatus.....	144
APPENDIX C VERTICAL CREEP CALCULATIONS.....	145
C.1 Loading Details	146
C.2 Summary of Results	146
APPENDIX D OVERVIEW OF BEAM DEFLECTION CALCULATIONS.....	148
APPENDIX E EFFECTIVE MOMENT OF INTERIA CALCULATIONS	150
E.1 Loading Details	151
APPENDIX F ENGINEERING DRAWINGS FOR TEST APPARATUS	152
APPENDIX G DESIGN LIMITS OF TEST APPARATUS.....	159
APPENDIX H WALL LIFT DETAILS.....	161
H.1 Conceptual Design	162
APPENDIX I WALL DEFORMATION CALCULATIONS.....	164
I.1 Overview	165
I.2 Conclusions	167
APPENDIX J TESTING DETAILS	168
J.1 Logbook Summary	169
J.2 LVDT Locations.....	170

NOMENCLATURE AND ABBREVIATIONS

A	Area (mm^2)
a	Distance between points of zero shear in longer direction (mm)
b	Distance between points of zero shear in the shorter direction (mm)
B	Bottom line of grid system, representing the bottom of the infill wall
C_e	Exposure factor
C_f	Factored compressive demand (MPa)
C_g	Gust effect factor
C_p	External pressure coefficients
C_r	Maximum factored wall resistance (kN)
CT	Top line of grid system, representing the top beam of the concrete frame
CB	Bottom line of grid system, representing the bottom beam of the concrete frame
CM	Middle line of grid system, representing mid-height of the concrete columns
d	Diameter (mm)
D	Dead Load (kN/m)
D_s	Sustained Dead Load (kN/m), or smaller plan dimension of a building (m)
e	Eccentricity (mm)
E_c	Elastic Modulus of Concrete (MPa)
FRR	Fire resistance rating stated by the NBCC
f_c'	Compressive strength (MPa)
f_y	Yield Strength (MPa)
H	Height of building (m), vertical height of infill wall (mm)
H'	Horizontal differential displacement of test apparatus (m)
H_{DT}	Distance between the top and bottom LVDT (m)
h	Height of storey (m)
HSS	Hollow Structural Section
I	Moment of Inertia (mm^4)
I_{cr}	Cracked Moment of Inertia (mm^4)
I_g	Gross Moment of Inertia (mm^4)
I_e	Effective Moment of Inertia (mm^4)
IRLBH	Insurance Research Lab for Better Homes
L	Span length (m)
L_{max}	Maximum length (m)
L	Live Load (kN/m), Steel Angle
LLRF	Live Load Reduction Factor

LVDT	Linear Variable Displacement Transducer
ℓ_n	Clear span (m)
M_a	Applied Moment (kN.m)
M_{cr}	Cracking Moment (kN.m)
M	Middle line of grid system, representing the midheight of the infill wall
n	Number of storeys
o/c	On-center
OSB	Oriented Strand Board sheathing
P_c	Axial Force due to dead load (kN)
P_h	Load applied horizontally at the top corner for the frame (kN)
P_v	Load applied vertically at the bottom left column (kN)
PLA	Pressure Load Actuator
R_{ext}	Resultant force at an exterior support (kN)
R_{int}	Resultant force at an interior support (kN)
SPF	Refers to a type of lumber that combines spruce-pine-fir
SLS	Serviceability limit states
T	Top line of grid system, representing the top of the infill wall
q	50-year reference velocity pressure (kN/mm)
ULS	Ultimate limit states
QB	Quarter line of grid system, representing the lower quarter of the infill wall
QT	Quarter line of grid system, representing the upper quarter of the infill wall
w_f	Total factored load (kN/m)
W	Wind Loading (kN/m), Mid-span wall deflection (mm)
Δ	Displacement seen at various locations on the test apparatus and specimen (mm)
Δ_B	Deflection of the wall near the bottom connection (mm)
Δ_D	Deflection due to the specified dead load
Δ_c	Column shortening of an exterior column due to creep (mm)
Δ_H	Point of maximum horizontal deflection (mm)
Δ_i	Column shortening of an interior column due to creep (mm)
Δ_{iL}	Deflection due to immediate live load (mm)
Δ_L	Lateral (or sway) deformation of the column over one storey (mm)
Δ_M	Measured midspan displacement of the wall (mm)
Δ_{SD}	Deflection due to sustained dead load (mm)
Δ_{SL}	Deflection due to sustained live load (mm)
Δ_T	Deflection of the wall near the top connection (mm)

Δ_{vc}	Accumulated differential vertical deflection of the columns due to creep (mm)
Δ_{vb}	Vertical deformation of the beam between the columns including any long-term deflection due to sustained loading (mm)
Δ_w	Deflection at midspan of the wall, deflection due to wind loading (mm)
λ	Change in gap (mm), long-term deflection multiplier
ν	Poisson's ratio

1 INTRODUCTION

1.1 OVERVIEW

1.1.1 INTRODUCTION

Wood and concrete have been used separately as effective structural materials in two-storey residential housing and low-rise multi-storey structures. With the recent seismic test of a six-storey light-frame wood structure in the NEESwood project (van de Lindt, 2010) and changes to the BC Building Code that increase the maximum number of storeys permissible using combustible building materials to six (BCBC, 2009), there is incentive to explore the boundaries of light-frame wood construction. The feasibility of a hybrid mid-rise design seems realistic given the potential synergy of pairing the strength and durability of concrete with the light weight and sustainability of wood. Currently there is no literature, however, that reviews light-frame wood and concrete hybrid systems for mid- to high-rise structures.

There has been some research on wood/concrete connection detailing, but past tests have focused on heavy timber construction, such as a post-and-beam wood frame with a concrete shear wall (e.g. Sakamoto, 2004). When subjected to simulated earthquake loading, failure occurred in both the concrete and the wood at their interconnection point. There are no references in the literature that specifically refer to hybrid light-frame wood/concrete methods of construction. The benefit of using light framing, instead of heavy timber, is that the load can be distributed throughout the wall system. This requires more connection points between the two materials but reduces the load on each

individual connection and so has the potential to add redundancy to the system. Light-frame members are more readily available than heavy timber members, which are now typically used as built-up sections (van de Lindt, 2010).

Additional research must be done to assess the interaction of light-frame wood and concrete in buildings. The connection of these materials is not discussed within CSA design standards and has been recognized as essential to the development of future design methods (CSA, 2010a; CSA, 2010c). This is further emphasized in Commentary B of the NBCC (2010) – Part 4, Division B, which states that “situations where structural integrity may require special attention include medium-rise and high-rise building systems made of components of different building materials, whose interconnection is not covered by existing CSA design standards” (emphasis added) (NBCC, 2010).

1.1.2 COMPLEMENTARY MATERIALS

Table 1-1 summarizes typical material properties of light-frame SPF wood (CSA, 2010c) and normal-weight concrete (MacGregor and Bartlett, 2000). Some of these properties are complimentary, suggesting hybrid wood/concrete construction may be feasible. For example, concrete is denser, stiffer and markedly stronger in compression, where as wood is lighter and stronger in tension.

Table 1-1 - Material Properties for Wood and Concrete

Material Properties	Wood	Concrete	Wood-to-Concrete Ratio
	Parallel to/Across Grain		
Density (kg/m ³)	550	2400	1:4.4
Specified Compressive Strength (MPa)	11.5/5.3	30	1:2.6 / 1: 5.7
Specified Tensile Strength (MPa)	5.5	3	1:0.5
Elastic Modulus (MPa)	9500	25000	1:2.6
Elastic Modulus (5% fractile) (MPa)	6500	25000	1:3.8

For wood/concrete hybrid systems to be feasible, potential material incompatibilities need to be resolved. Wood and concrete have different coefficients of thermal expansion that can potentially create high stresses at their interconnection points (Cook, 1977; Fragiacomio, 2010). Swelling and shrinkage of the wood is also a concern, especially in horizontal members such as floor joists, wall plates and beams (Wallace, 1998). It is unclear whether a moisture barrier is necessary between wood and concrete surfaces in contact in residential construction (CMHC, 1970). Without the barrier, the system may need to sustain the repeated swelling and contraction of the wood and the wood may wick moisture from the concrete causing deterioration (Holmes, 2006). Recent hybrid wood/concrete bridge construction practices have, however, involved successfully casting concrete against wood without a moisture barrier (Krisciunas, 2010). The National Building Code of Canada (NBCC) 2010 states that "wood framing members that are not pressure treated with a wood preservative and that are supported on concrete in contact with the ground or fill shall be separated from the concrete by not less than 0.05mm polyethylene film or Type S roll roofing". The same section also states that this is "not required where the wood member is at least 150mm above the ground", implying that

there will be no moisture in the concrete above such elevations. Load transfer mechanisms in future wood/concrete hybrid systems in mid-rise structures must accommodate these material incompatibilities.

1.1.3 POTENTIAL BENEFIT

A major benefit of including concrete in a mid-rise wood structure is the potential of increasing its fire resistance. A load-bearing wall within a structure of any size that is sprinklered can be classified as a firewall if it has a Fire Resistance Rating (FRR) of 2 hours (NBCC, 2010). If the building has six storeys, satisfies the area limitations specified in Part 3 of the NBCC (2010) and is made of a non-combustible material, then it requires have a FRR of only 1 hour. Provisions for six-storey structures were recently added to the BC Building Code to allow the use of combustible construction materials with a FRR of 1 hour (BCBC, 2009).

A potentially feasible design is a light-frame wood structure with a concrete elevator shaft, or stairwell, and a hybrid wood/concrete floor system in the corridors, as shown in Figure 1-1. This design takes advantage of the fire resistance of concrete by increasing its use in areas that require a higher FRR, such as stairwells. This design also addresses the need for the hybrid flooring to expand and contract, as accommodated by the connection detail shown. Implementation of this structure requires close consideration of the various wood/concrete connection details, particularly those around the concrete core.

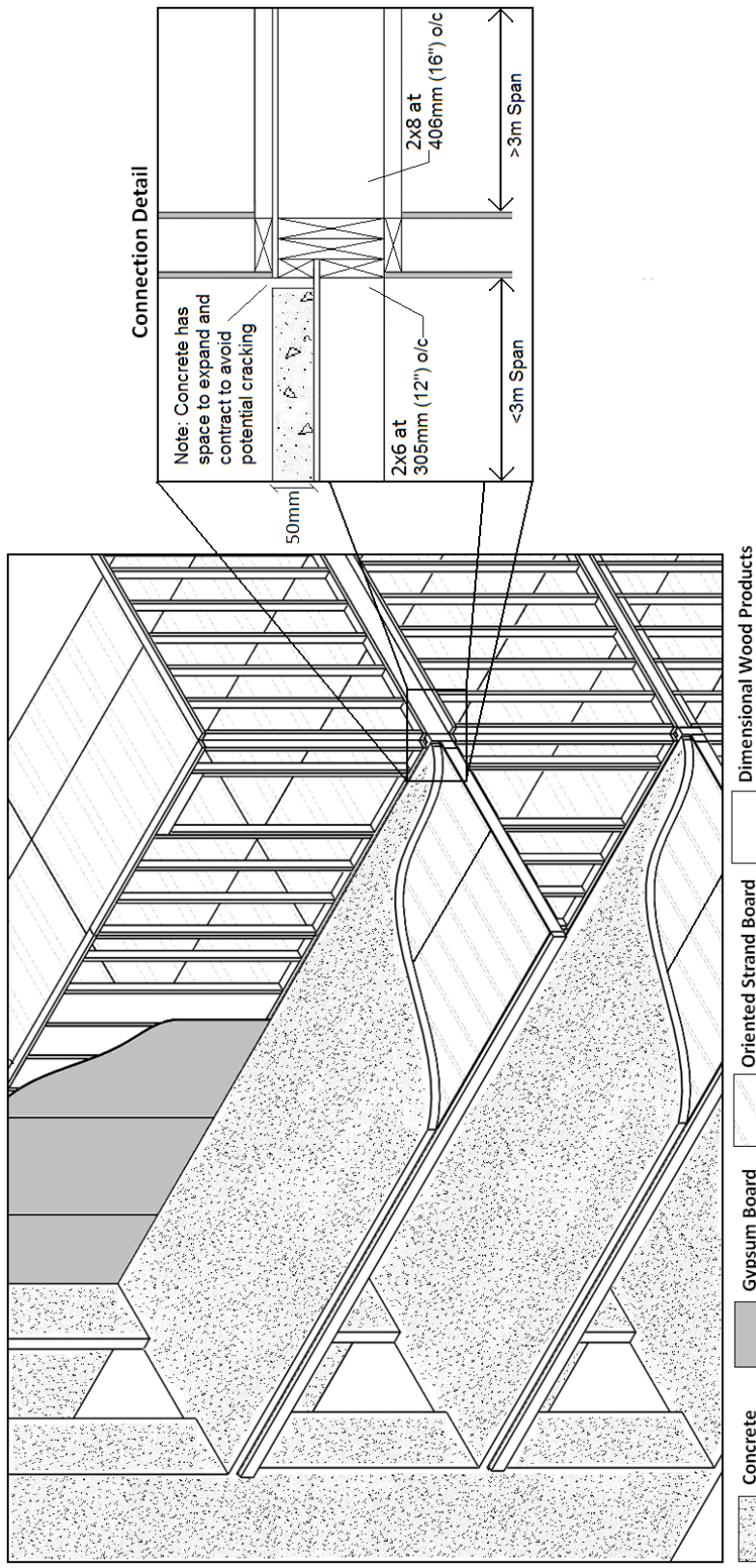


Figure 1-1 - Section of a Feasible Light-frame Wood/concrete Mid-rise Structure

1.2 NEWBUILDS

The NSERC Strategic Network on Innovative Wood Products and Building Systems (NEWBuildS), who funded the research reported in this thesis, focuses on increasing "the use of wood products in mid-rise buildings for residential and non-residential purposes in Canada and elsewhere" (Chui, 2009). This network includes "industrial associations (Canadian Wood Council, Canadian Home Builders Association), industrial research organization (FPInnovations), building product approval agency (NRC Canadian Construction Materials Centre), consulting engineers (structural and fire), engineered wood product manufacturers, and university researchers". The research activities of the network are classified within the four following themes:

- Theme 1: Cross Laminated Timber, focusing on material characterization and structural performance;
- Theme 2: Hybrid Building Systems, focusing on structural performance;
- Theme 3: Building Systems, focusing on fire performance, acoustic and vibration serviceability; and
- Theme 4: Building Systems, focusing on durability, sustainability and enhanced products.

The present study is part of Theme 2, listed as Project T2-2-C4: "Niche for and Feasibility of Reinforced Concrete Frame Multi-material Mid-rise Hybrid Systems".

1.3 RESEARCH OBJECTIVES

The broad objectives of this study are to:

1. identify and investigate niche areas for wood/concrete hybrid systems in mid- to high-rise buildings that can be practically implemented, accounting for the potential contributions of current or upcoming research, to highlight existing knowledge gaps that have prevented development to date (presented in Chapter 2), and;
2. explore some of the existing structural engineering challenges for a specific niche area to meet conventional limit states design requirements, including serviceability, safety and durability, and further its practical development (presented in Chapters 3 and 4).

Wind-bearing light-frame wood infill walls in reinforced concrete frame structures has been chosen as the niche area worth pursuing. This led to the following specific objectives:

- A. Quantify the deformed shape of a typical reinforced concrete frame structure under wind loading to identify critical frame sway deflection magnitudes.
- B. Develop a methodology for testing full-scale non-load-bearing infill wall specimens under realistic in-plane racking deformations and out-of-plane wind loads at both serviceability and ultimate limit states
- C. Design and construct a full-scale test apparatus that can replicate these critical racking deformations and apply the required wind loads to investigate,

experimentally, the interaction between the reinforced concrete frame and the wood infill wall.

- D. Design, prototype and test a connection that accommodates the predicted in-plane sway deflections of the reinforced concrete frame and yet withstands the localized out-of-plane wind loads at both serviceability and ultimate limit states.

1.4 OUTLINE OF THESIS

Chapter 2 investigates a spectrum of potential niche areas for wood/concrete hybrid systems in mid- to high-rise structures using traditional light-frame wood construction. Certain niches areas are deemed to be more feasible than others and are further investigated to quantify their feasibility using a limiting criterion such as the maximum number of storeys. A single niche, light-frame wood infill walls in reinforced concrete frame structures, is then chosen to be the focus of the rest of the study.

Chapter 3 focuses on the design and construction of the full-scale reinforced concrete frame test apparatus and the light-frame wood infill wall specimen. The test apparatus is used to replicate the realistic vertical and lateral frame deformations, identified by an investigation of a 9-storey reinforced concrete frame prototype structure, and to apply out-of-plane wind loading. A description of the connection design concept for the light-frame wood infill wall is also presented.

Chapter 4 presents the procedure for and results from the in-plane lateral sway and vertical racking tests, as well as three out-of-plane pressuring tests, performed using the test apparatus and wall specimen. A comparison of observed and predicted response of test apparatus and wall test specimen during the first out-of-plane test and the in-plane

tests are presented. The sequential out-of-plane tests were performed in-between each in-plane test to investigate their effect on the out-of-plane stiffness of the wall using a repeatability assessment.

Chapter 5 summarizes the research program and presents the conclusions of this research. Recommendations for future work are also presented.

2 NICHE AREAS FOR MID-RISE LIGHT-FRAME WOOD/CONCRETE HYBRID CONSTRUCTION

2.1 INTRODUCTION

2.1.1 OBJECTIVE

The objective of this chapter is to identify niche areas for wood/concrete hybrid systems in mid- to high-rise structures using traditional light-frame wood construction and to determine their feasibility for future use in practice.

2.1.2 DEFINING TERMS

A variety of terms have been used in the literature on hybrid systems (i.e., Elliot, 2003; Sakamoto, 2004). The present study will adopt the definition by Gagnon *et al.* (2006, 2007) which uses the term "hybrid" to describe two different materials that are combined to take advantage of each other's properties. These two materials may be interconnected as a system, or participate in parallel to achieve a common purpose. The term "composite" will refer to the action created between these two materials when connected integrally, such as the composite action in wood/concrete hybrid floor systems that is created by shear connectors. The terms "mixed construction", which generally refers to two materials combined without optimizing the benefits of each, and "dual system" will not be used. This study will also focus on the global perspective of a structure, as other research tends to incorporate the elements of a structure as well (Isoda, 2000; Gagnon, 2007). Thus, the present study will be focused on assessing the overall structure with

respect to the systems and assemblies within the structure. The study of individual elements, such as a single wood/concrete hybrid beam, will not be addressed.

2.2 EVALUATION OF NICHE AREAS

2.2.1 SCOPE

Figure 2-1 shows the spectrum of light-frame wood and concrete hybrid niche areas that have been considered within the scope of this project. Light-frame wood structures are listed at the top, representing one end of the spectrum. Concrete components are progressively added to create other niche areas, leading to all-concrete structures shown at the bottom. Each niche has been investigated to establish its potential as an area of growth for the Canadian wood industry. Past research has considered a variety of heavy timber wood/concrete hybrid systems (i.e. Sakamoto, 2002; Gagnon, 2007) but these will not be considered in the present study. There are a number of light-frame wood/concrete hybrid designs that have already been constructed successfully, however, generally these existing designs address the use of wood and concrete as materials in distinct separate structures, or uses one of the materials as a non-structural element. Other systems shown require the wood and concrete to be designed as a hybrid system. Research on some of these niche areas is ongoing elsewhere, such as in NEWBuildS Network Projects T2-1-C3: "Techniques for forming multi-functional construction interfaces in hybrid-buildings" and T2-9-C6: "Movements and deformation incompatibilities of materials in light wood frame residential buildings" (Chui, 2009). As implied by Figure 2-1, this chapter will address each of the niche areas listed and then further explore the feasibility of the following niches: Wood Structure with Wood/concrete Floor Systems, Wood

Structure with Concrete Lateral-load-resisting System and Reinforced Concrete Frame
Structure with Exterior Light-frame Wood Infill Walls.

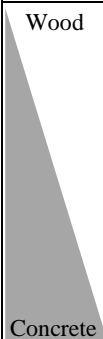
Spectrum	Potential Wood/Concrete Hybrid Systems	Reviewed Only	Further Investigated
Light-Frame Wood Structure			
Wood 	Wood Structure with Wood/Concrete Floor Systems		√
	Wood Structure with Concrete Foundation and Lower Storeys	√	
	Wood Structure with Concrete Lateral-load-resisting System		√
	Hybrid Structure with Compartmentalization	√	
	Reinforced Concrete Structure with Wood/Concrete Floor Systems	√	
	Reinforced Concrete Structure with a Wood Roof or Wood Upper Storeys	√	
	Reinforced Concrete Structure with Interior Partition Walls	√	
	Reinforced Concrete Structure with Exterior Light-frame Wood Infill Wall		√
Concrete	Reinforced Concrete Structure		

Figure 2-1 – Spectrum of Potential Wood/concrete Hybrid Systems

2.2.2 LIGHT-FRAME WOOD STRUCTURE

Figure 2-1 shows this niche is outside of the spectrum of wood/concrete hybrid systems. Light-frame wood structures are, however, used in this study as a guide to compare the storey restrictions placed on existing structures by current design codes. In countries such as the United Kingdom, United States, Germany, Norway, Italy and Switzerland, the height limit for a multi-storey wood-frame building is set between 5 and 7 storeys (Smith, 2008a; Surprenant, 2010). Currently the NBCC (2010) allows the construction of multi-storey wood-frame structures with up to 3 storeys with floor area restrictions. Four storey wood-frame structures are also allowed provided they have automatic extinguishers, satisfy floor area restrictions, are located on a street and have a limited number of

occupants. These limitations are mainly due to fire prevention considerations (Surprenant, 2010). Projects such as the Timber Frame 2000 Project (Enjily, 2006; Johal, 2009) and the NEESWood Project (van de Lindt, 2010) led to recent provisions to the BC Building Code which now allow the use of combustible materials in structures up to 6 storeys as of April 6th, 2009 (BCBC, 2009).

2.2.3 WOOD STRUCTURE WITH WOOD/CONCRETE FLOOR SYSTEMS

Figure 2-1 shows the feasibility of wood structures with wood/concrete floor systems will be further investigated in this study. Currently these systems are used in low-rise structures, but do not exist in mid-rise light-frame wood structures. This is because the accumulation of vertical shrinkage in the wood is considered negligible for structures with fewer than four storeys (Cheung, 2000). The present study includes a general survey of this niche, however, in-depth work is being done by NEWBuildS Network – Project T2-4-C3: "Innovative post-tension composite systems for long-span floor construction" (Chui, 2009).

Wood/concrete floor systems can be composite or non-composite. Non-composite floor systems include the use of concrete topping to add fire-resistance and sound-absorbent properties to the wood floor. This type of design is occasionally used (Cheung, 2008) and is considered in some sources to be standard practice (e.g. CWC, 2010). Composite floor systems use shear connectors to ensure full or partial composite behaviour between the concrete and the wood. They were first researched as floor systems in the 1940s (Lukeszeska, 2010), however they were used as decking for wood bridges in the 1930s (Cooke, 1977; Dolan, 2005; Clouston, 2008; Rautenstrauch, 2010; Gutkowski, 2010).

More recently they have been used for restoring historic buildings (Piazza, 2000) and specific connection designs are being used in practice to create hybrid flooring systems (Lukaszewska, 2008). The use of wood increases the efficiency of the system (load carrying capacity per unit self-weight), reduces load for better seismic performance, and markedly reduces environmental impact compared to a concrete slab (Yeoh, 2010). The concrete improves acoustics, decreases deflection and so increases span length, and enhances the fire resistance and floor diaphragm stiffness when compared to a timber-only floor (Gagnon, 2007; Clouston, 2008).

The benefits of wood/concrete composite floor systems have generated considerable research on innovative shear connectors between the two materials to facilitate an optimized and predictable composite system (Gagnon, 2007). Current challenges include: effectively achieving composite action between the materials, long-term behavior of the wood, creep effects due to the weight of concrete, plasticity developed before collapse, and the risk of fatigue failure from repetitive loading. There also remains uncertainty concerning the effect of water in the concrete on the durability of the wood members; however it is suggested that using precast concrete would resolve this, while also limiting concrete shrinkage and reducing construction costs (Lukaszewska, 2010). A film could also be applied as a moisture barrier between the wood and the concrete to protect the wood from excessive moisture (Clouston, 2005).

In general, the reported range of recently used concrete thicknesses in composite wood/concrete floor systems is 63.5-120mm for normal-weight concrete and 50-60mm for high-strength concrete, whether precast or cast in-situ (Clouston, 2005, 2008; Yeoh, 2010; Gutkowski, 2010; Crocetti, 2010; Lukaszewska, 2008, 2010; Kuhlmann, 2008;

Chuan, 2009). Spans reported in these studies range from 3.6m to 10.0m with various type of timber used (traditional lumber, laminated veneer lumber, glued laminated timber, etc.). The extensive available research on wood/concrete flooring systems has been summarized by Gagnon *et al.* (2007), Clouston *et al.* (2005, 2008), Gutkowski *et al.* (2010) and Lukaszewska *et al.* (2010). Despite this research, such systems are rarely used because of the difficulty in providing efficient connections, uncertainty in predicting long-term changes of the system and the lack of guidelines for design (Lukaszewska, 2010). The potential composite action is unclear: some claim that over 95% composite action can be achieved using a well-designed system (Clouston, 2005; Yeoh, 2010; Lukaszewska, 2010), while others state that the interaction between the two materials should be classified as only partially composite (Crocetti, 2010).

2.2.4 WOOD STRUCTURE WITH CONCRETE FOUNDATION AND LOWER STOREYS

Figure 2-1 indicates that this niche will not be further investigated because existing wood-to-concrete connections and current code restrictions limit the height of current mid-rise light-frame wood structures. These connections are required to resist large uplift and torsional forces to ensure adequate performance of the light-frame wood structure, while maintaining proper load transfer to the concrete substructure. Elaborate connection systems used for this type of construction (i.e., holdowns, strappings and continuous tie down, etc.) have helped to increase the maximum number of storeys with respect to all-wood structures (Shackelford, 2007). This niche is sensitive, however, to the similar code restrictions and design limitations placed on light-frame wood structures. Therefore,

further development of these connections seems to be limited and this niche will not be further addressed within this study.

2.2.5 WOOD STRUCTURE WITH CONCRETE LATERAL-LOAD-RESISTING SYSTEM

Figure 2-1 indicates that a wood structure with a concrete lateral-load-resisting system will be further developed within this study. Obvious design challenges are material incompatibilities, such as creep and differential shrinkage, in addition to the questionable behavior of the structure under lateral loading due to the connection detailing (Wallace, 1998; Sakamoto, 2002). Designs for these connections have been discussed suggesting that the wood and concrete structural systems be designed to act independently (Cheung, 2000). Further research is being conducted by the NEWBuildS Network – Project T2-9-C6: "Movements and Deformation incompatibilities of materials in light wood frame residential buildings" (Chui, 2009; Zhou, 2009).

2.2.6 HYBRID STRUCTURES WITH COMPARTMENTALIZATION

Figure 2-1 indicates that hybrid structures with compartmentalization will not be further considered within this study. This concept is potentially feasible in the long term. Its current potential is limited, however, and since the focus of this study is short-term feasibility, it will not be further developed. Smith *et al.* (2008b) developed a conceptual design of a "high-performance composite-construction system for a tall building", shown in Figure 2-2, based this approach. It is only theoretical at this point, yet has the potential to amalgamate a number of wood/concrete hybrid systems. The benefits allow the separation of components of the structural system to prevent, for example, the spread of

fire. This approach could also be applied to control shrinkage and creep within each compartment. To exploit this niche, the challenges of wood/concrete material incompatibility still require resolution. Further work is being done by NEWBuildS Network – T2-1-C3: "Techniques for forming multi-functional construction interfaces in hybrid-buildings" (Chui, 2009).

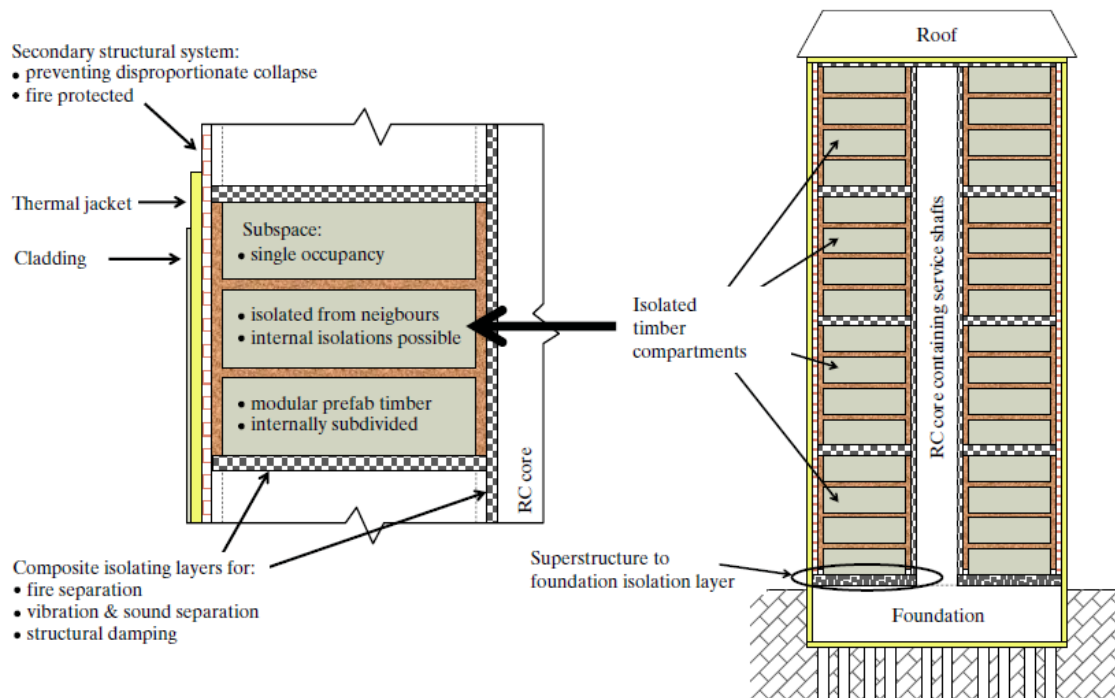


Figure 2-2 - Conceptual 16 storey Wood/concrete Hybrid Building (Smith, 2008b)

2.2.7 REINFORCED CONCRETE STRUCTURES WITH WOOD/CONCRETE FLOOR SYSTEMS

Figure 2-1 shows that reinforced concrete structures with wood/concrete floor systems will not be further considered in the present study due to the consideration of realistic design criteria when considering light-frame wood versus heavy timber. The wood floor

system is likely to be constructed within the structure, confined from expansion and contraction by concrete beams and/or walls, suggesting that material incompatibilities may be a concern. These connections will likely need to resist differential changes and potential moisture transfer while accommodating the deformed shape of the structure under lateral loading. Most heavy timber systems are typically engineered wood products and so are potentially more suitable because they exhibit much less expansion and contraction than light-frame systems. Since the floor system transfers gravity loads to the concrete walls, instead of the light-frame wood walls discussed in Section 2.2.2, they will be able to resist the large point loads created by heavy timber beams. Given these features, as well as the benefit of longer spans, it seems likely that a heavy timber would be preferable in this type of floor system, limiting the potential of a light-frame wood/concrete floor system in a reinforced concrete structure.

2.2.8 REINFORCED CONCRETE STRUCTURE WITH A WOOD ROOF OR WOOD UPPER STOREYS

Figure 2-1 indicates that a reinforced concrete structure with a wood roof or upper storey will not be further investigated. Although structurally similar to the ‘Wood Structure with Reinforced Concrete Foundation or Lower Storeys’ described in Section 2.2.3, the feasibility of this niche is mainly dependant on the potential fire risks in a high-rise light-frame wood structure. Current design restrictions are largely influenced by the ability to extinguish the fire on the top storey (Surprenant, 2010) and it is unrealistic to assume that these restrictions would apply to mid- to high-rise construction in this niche. This design potentially leads to larger structures, however fire constraints limit its overall feasibility.

2.2.9 REINFORCED CONCRETE STRUCTURE WITH INTERIOR WOOD PARTITION WALLS

Figure 2-1 shows that reinforced concrete structures with interior partition walls will not be further considered because, in North America, light-frame wood walls are already commonly used as interior non-load-bearing partition walls where the primary structure is constructed of a non-combustible material such as concrete or steel (Gagnon, 2006). These walls are frequently used in mid- to high-rise residential and non-residential construction and are comparable to similar wall systems that use light-gauge steel studs or masonry (Gagnon, 2007). With the potential for excellent acoustic performance and the use of prefabricated construction, light-frame wood walls can be optimal, especially compared to heavy masonry wall systems. The NBCC (2010) states that light-frame wood partition walls can be used in non-combustible structures if they are: sprinkled throughout; not used as a care, treatment or detention occupancy; and not located in exit enclosures.

2.2.10 REINFORCED CONCRETE STRUCTURE WITH EXTERIOR LIGHT-FRAME WOOD INFILL WALLS

Figure 2-1 shows that reinforced concrete structures with exterior light-frame wood infill walls is considered in the present study and, although touched on briefly in this chapter, will be further developed in the following chapters. A large majority of high-rise structures use concrete, either precast or cast-in-place, as the primary structural system and use other materials, such as masonry or light-gage steel framing, for infill walls. These infill components are typically non-loadbearing; exterior infill walls are only

required to transfer localized out-of-plane wind loads to the surrounding concrete frame. There are currently exterior light-frame wood infill walls in Scandinavia (where they were introduced in the 1950s), Netherlands, Germany, France, United Kingdom, Austria and China (Eriksson, 2005). Many existing examples of this system are low-rise structures or high-rise structures in geographic locations where there is no seismicity, such as Sweden. These wall systems are cost-competitive up to 20 storeys, especially current requirements for energy efficiency (EWC, 2010). There is little indication, however, that this hybrid system is used in North America (Wang, 2011). One of the current knowledge gaps concerning exterior wood infill walls involves quantification of the space required between the concrete frame and the infill wall panel. This space and the connection details must accommodate material volume change incompatibilities, deformations of the structure due to lateral loading and realistic construction tolerances of both the wood infill panel and the concrete frame. Light-gauge steel and masonry exterior wall systems are currently preferred in North America, mainly due to their non-combustibility.

2.3 ASSESSMENT OF POTENTIAL NICHE

2.3.1 APPROACH

The next goal is to assess the feasibility of the three highlighted niche areas shown in Figure 2-1 to be 'further investigated'. This is done by computing the potential maximum number of storeys of each niche alternative and comparing it to a feasibility limit criterion, which for this study is set at 7 or more storeys. This limit has been chosen to facilitate surpassing the current code restrictions for light-frame wood structures,

discussed in Section 1.1.1, which states that the maximum height of a wood structure in Canada is currently 6 storeys (in British Columbia). It also exceeds the limit of the full-scale light-frame wood structures that have been tested in the Timber Frame 2000 Project (Enjily, 2006; Johal, 2009) and the NEESWood Project (van de Lindt, 2010).

2.3.2 WOOD STRUCTURE WITH WOOD/CONCRETE FLOOR SYSTEM

The load path for a wood structure carrying gravity loads can easily be followed through the light-frame sheathed wood stud walls, leading directly to the foundation of the structure. The compressive capacity of these sheathed stud walls will be used in this study to estimate the maximum number of storeys for various loadings, material types and floor alternatives.

Figure 2-3 shows the cross-section of the simplified interior span investigated. Pin connections are assumed at the top and bottom of each wall. The floor is assumed to be continuous over, and so transfers a significant reaction to, the interior supporting wall, which is therefore the focus of this study. An exterior wall with the same axial capacity as the interior wall can support a span that is 3.3 times longer. For this simple idealized structure, the interior wall capacity becomes directly dependent on the properties of its constituent materials, readily facilitating comparisons for various loading criteria given different stud sizes and spacings.

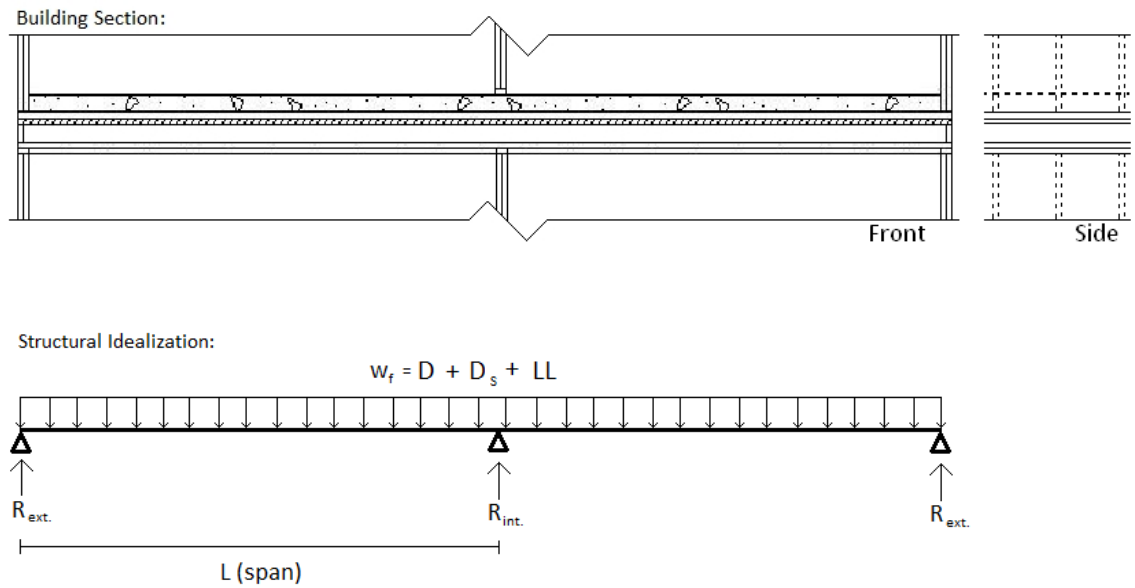


Figure 2-3 - Load Arrangement for Maximum Internal Reaction

The compressive demand, C_f , on the centre interior wall is:

$$[2.1] \quad C_f = 1.25 L n w_f$$

where L is the span between two walls and n is the number of storeys supported by the wall. The total factored load, w_f , is due to dead load, D , and live loads, L , specified in the NBCC (2010). Snow loads were neglected since they add limited gravity loading to the ground floor walls of structures with more than 4 storeys. The capacity of a 1m section of wall with a maximum stud spacing of 610 mm (24") on-center (o/c) was determined in accordance with CAN/CSA-O86-01 (CSA, 2010c). Given the wall capacity, C_r , the maximum number of storeys that can be supported for a given span can be computed for Eq. [2.1] for $C_f = C_r$. A clear storey height of 2.4m was assumed and the lumber was assumed to be dry, untreated SPF No. 1/2. No live load reduction was included as it is

unclear how to compute tributary areas for walls in accordance with NBCC (2010), Commentary F. For example, Figure 2-4 is a plan view of tributary area $a \times b$ that could be assigned to a floor supported on discrete walls, where a is the distance between two lines of zero shear in shorter direction and b is the distance between two lines of zero shear in the longer direction. If the wall is continuous, however, the length of the tributary area along the length of the wall, a , is unclear.

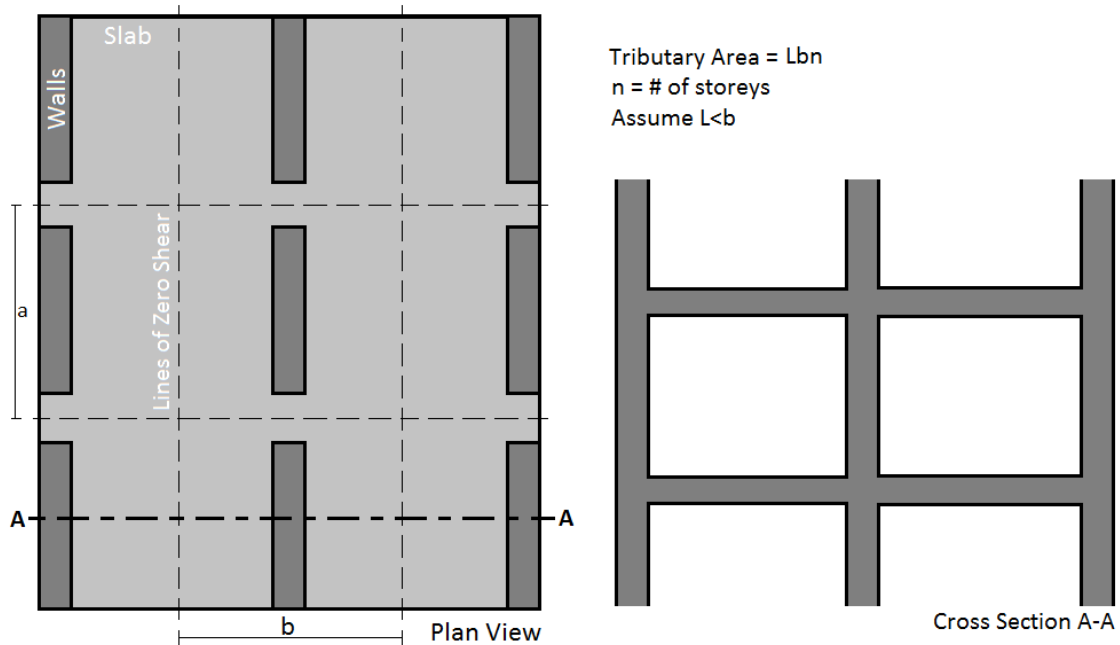


Figure 2-4 - Tributary Area for a Wall

Maximum span lengths for traditional wood products were based on bending moment capacities for various combinations of lumber joist depths and spacings calculated in accordance with CAN/CSA-O86-01 (CSA, 2010c). Deflection and floor vibration criteria were also considered. A 90mm concrete topping was assumed, to achieve the minimum 1 hr FRR specified in the NBCC (2010). As shown in Table 2-1, the maximum span length

is 5m and requires the use of 38mm x 286mm (2x12) joists at a spacing of 300mm. Realistically it is likely that the maximum span length will be 4m for dimensional lumber joists. Engineered wood products or wood/concrete hybrid floor systems have the potential to increase the maximum span, so longer spans have also been considered in this study.

Table 2-1 – Maximum Spans for Wood Joists

Span (m)	Joist Spacing (mm)			
	300	400	500	600
3	2x8	2x8	2x10	2x10
4	2x10	2x12	--	--
5	2x12	--	--	--

Table 2-2 shows the parameters and parameter ranges considered in the sensitivity analysis. Three different floor concrete thicknesses were investigated: non-structural concrete topping recommended in the Wood Design Manual (CWC, 2010) and permitted by NBCC (2010) to enhance FRR to at least 1 hr., wood/concrete composite floor systems described in current literature, and concrete slabs with span-to-thickness ratios that meet the empirical limits for deflection in CSA Standard A23.3-09 (CSA, 2010a).

Table 2-2 - Parameter Ranges Investigated

Variable	Range	Reference
Occupancy Classification	A - F	NBCC (2010) - Table 3.1.2.1
Live Load (kPa)	1.9 - 4.8	NBCC (2010) - Table 4.1.5.3
Super-imposed Dead Load (kPa)	1.6	CISC, 2006
Density of Concrete, γ_c , (kg/m ³)	1430-2400	MacGregor, 2000
Live Load Reduction Factor	1.0	NBCC (2010) Div. B - 4.1.5.9
<i>Wood Design Manual Suggested Values</i>		
Concrete Topping Height (mm)	36-50	CWC, 2010
<i>Wood/concrete Composite Floor System</i>		
Concrete Height (mm)	50-120	Crocetti, 2010; Clouston, 2005
<i>Concrete Design Manual Deflection Criteria</i>		
Maximum Length, L_{max} (m)	2.6-6.3	CSA, 2010a
Concrete Slab Thickness, t (mm)	150-350	-

Table 2-3 lists the seven cases investigated. Each case investigates the effect on the maximum number of storeys of changing the parameters shown in **'bold'** font. The various cases are further described as follows:

- Case 1 represents a wood structure with a wood floor system.
- Case 2 uses a 50mm thick concrete topping that allows a wood floor system to meet deflection criteria, and achieves the required 1-hour FRR using a combination of concrete and plywood (CWC, 2010). This case results in the least severe loading for any of the wood/concrete flooring alternatives investigated.
- Case 3 is the principal case. The 90mm concrete topping acts as the necessary flexural compressive zone within the assumed wood/concrete hybrid floor system and achieves the necessary 1- hr FRR specified in the NBCC (2010). This concrete thickness was chosen by assessing various wood/concrete test specimens

reported in current literature and has the potential to increase the span length beyond the limits shown in Table 2-1 (Chuan, 2009; Clouston, 2005, 2008; Crocetti, 2010; Gutkowski, 2010; Kuhlmann, 2008; Lukaszewska, 2008, 2010; Yoeh, 2010).

- Case 4 uses a non-prestressed one-way solid slab that satisfies the CAN/CSA-A23.3-09 deflection requirements (CSA, 2010a). The slab is assumed to be the only load-carrying element spanning between the load-bearing walls. To eliminate damage to non-structural elements from large deflections, the maximum length allowed, L_{\max} , for light-weight concrete is, from Table 9.2(a) of CSA A23.3-09 (2010a):

$$[2.2] \quad L_{\max} = 20 t (1.65 - 0.0003\gamma_c)$$

where t is the slab thickness and γ_c is the concrete density in kg/m^3 . A slab thickness of 200mm was found to be optimal, achieving the maximum number of storeys due to material capacity of the wood wall system while satisfying code deflection requirements.

- Cases 5-7 investigate the effects of changing the occupancy classification from residential to business, the concrete type from normal weight to lightweight and both the occupancy classification and concrete type, respectively, with respect to Case 3.

Table 2-3 - Multi-Storey Wood Structures with Wood/concrete Flooring

Variable	Assumed Values						
	Case 1	Case 2	Case 3	Case 4	Case 5	Case 6	Case 7
Occupancy Classification	C –Res.	C –Res.	C –Res.	C –Res.	C –Res.	D - Bus.	D - Bus.
Live Load (kPa)	1.9	1.9	1.9	1.9	1.9	2.4 / 4.8	2.4 / 4.8
Density of Concrete, γ_c (kg/m ³)	-	1800	1800	1800	2400	1800	2400
<i>Wood Design Manual Suggested Values</i>							
Concrete Topping Height (mm)	-	50	-	-	-	-	-
<i>Wood/Concrete Composite Floor System</i>							
Concrete Topping Height (mm)	-	-	90	-	90	90	90
<i>Concrete Design Manual Deflection Criteria</i>							
L_{max} (m)	-	-	-	3.6	-	-	-
Concrete Slab Thickness, t (mm)	-	-	-	200	-	-	-

Figure 2-5 shows the output for Case 1. The light-frame wall studs considered are 38mm x 89mm (2x4), 38mm x 140mm (2x6) and 38mm x 184mm (2x8) at varying spacings of either 152mm (6”), 203mm (8”), 305mm (12”), 406mm (16”), 508mm (20”) or 610mm (24”) o/c. The area under each curve represents the feasible domain. The maximum number of storeys reduces as the span length increases. As an example, Figure 2-5 shows that the maximum span that can be supported by the interior wall of a 7-storey structure consisting of 38mm x 184mm (2x8) studs at 152mm (6”) o/c is 5m. As a comparison, Figure 2-6 shows that Case 3 is unable to withstand the loads required for a 7 storey structure. The results for all cases are presented in Appendix A. A combination of different dimensional lumber sizes and spacing can be used throughout the storeys of the structure. For example, Figure 2-5 shows the 7-storey structure with 5m spans requires 38mm x 184mm (2x8) studs at 152mm (6”) o/c for the bottom two storeys, 38mm x 184mm (2x8) at 203mm (8”) o/c for the next two storeys and 38mm x 184mm (2x8) at

305mm (12") o/c for the remaining upper storeys. Regardless, the maximum wall compressive capacity in all cases is for 38mm x 184mm (2x8) studs at 152mm (6") o/c and this capacity was used to determine the maximum number of storeys for each case.

Table 2-4 summarizes the results for all seven cases. In assessing the maximum number of storeys it is assumed that the minimum acceptable span is 4.0m. This limit is realistic for residential construction: for example, the spans used in the NEESWood Project were approximately 4.0m (van de Lindt, 2010). The maximum span lengths are variables in the results for Cases 1-7. In all cases, the maximum number of storeys decreases as the span is increased. Therefore the use of span lengths greater than those shown in Table 2-1 will markedly reduce the maximum number of storeys.

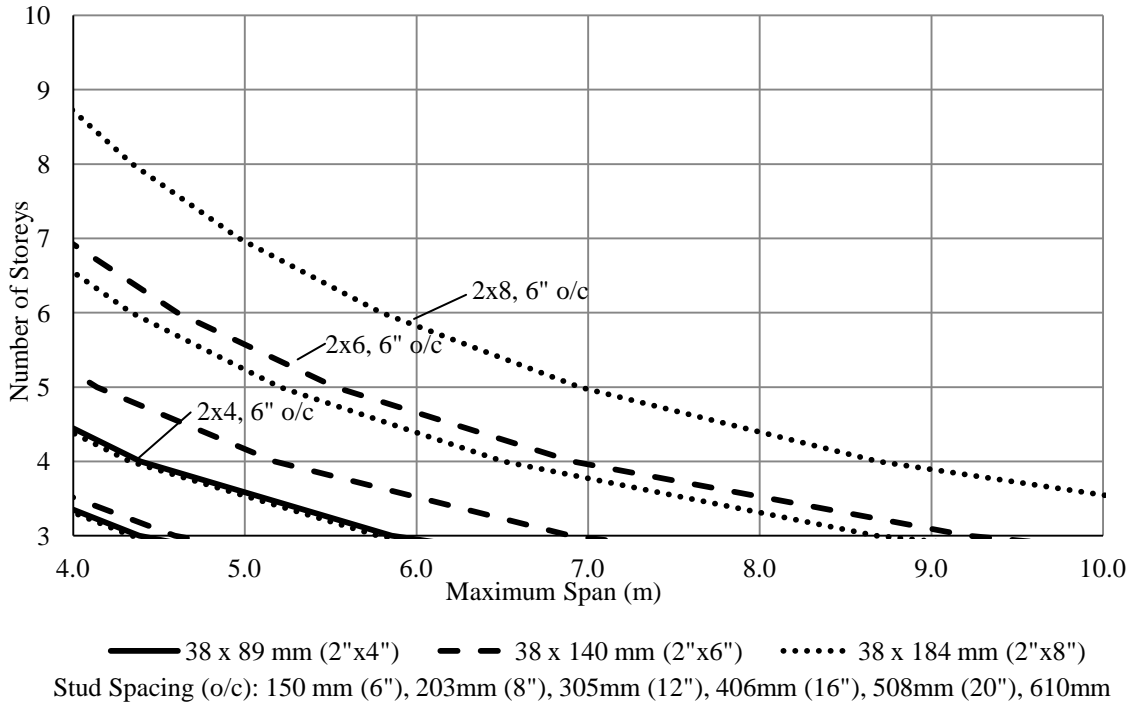


Figure 2-5 - Results for Case 1: Wood Structure under Residential Occupancy

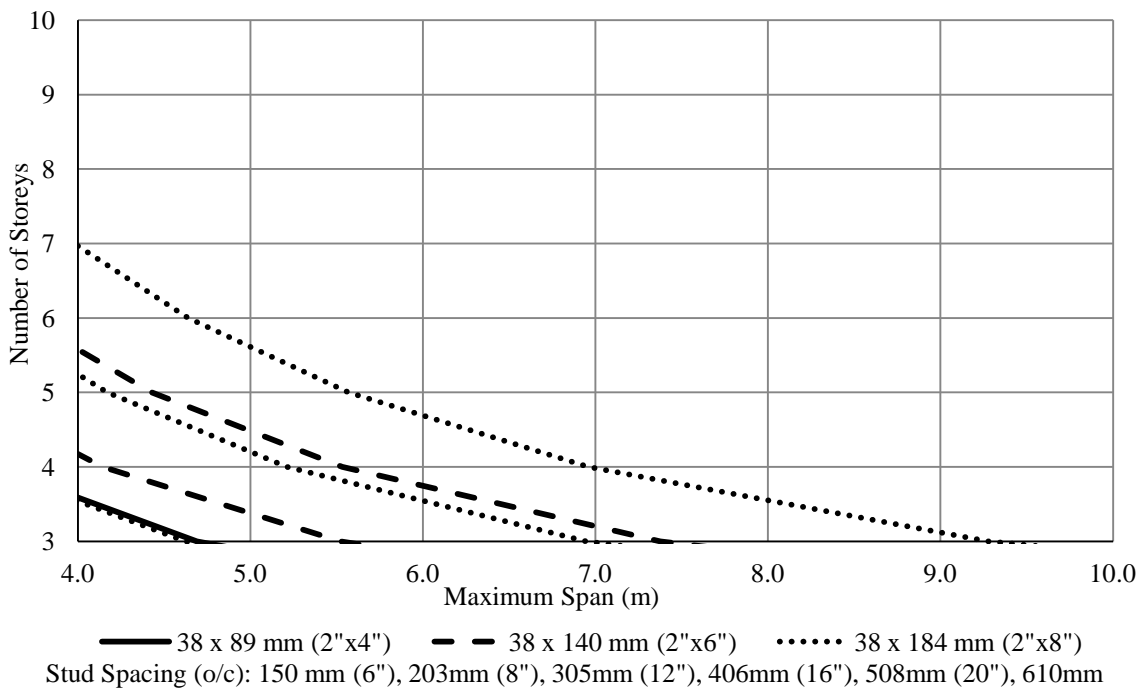


Figure 2-6 - Results for Case 3: Wood Structure with Light-weight Concrete and Wood Composite Flooring under Residential Occupancy

Table 2-4 shows that, for this simplified structure, Cases 1 and 2 give the greatest number of storeys, 8, with 4.3m and 4.0m spans, respectively. For Case 2, this can be attributed to the thin light-weight concrete topping on the floor system. Case 3 uses 90mm of concrete and this extra weight reduces the maximum number of storeys by one, irrespective of the wall stud size. Case 4 shows it is not feasible to design the concrete slab to be a structural element in a mid-rise structure with wood stud walls as it requires a slab thickness that markedly increases the dead load and reduces the maximum number of storeys to 5. When the occupancy classification is changed from C (Residential), Case 3, to D (Business), Case 6, the increased live load reduces the maximum number of storeys by two to 5. Normal-weight concrete reduces the maximum number of storeys by one to 6, as seen in the comparison between Case 5 with Case 3, and hence has potential to be feasible. When combining the effects considered in Cases 5 and 6, as shown in Case 7, there is little merit in pursuing a hybrid design for business occupancies using normal-weight concrete.

Table 2-4 – Maximum Number of Storeys: Gravity Loading Only

Stud Size	Result Criteria	Case						
		<i>1</i>	<i>2</i>	<i>3</i>	<i>4</i>	<i>5</i>	<i>6</i>	<i>7</i>
38x184mm (2x8)	Max. Number of Storeys:	8	8	7	5	6	5	4
	Span (m):	4.3	4.0	4.0	4.1	4.2	4.2	4.6
38x140mm (2x6)	Max. Number of Storeys:	6	6	5	4	5	4	< 4
	Span (m):	4.6	4.2	4.4	4.1	4.0	4.0	
38x89mm (2x4)	Max. Number of Storeys:	4	4	< 4	< 4	< 4	< 4	< 4
	Span (m):	4.4	4.0					

The results in Table 2-4 define the maximum number of storeys that can be supported by a structure with light-frame wood walls with various floor systems considering gravity loads only. These results suggest that residential occupancies with light-weight concrete or, if a slight reduction in the number of storey is accepted, normal-weight concrete are promising. Practically, however, the consideration of lateral loading may limit the maximum number of storeys in these mid-rise structures.

The current limit on light-frame wood construction, as reflected in recent changes to the BC Building Code (BCBC, 2009) and in the scale of the largest light-frame wood structure tested (van de Lindt, 2010), is 6 storeys. These structures have been designed to resist all lateral loads and use advanced design techniques, such as tie rods and built-up stud packs, to resist the large overturning moments (van de Lindt, 2010). In the current study, Case 1 represents a similar, although idealized, wood structure and has a theoretical limit of 8 storeys with 2x8 (38x184mm) studs at 6" (150mm) o/c. Comparing this height with currently accepted practice, it is realistic to assume that the consideration of lateral loading will reduce the storey limits shown in Table 2-4 by 1 or 2 storeys. This deduction has been applied to all the cases, yielding the reduced maximum numbers of storeys shown in Table 2-5. For example, Case 3 has a theoretical limit of 7 storeys with 2x8 (38x184mm) studs at 6" (150mm) o/c, Table 2-4, and should therefore be deemed to be restricted to a maximum of 5 storeys if lateral loading is considered, Table 2-5. Therefore, these results show, within reason, that wood structures with wood/concrete floor systems have limited feasibility for mid-rise structures with 7 or more storeys.

Table 2-5 - Maximum Number of Storeys: Lateral Load Included

Stud Size	Result Criteria	Case						
		<i>1</i>	<i>2</i>	<i>3</i>	<i>4</i>	<i>5</i>	<i>6</i>	<i>7</i>
38x184mm (2x8)	Max. Number of Storeys:	6	6	5	3	4	3	2
	Span (m):	-	-	-	-	-	-	-
38x140mm (2x6)	Max. Number of Storeys:	4	4	3	2	3	2	<< 4
	Span (m):	-	-	-	-	-	-	
38x89mm (2x4)	Max. Number of Storeys:	2	2	<< 4	<< 4	<< 4	<< 4	<< 4
	Span (m):	-	-					

2.3.3 WOOD STRUCTURE WITH CONCRETE LATERAL-LOAD-RESISTING SYSTEM

Consideration of lateral loading has shown to be critical when assessing the capacity of the simplified structures investigated. The addition of a separate concrete lateral-load-resisting system may therefore seem beneficial to minimize the transfer of lateral loading to the wood structure. The feasibility of this niche has been further explored by examining hybrid systems consisting of light-frame wood structures with a concrete elevator core or stairwell. It is assumed, perhaps optimistically, that the monolithic nature of the core and floor topping would create full rotation fixity at one exterior support and so reducing the reaction at the interior wall, yielding:

$$[2.3] \quad C_f = 1.14 L w_f n$$

This 8.5% reduction of the reaction, compared to Eq. [2.1], increases the maximum number of storeys by one. Table 2-6 shows the modified results for each case and

demonstrates that attaching a concrete core to the wood structure with wood/concrete floors creates further potential for this niche area.

Table 2-6 - Maximum Number of Storeys: Gravity Loading with Lateral-load-resisting System

Stud Size	Result Criteria	Case						
		<i>1</i>	<i>2</i>	<i>3</i>	<i>4</i>	<i>5</i>	<i>6</i>	<i>7</i>
38x184mm (2x8)	Max. Number of Storeys:	9	9	8	6	7	6	5
	Span (m):	4.3	4.0	4.0	4.1	4.2	4.2	4.6
38x140mm (2x6)	Max. Number of Storeys:	7	7	6	5	6	5	<5
	Span (m):	4.6	4.2	4.4	4.1	4.0	4.0	
38x89mm (2x4)	Max. Number of Storeys:	5	5	<5	<5	<5	<5	<5
	Span (m):	4.4	4.0					

Within this study, the maximum number of storeys for a wood structure with a wood/concrete floor system, whether attached or not attached to a concrete lateral-load-resisting system, has been shown to be limited to 8 or 9 storeys. This limit is based on optimistic assumptions and is dependent on large 38mm x 184mm (2x8) studs at small 152mm (6") spacings and short 4m spans. When considering the effect of lateral loading and incompatibilities between the two materials, the use of light-frame wood as load-bearing elements in mid-rise wood structures with composite wood/concrete floors is generally not feasible. Even with future research, there is limited potential to reach more than eight storeys with load-bearing light-frame timber. The use of non-traditional timber sizes (i.e., 3"x6", 910mm x 1830mm) may be necessary to realize the feasibility of hybrid

systems with load-bearing wood walls. In Europe, "light-frame" wood construction includes wood members with a minimum cross-sectional area dimension of 160mm (Frangi, 2011).

There is little literature on hybrid light-frame wood/concrete systems and currently this type of design is restricted to structures with up to 4 storeys (Gagnon, 2006) due to the accumulation of material incompatibilities in taller structures. Further work is currently being done within the NEWBuildS Network (Chui, 2009) to assess the interaction of the two materials.

2.3.4 REINFORCED CONCRETE STRUCTURE WITH LIGHT-FRAME WOOD INFILL WALLS

This niche alternative considers light-frame wood walls in conventional reinforced concrete frame structures. It has been shown in Sections 2.3.3 that a light-frame wood wall has limited load-bearing capacity, especially for taller structures. To further investigate whether these walls are capable participating with the concrete load-carrying system, the maximum compressive capacity of a 1m wide wall for dry, untreated SPF timber was computed and compared to the compressive demand due to overturning from lateral loading, combined with gravitational loads, for a 10 storey reinforced concrete structure with an aspect ratio of 0.7. The compressive demand at the base of the structure is approximately twice the capacity of a 1m wide section of a sheathed wood wall comprising of 2x8 (38mm x 184mm) SPF studs at 6" (152mm) o/c. It was therefore deemed unrealistic to use light-frame exterior wood infill walls as load-bearing elements within a mid- to high-rise structure.

Non-load-bearing infill walls have been successfully implemented in Europe, including use in high-rise buildings in non-seismic zones (Eriksson, 2005). This type of infill wall system is popular due to high energy conservation properties of wood and the simple construction techniques that can be adaptable to various building systems (Wang, 2011; Gagnon, 2006). Despite this, the associated design criteria and available literature is limited. There is little information on design limitations, such as structure height, and current knowledge seems to be experience-based with little basis in the fundamentals of structural mechanics.

Standard practice for existing wood infill wall designs feature a gap of 15 to 20mm (Eriksson, 2005) around the perimeter of the wall to accommodate in-plane deformations of the reinforced concrete frame and ensuring the infill wall remains non-loadbearing. This gap also helps to avoid potential material incompatibility issues, as the concrete and wood are free to expand and contract without being restrained by the other material. In fact, these material changes are mainly limited to the concrete as the expansion and contraction of the wood infill wall will only occur in the top and bottom plates in the radial and tangential directions (i.e., parallel to the grain) (Keenan, 1986). This avoids accumulated stresses over the height of the structure from attached wood systems, a concern relevant to other wood/concrete hybrid systems, as well as any significant contribution from the infill wall to the change in gap. The gap also has the potential to accommodate concrete construction tolerances. On-site geometric tolerances, however, may be substantially less or substantially greater than these values since other types of exterior cladding and wall systems, such as light-gauge steel framing and precast concrete panels, recommend a tolerance of +/- 1.5 in. (38.1mm) (e.g. CSSBI, 1992).

Further research within the present study will focus on connections that effectively transfer load and isolate material incompatibilities, are readily constructed using conventional methods and accommodate realistic concrete construction tolerances.

The structural performance of these wall systems is important, however, fire resistance of the walls may be a more serious constraint. The NBCC (2010) permits an exterior non-load-bearing wall assembly that includes combustible components to be used in a building of non-combustible construction, such as a wood infill wall in a concrete frame, only if the building is sprinklered and the interior surface of the wall assembly is protected by a thermal barrier. These requirements are readily addressed. Currently, the most stringent Canadian requirement is that the exterior walls must conform to the 'Fire Test of Exterior Wall Assemblies' (NBCC, 2010), especially if untreated exterior cladding is used (Mehaffey, 2010). This needs to be addressed before a light-frame wood wall can be successfully implemented in mid- or high-rise structures.

2.4 SUMMARY AND CONCLUSION

This investigation has defined a spectrum of potential niche areas for light-frame wood/concrete hybrid systems in mid-rise structures. Each alternative considered represents a hybrid system that allows the two materials to complement each other. A number of niche areas were reviewed that were limited by challenges such as material incompatibilities and fire resistance. The following three, out of the eight, potential niche areas were chosen to be assessed in further detail:

1. Load-bearing light-frame wood walls combined with floor systems featuring non-composite concrete topping, wood/concrete composite construction or concrete

one-way slabs. The feasibility study investigated various combinations of gravity loading where the axial capacity of the stud wall at the base of the structure was used to determine the maximum number of storeys. These results were then compared to existing structures to determine the potential contribution of lateral loading. With these assumptions, an approximate maximum number of storeys was determined.

2. Gravity-load-resisting light-frame wood structure with a reinforced concrete lateral-load-resisting system, such as concrete elevator shafts and stairwells. Introducing these systems into a largely light-frame wood structure could mitigate fire resistance and enhance the overall stability of the structure. The same procedure used to assess the wood structure without the lateral-load-resisting system was adopted. The results indicate that the concrete lateral-load-resisting system allows an increase of an extra storey since the connection of the wood system to the concrete system is assumed to be fixed. Also, any reduction in storeys due to the additional demands caused by lateral loading is avoided.
3. Light-frame wood infill walls in reinforced concrete frame structures. A brief investigation was carried out on a load-bearing infill wall system. There are existing applications of this type of system throughout Europe, include high-rise buildings, yet they seem unfeasible according to the requirements of Canadian codes. Further structural research includes connection detailing, concrete geometric tolerances that must be accommodated and storey restriction necessary to ensure minimal damage from the sway deflections of the concrete structure.

Upon further review of the three potentially feasible niche areas, the following conclusions can be made:

1. Light-frame wood structures with wood/concrete floor systems are most preferable for residential occupancies, where a maximum of 6 storeys is possible if light-weight concrete topping is used. The use of normal-weight concrete reduces the maximum number of storeys by one. Such systems are clearly not feasible for buildings with business occupancies, particularly as such structures require span lengths longer than 4m to create open-concept floor layouts. They are also not feasible for the case of a full-depth concrete slab as the floor system.
2. Overall, there is limited feasibility in pursuing light-frame wood structures combined with wood/concrete floor systems for 7 or more storeys, if the maximum span is 4m and current techniques for light-frame wood structures is used for resisting lateral loads. The compressive capacity of the load-bearing dimensional lumber is a limiting factor, however alternatives with larger cross-sections and/or use engineered wood products, as well as the use of combining studs to create built-up stud packs, may need consideration.
3. Similar conclusions can be made for gravity-load-resisting light-frame wood structures with a concrete lateral-load-resisting system, although such systems have the potential to reach 9 storeys. Material incompatibilities are still a challenge, however, since their effects accumulate as the height of the structure increases. These issues are currently being investigated by projects within the NEWBuildS Network and may therefore be deemed feasible in the future.

4. Preliminary calculations have demonstrated that light-frame wood infill walls are not feasibly for use as a load-bearing element.
5. The most promising niche is the use of light-frame wood infill walls in reinforced concrete frame structures. These wall systems must remain non-load-bearing during in-plane deformations of the reinforced concrete frame structure and so require a gap around the perimeter of the wood wall. Design limitations for this type of wood/concrete hybrid system, such as the size of the gap, need to be quantified in the context of Canadian standards before this construction can be used in mid- to high-rise structures.

3 TEST DESIGN AND CONSTRUCTION

3.1 OBJECTIVE

Chapter 2 identified non-load-bearing light-frame wood infill walls in mid- to high-rise reinforced concrete frame structures as a feasible niche area for hybrid wood/concrete construction. The research presented in this chapter investigates realistic in-plane boundary conditions at serviceability and ultimate limit states for a light-frame wood infill wall created by the deformations of a reinforced concrete frame, and a means to subject a full-scale wall specimen to these deformations in the laboratory. The application of out-of-plane wind loading will also be presented.

The specific objectives are:

- To quantify the critical storey deformations in a typical multi-storey reinforced concrete frame due to in-plane wind loading and differential column creep.
- To design a test apparatus that can replicate these critical concrete frame deformations, and also facilitate out-of-plane wind loading on a full-scale infill wall specimen.
- To design the full-scale light-frame wood infill wall, including its connection to the concrete frame.

The experimental investigation of its response to realistic in-plane and out-of-plane loading will be presented in Chapter 4.

3.2 PROTOTYPE STRUCTURE

Figure 3-1 shows the simple sway frame structure from the Cement Association of Canada Concrete Design Handbook, 2nd Edition (CAC, 1984), that was used as the prototype structure for the present study. The frame is 8 storeys tall, excluding the basement floor, with a typical storey height of 3.3m and a first storey height of 5.5m. The column lines are at 6.5m o/c in both directions. Analysis of this frame is well documented, allowing a new second-order analysis to be carried out using SAP2000 (SAP, 2009) which was checked by comparing the predicted first-order analysis response to that originally reported (CAC, 1984), and to other previous work (Stead, 2010). Separate linear elastic analyses were conducted to quantify the response for specified and factored load levels.

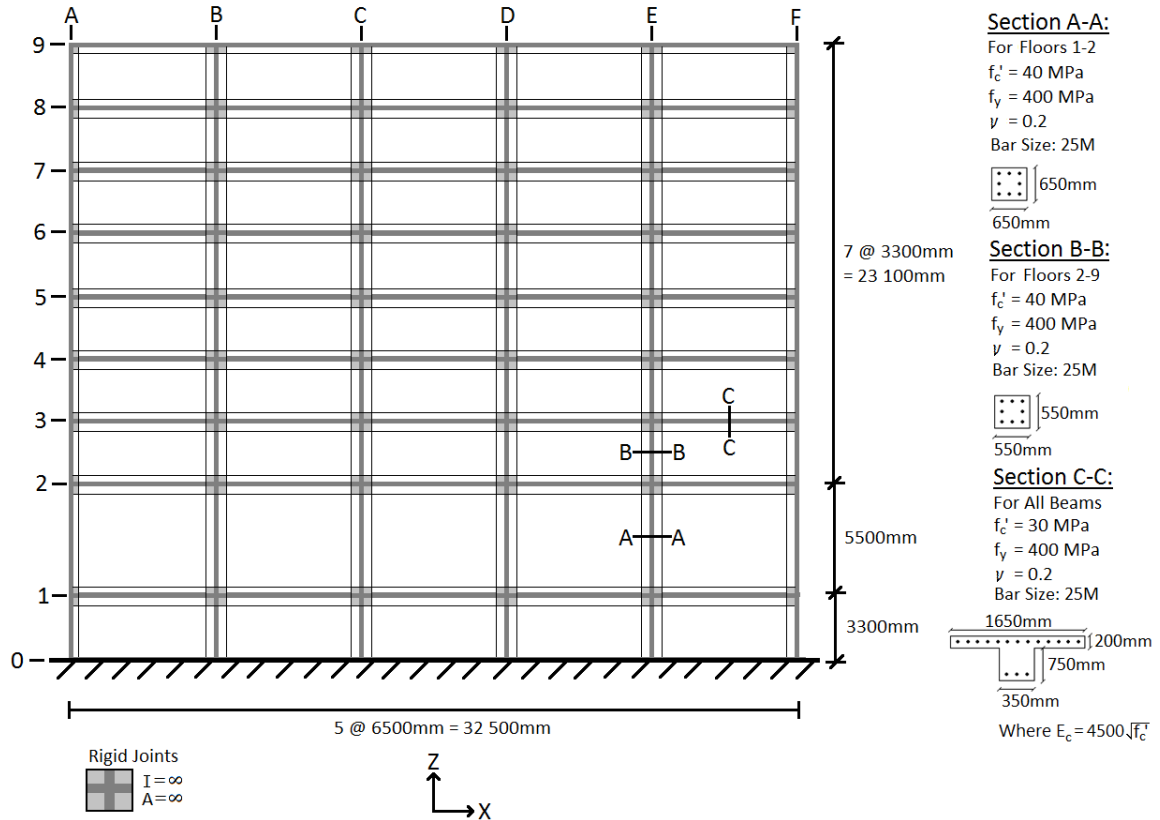


Figure 3-1 - Summary of Prototype Structure

3.2.1 IDEALIZATION

The following idealizations were made:

- Joints were assumed to have infinite stiffness within each beam-column core to predict joint rotations and frame deflections more accurately.
- Connections at the base of the structure were assumed fixed to represent the effect of the basement floor and foundation.
- An effective slab width of 1650mm (CSA, 2010a) was assumed. Any width of the floor slabs beyond the beam stems was originally neglected (CAC, 1984). The

current idealization increases the moment of inertia of the beams and, therefore, reduces the overall deflections.

- The column stiffnesses assumed to assess the response at specified load levels to check Serviceability Limit States (SLS) are the gross (i.e., uncracked) values whereas the beam stiffnesses are 50% of the gross values to account for cracking. To investigate Ultimate Limit States at factored load levels, both the beam and column stiffnesses were reduced by 30% to account for cracking of the concrete and yielding of steel reinforcement (CSA, 2010a).

3.2.2 LOADING ASSUMPTIONS

A sustained dead load of 7.5 kPa (CAC, 1984) was applied. This accounts for the slab weight of 4.8 kPa and the T-beam stems, equivalent to an additional dead load of 1.9 kPa. The additional dead load is due to ceiling and floor finishes, etc. A live load of 5 kPa (CAC, 1984), comparable to the specified office occupancy load of 4.8 kPa (NBCC, 2010), was also used. The live load was reduced by a Live Load Reduction Factor (LLRF) of 0.47, which is appropriate for a ground floor interior column (NBCC, 2010).

The wind loads, specified by the NBCC (2010), were derived using the following parameters:

- A 50-year reference velocity pressure, q , of 0.53 kN/m^2 , chosen to represent the higher pressures specified for a building located in Ontario.
- A gust effect factor, C_g , of 2.0 as is appropriate for a slender high-rise structure with $H > 20\text{m}$ and $H/D_s > 1$, where H is the height of the building and D_s is the smaller plan dimension.

- An exposure factor, C_e , corresponding to rough terrain that increases with the height on the windward side and is uniform on the leeward side.
- External pressure coefficients, C_p , of 0.8 (windward side) and -0.5 (leeward side).

A summary of the wind loading details are presented in Appendix B-1. The load combination at SLS, when wind is the principal action, is $D+0.5L+0.75W$ as specified in the NBCC (2010). The factored load combinations at ULS are $1.25D+1.5L+0.4W$ and $1.25D+0.5L+1.4W$. The combination with the wind as the principal transient load governs the sway deflections because the second-order effects are small.

3.2.3 PRINCIPAL IN-PLANE DEFLECTIONS

Figure 3-2 shows the three principal deflections that have been identified for this study, where:

- Δ_L is the lateral (or sway) deformation of the column over one storey;
- Δ_{vc} is the accumulated differential vertical deflection of the columns due to creep,
and;
- Δ_{vb} is the vertical deformation of the beam between the columns including any long-term deflection due to sustained loading.

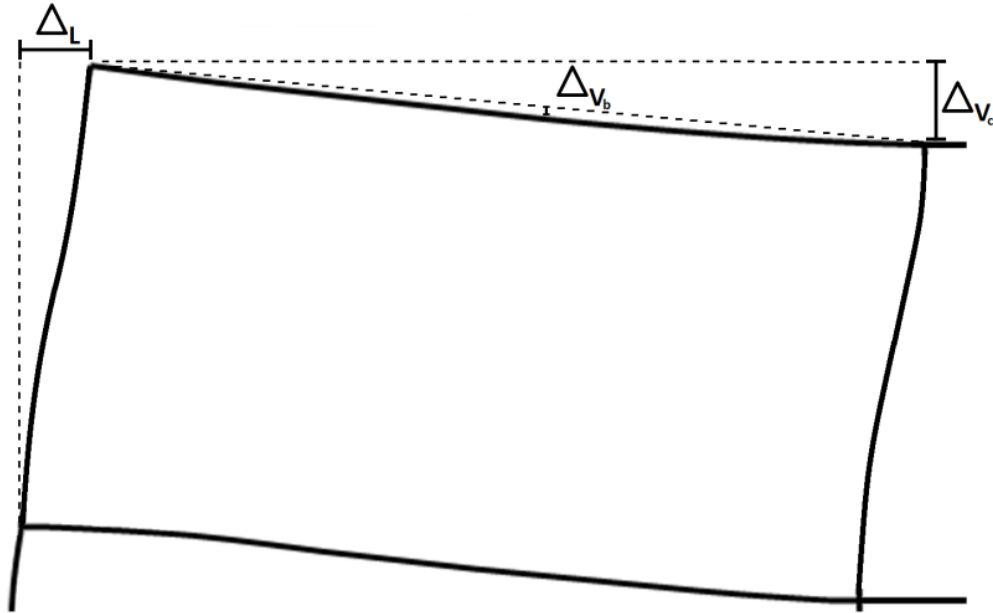


Figure 3-2 - Principal In-plane Deflections

Figure 3-3 shows the sway deformation of the structure at SLS and ULS, computed accounting for second order effects. The largest interstorey sway deflection occurs at Storey 1-2 where the shear force is large and the storey height is greatest. It is assumed unlikely that a wood infill wall would be used on this ground floor, however, so this study focuses on the upper storeys. The critical frame is therefore the exterior frame Storey 2-3, shown highlighted in grey, which has an interstorey sway deflection at SLS, using the $D+0.5L+0.75W$ load combination, of 0.7mm. The corresponding sway deflection limit (NBCC 2010) is $h/500$, where h is the height of the storey. Thus, for a storey height of 3300mm, the limit is 6.6mm, shown in Figure 3-4 as an approximate range of 6-7mm. The critical interstorey sway deflection of Storey 2-3 at ULS, using the $1.25D+0.5L+1.4W$ load combination, is 1.8mm, or 2.6 times the SLS deflection. This increase can be attributed to the combined effects of the cracking of the concrete (i.e., a

factor of $1/0.7=1.43$), and the increased factored wind load (i.e., a factor of $1.4/0.75 = 1.87$) which together correspond to a factor of 2.67. If the structure is designed to just satisfy the SLS deflection limit of 6.6mm, the corresponding approximate ULS sway deflection is 17-18mm, as shown in Figure 3-4.

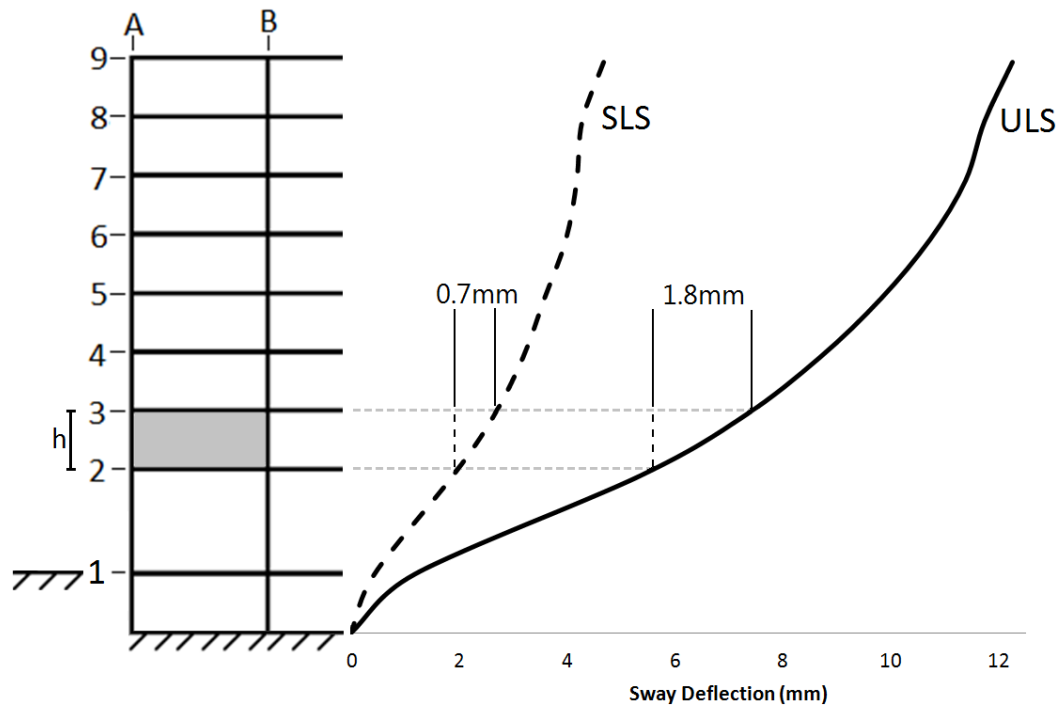


Figure 3-3 - Sway Deformation of the Prototype Structure at SLS and ULS

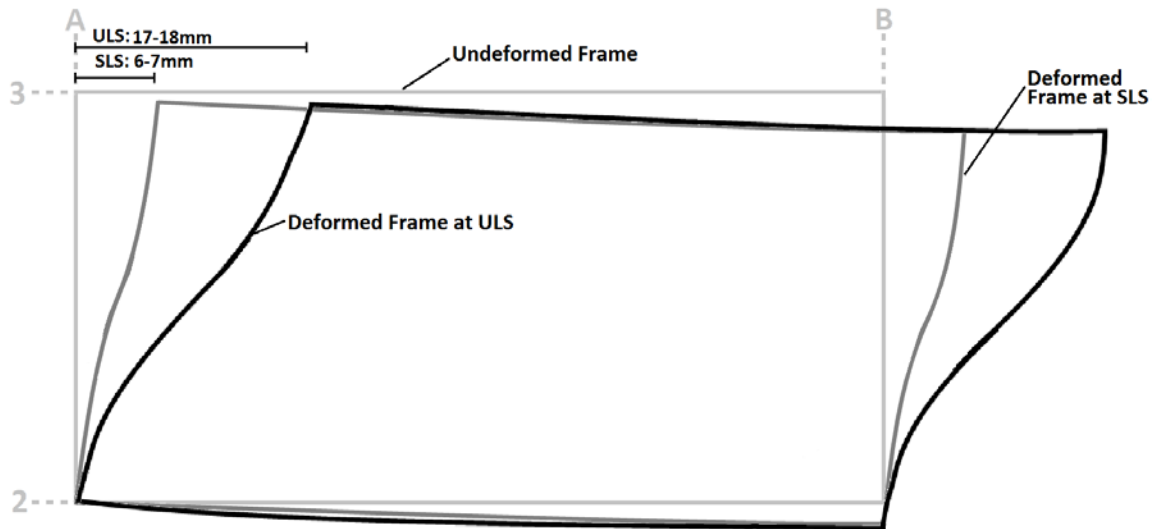


Figure 3-4 - Sway Deflection Limits for Critical Frame

The vertical creep deformations are due to differential shortening in the reinforced concrete columns. The creep deflection is calculated using CEB-FIB Model Code 1990 method (i.e., MacGregor and Bartlett, 2000) assuming a 25 year time period, a relative humidity of 50%, and that loading occurs 2 weeks after the concrete is cast. The axial force in the columns was determined using the SAP2000 model under 1.0D for SLS and 1.4D for ULS. Loading details and a summary of the results are presented in Appendix C. The tributary area of the interior column is twice as large as the exterior column, despite their having the same cross section, leading to twice the sustained dead load stress and thus causes a differential deflection over time. Figure 3-5 shows the accumulation of vertical shortening over the height of the prototype structure for exterior and interior columns at SLS and ULS. The greatest differential shortening occurs in the top storey of an exterior frame, shown highlighted in grey. The maximum differential shortening of the critical frame is 6.8mm at SLS and 9.5mm at ULS. There is no code limit on differential

vertical deflections at SLS so the critical range, rounded up slightly to account for creep analysis uncertainty, is 7-8mm, as shown in Figure 3-6. The corresponding range at ULS, accounting for the dead load factor, is 10-12mm, as also shown in Figure 3-6. Other factors including foundation settlement, construction tolerances, non-standard loading, etc., can increase the differential vertical deflection but are not reflected in these limits.

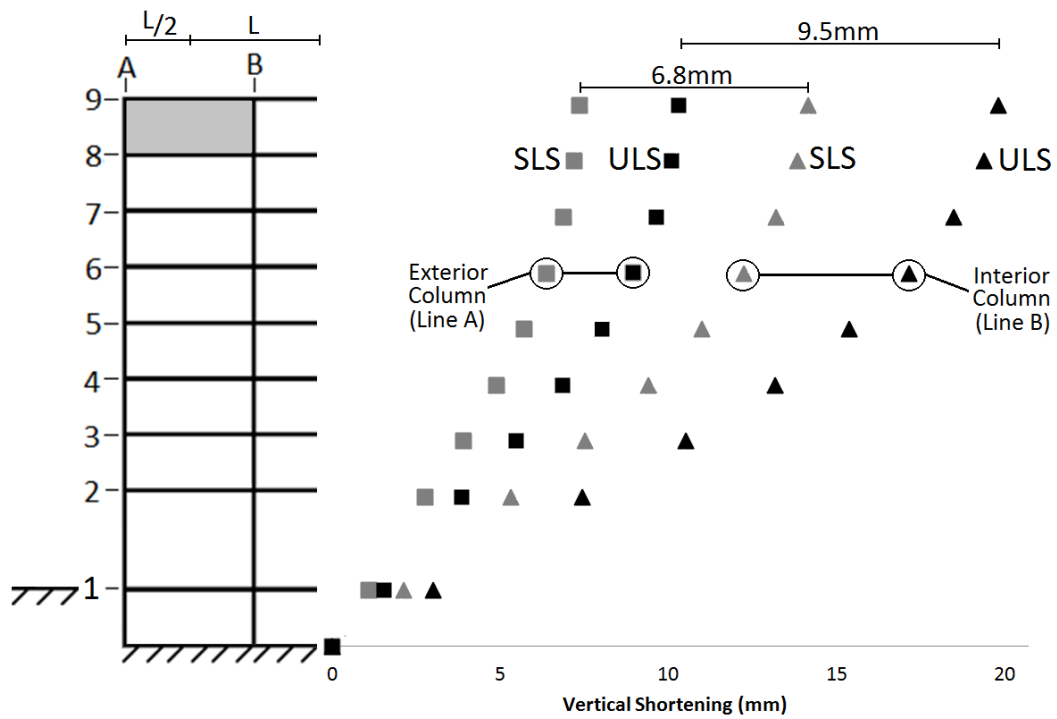


Figure 3-5 - Vertical Creep Deformation of Exterior and Interior Columns at SLS and ULS

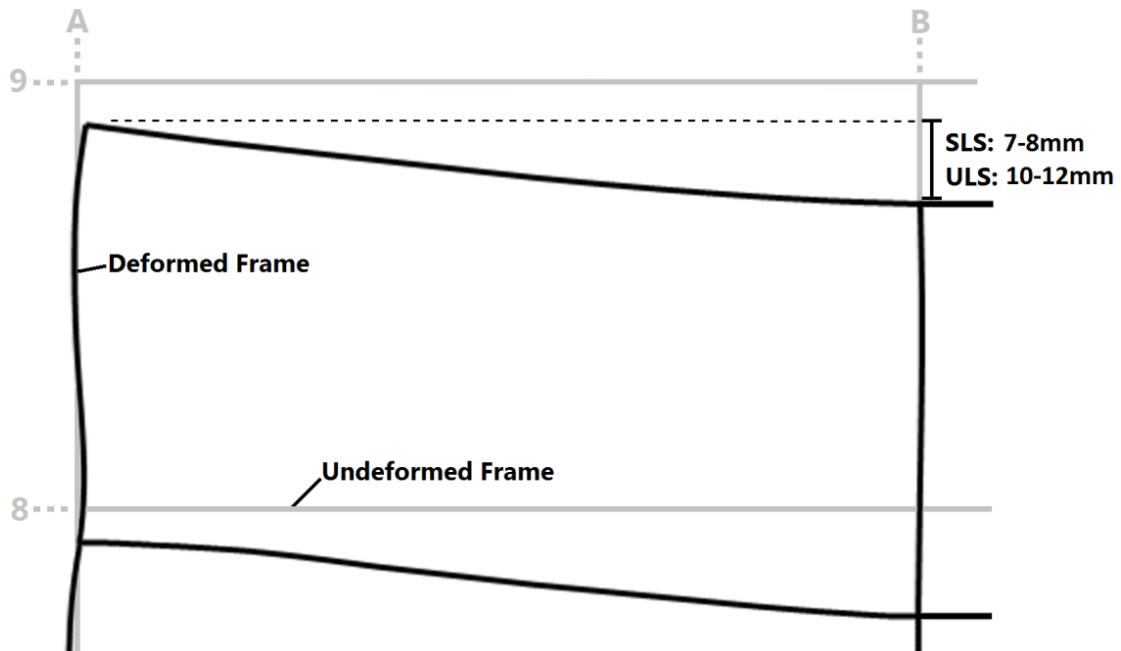


Figure 3-6 - Vertical Creep Deformation Limits for Critical Frame

The deflection of the beam is primarily due to the gravity loads and is increased for sustained loading. A LLRF of 0.78 was used considering the tributary area of an individual beam. All dead and live loads, neglecting snow loads, were assumed present to calculate deflections at SLS due to sustained loads. The long-term deflection after 5 years was computed assuming sustained loads were applied when the concrete was 3 months old. The critical beam is located in an exterior bay where there are no counteracting moments from a beam framing into the other side of the column joint to minimize the rotation, as there would be for an interior column. This causes a larger deflection at mid-span of the beam, which, as shown in Figure 3-7, is 1.1mm due to the immediate loading, plus the additional 1.1mm due to the sustained loading effect. Further of the deflection calculations are presented in Appendix D. Using CSA A23.3-04 (2010a) deflection limits for "roof or floor construction supporting or attached to non-structural elements likely to

be damaged by large deflections", the deflection limit is $\ell_n/480$, or 12.5mm. This value is much greater than the 2.2mm deflection computed from the "sum of the long-term deflection due to all sustained loads and the immediate deflections due to any additional live load" (CSA, 2010a).

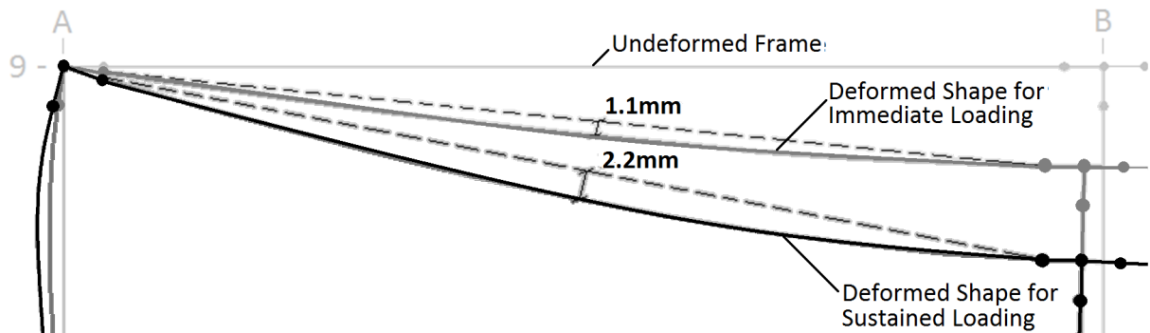


Figure 3-7 - Mid-span Deflection of Critical Beam

Table 3-1 summarizes the SLS and ULS deflection limits for Case A (interstorey sway) and Case B (differential creep) that the test apparatus must accommodate. The beam deflection was deemed not critical as beam deformations with similar magnitudes will occur during the lateral sway and vertical racking deformation.

Table 3-1 - Final Deflection Limits of the Prototype Structure at SLS and ULS

Deflection Case	Limit State	Principal Loading	Prototype Results	Critical Range
(A) Sway Column Deflection, Δ_L , at Second Floor, Exterior Bay	SLS	$D+0.5L+0.75W$	0.7 mm	6-7mm
	ULS	$1.25D+0.5L+1.4W$	1.8 mm	16-18mm
(B) Differential Column Shortening, Δ_{vc} , at Top Floor, Exterior Bay	SLS	1.0D w/ creep	6.8 mm	7-8mm
	ULS	1.4D w/ creep	9.5 mm	10-12mm

3.3 TEST APPARATUS

3.3.1 OBJECTIVE AND CONSTRAINTS

The test apparatus must accommodate the following in-plane tests:

- Lateral Sway Push Test, creating Case (A) deflections shown in Table 3-1;
- Lateral Sway Pull Test, creating Case (A) deflections; and
- Vertical Racking Test creating Case (B) deflections.

The loads acting on the concrete frame for the Lateral Sway Push Test are shown in Figure 3-8a), where load, P_h , is applied horizontally to the top corner for the frame. Conversely, P_h is applied in the reverse direction during the Lateral Sway Pull Test. The Vertical Racking Test applies similar loads to the concrete frame as the Lateral Sway Push Test, except the load, P_v , is applied vertically at the bottom left column.

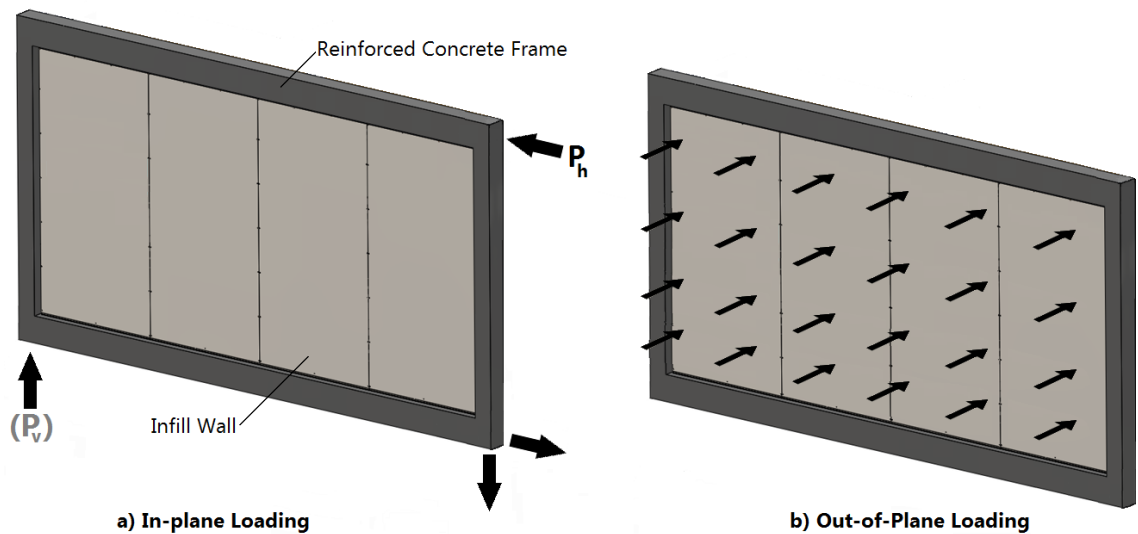


Figure 3-8 - Load Cases Investigated: a) In-plane; b) Out-of-plane

The Out-of-plane Pressure Test applies a uniform pressure, shown in Figure 3-8b), to the wood infill wall while restraining out-of-plane movement of the reinforced concrete frame. The test pressures, shown in Table 3-2, are in accordance with wind loading criteria in the NBCC (2010). The positive pressure case represents the combined effect of positive external and negative internal pressures, and vice-versa. The positive pressure is greater in magnitude because the external pressure coefficients for this case are greater. Details of the pressure calculations are presented in Appendix B-2.

Table 3-2 - Positive and Negative Test Pressures

Limit State	Positive Pressures (kPa)			Negative Pressures (kPa)		
	External	Internal	Total	External	Internal	Total
Serviceability	1.04	-0.4	1.44	-0.64	0.26	-0.9
Ultimate	1.94	-0.74	2.68	-1.19	0.49	-1.68

The test apparatus must also meet the following objectives:

- The aspect ratio of the test frame, length to height, must be approximately the same as in the prototype structure, i.e., 2.0
- The vertical clearance between the concrete beams must accommodate an infill wall of height 95 5/8" (2429mm), which accounts for pre-cut studs and single top and bottom plates.
- The horizontal clearance between the concrete columns must accommodate an infill wall of length 16ft (4877mm).

- The ratio of the column to beam moments of inertia of the test apparatus must be approximately the same as that in the prototype structure (i.e., 0.33 based on the cross section properties).
- The floor connections must provide boundary conditions that replicate the deformed shape of a single storey within the prototype structure.

The test apparatus must also meet the following constraints:

- The anchor plates in the existing strong floor are spaced at 2439mm (8') o/c in the direction of the axis of the frame and 1219mm (4') o/c normal to the frame axis.
- The maximum applied load should not exceed the capacity of the load cell, 46kN, and must not exceed the capacity of the actuator, 90 kN.
- The weight of any unit must not exceed the capacity of the existing overhead crane, 17.8kN (2 tons).

3.3.2 FINAL DESIGN

The final design of the test apparatus, shown in Figure 3-9, has been constructed at the Insurance Research Lab for Better Homes (IRLBH). The steel frame acts as a reaction frame for all in-plane tests with two connection points at the joints of the reinforced concrete frame. A removable base at the bottom left corner facilitates the Vertical Racking Tests and an Out-of-Plane Pressure Loading System is attached on the 'exterior' side of the apparatus for out-of-plane pressure testing.

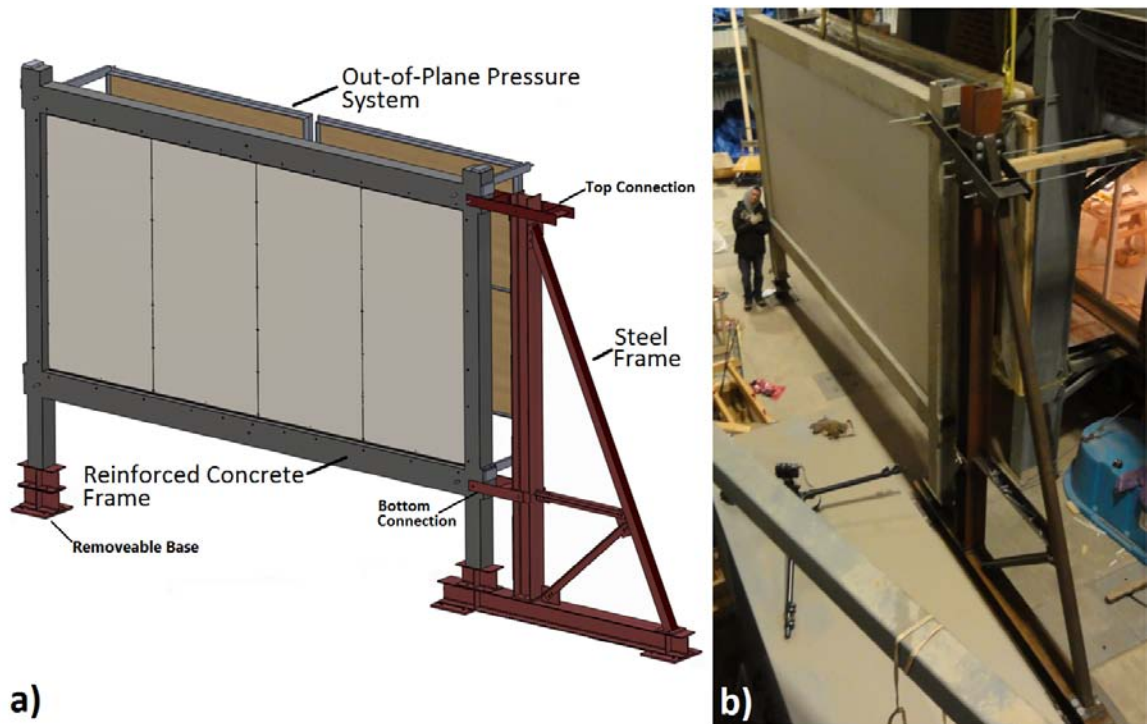


Figure 3-9 - Final Test Apparatus: a) As Designed; b) As Constructed at IRLBH

Figure 3-10 shows that the interior dimensions of the concrete frame must accommodate a 8' x 16' (2438mm x 4877mm) light-frame wood wall, leading to an aspect ratio of 1.9 for the concrete frame. The desired deformed shapes can be achieved using relatively slender concrete beams and columns that reduce the necessary applied loads. The depth of the columns and beams, 175mm and 250mm respectively, was selected to achieve the desired stiffness ratio. The width of the concrete frame, 184mm (7 1/4"), was selected to satisfy the weight constraints and allow the use of nominal 2x8 (38mm x 184mm) lumber as the formwork. The concrete columns extend past the bottom concrete beam to permit rotation at the joints, similar to the prototype structure. The width of the Out-of-plane Loading System accommodates the existing strong floor anchor plate locations. Also, the instrumentation grid system is shown that will be referred to throughout this study.

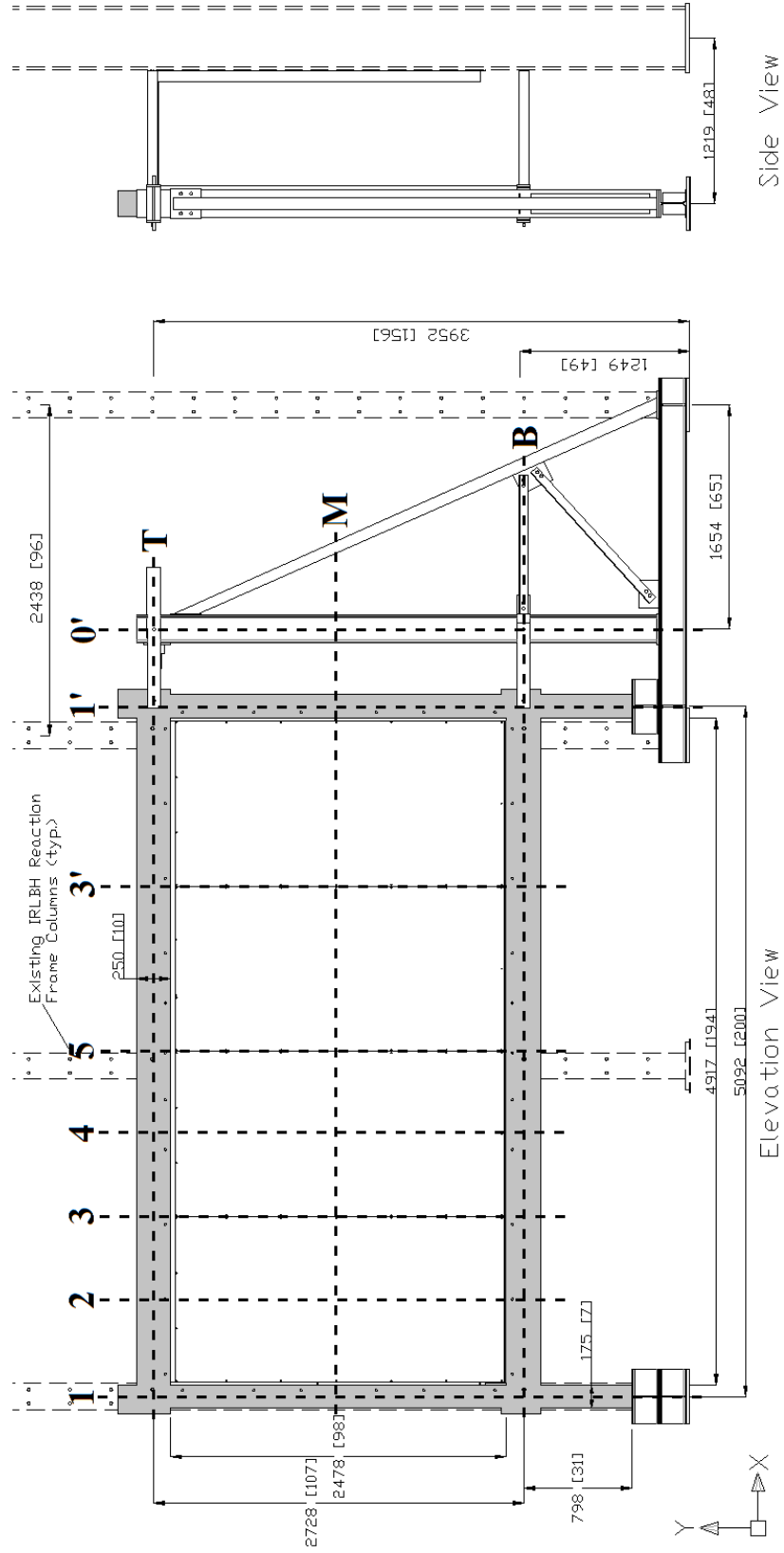


Figure 3-10 - General Layout of Test Apparatus with Instrumental Grid System

Figure 3-11 is an elevation of the reinforced concrete and steel frames as idealized using SAP2000 (SAP, 2009), where the steel has an elastic modulus of 200000 MPa and a yield strength of 350 MPa and the concrete has an elastic modulus of 26600 MPa and a compressive strength of 35 MPa. The analytical results for the model were independently validated by a first-order sway analysis using the displacement method (e.g. Hibbler, 2006). The stiffness modifiers, I_e/I_g , shown account for the stiffness loss due to cracking of the concrete (MacGregor and Bartlett, 2000). The calculations are described in further detail in Appendix E.

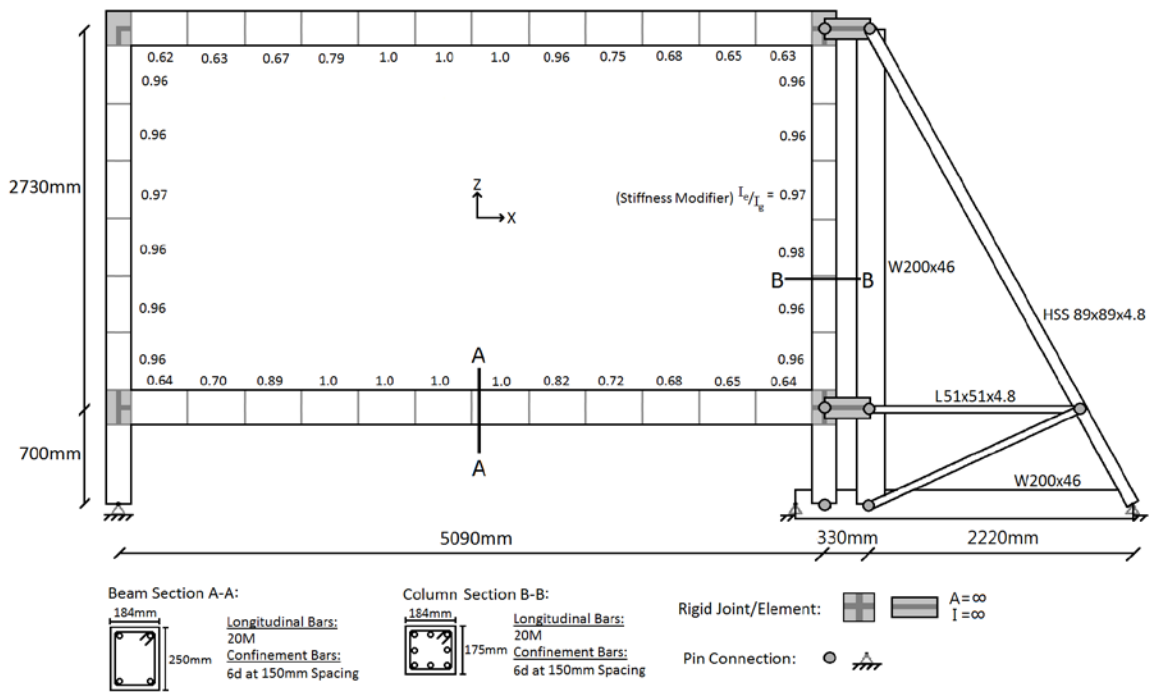


Figure 3-11 - Test Apparatus Details for SAP Model

The reinforced concrete frame was designed using CSA A23.3-04 (CSA, 2010a) and the steel frame using CSA-S16-09 (CSA, 2010b). The force effects due to the applied loads were based on results from a SAP2000 model using a load factor of 1.5. Detailed engineering drawings for both frames are shown in Appendix F and limits used for design are presented in Appendix G. To minimize costs, only the following three steel shapes were used for the steel frame: W200x46, HSS 89x89x4.8 and L51x51x4.8. All components were connected using pretensioned ASTM A325 3/4" (19mm) diameter bolts. Table 3-3A and Table 3-3B shows the prototype and test apparatus deflections under a lateral loading sway case at SLS and ULS, respectively, where the deflected shape and points of interest are identified in Figure 3-12 and the horizontal displacement at Δ_{T1} is used as the control displacement. The difference between the prototype structure and test apparatus is also shown, where the values without brackets show that the predicted deflection overestimates the observed response and the values with brackets show that the predicted deflection underestimates the observed response. A difference of over 0.5mm, highlighted in **bold**, has been used to identify points that have not been accurately predicted. These results shows that the overall deflected shapes are similar, however the test apparatus does not include the vertical component due to the self-weight of the structure and live loads seen in the prototype structure. This is shown as an increased difference between the vertical displacements on the left side of the frame (i.e., Δ_{T1y} and Δ_{B1x}) to the right side of the frame (i.e., $\Delta_{T1'y}$ and $\Delta_{B1'y}$). Despite this, the test apparatus predicts the prototype structure to be within 2.4mm at SLS and 3.3mm at ULS, which has been deemed to be sufficient.

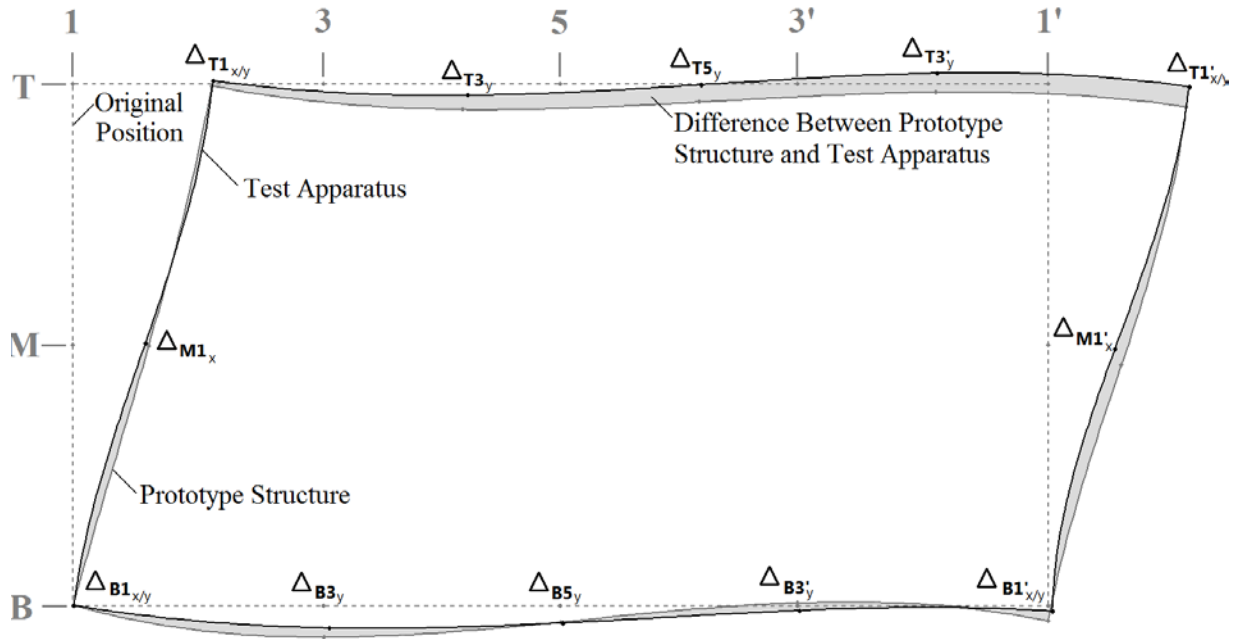


Figure 3-12 - Prototype Deflections vs. Test Apparatus Deflections for Lateral Racking

Table 3-3A - Deflection of Concrete Frame under Lateral Sway Loading at SLS

Deflection (mm)	Top Beam							Middle of Columns		Bottom Beam						
	Δ_{T1x}	Δ_{T1y}	Δ_{T3y}	Δ_{T5y}	$\Delta_{T3'y}$	$\Delta_{T1'y}$	$\Delta_{T1'x}$	Δ_{M1x}	$\Delta_{M1'x}$	Δ_{B1x}	Δ_{B1y}	Δ_{B3y}	Δ_{B5y}	$\Delta_{B3'y}$	$\Delta_{B1'y}$	$\Delta_{B1'x}$
Prototype Structure	6.5	-0.4	-1.8	-1.9	-1.8	-2.6	6.5	3.7	3.4	0.0	0.0	-2.0	-1.6	-0.8	-1.6	0.0
Test Apparatus	6.5	0.0	-1.5	-1.2	-0.3	-0.2	6.5	2.8	3.4	0.0	0.0	-0.4	-0.1	0.4	-0.2	0.0
Difference	-	(0.4)	(0.3)	(0.7)	(1.5)	(2.4)	-	(0.9)	-	-	-	(1.6)	(1.5)	(1.2)	(1.4)	-

Table 3-3B - Deflection of Concrete Frame under Lateral Sway Loading at ULS

Deflection (mm)	Top Beam							Middle of Columns		Bottom Beam						
	Δ_{T1x}	Δ_{T1y}	Δ_{T3y}	Δ_{T5y}	$\Delta_{T3'y}$	$\Delta_{T1'y}$	$\Delta_{T1'x}$	Δ_{M1x}	$\Delta_{M1'x}$	Δ_{B1x}	Δ_{B1y}	Δ_{B3y}	Δ_{B5y}	$\Delta_{B3'y}$	$\Delta_{B1'y}$	$\Delta_{B1'x}$
Prototype Structure	17.0	-0.3	-3.2	-1.9	-0.5	-2.9	17.0	9.4	9.0	0.0	0.0	-4.2	-1.9	0.8	-1.9	0.0
Test Apparatus	17.0	0.0	-2.7	-1.5	0.4	-0.5	17.0	7.7	8.7	-0.2	-0.5	-0.9	0.0	0.9	-0.5	-0.2
Difference	-	(0.3)	(0.5)	(0.4)	0.9	(2.4)	-	(1.7)	(0.3)	(0.2)	(0.5)	(3.3)	(1.9)	-	(1.4)	(0.2)

Note: **bold** values represent noteworthy results and values in brackets represent test apparatus deflections that are lower than those predicted in the prototype structure

Similarly, Table 3-4A and Table 3-4B show prototype and test apparatus deflections under a vertical racking loading case at SLS and ULS, where the deflected shape, and points of interest, are identified in Figure 3-13 and the vertical displacement at Δ_{B1} is used as the control displacement. The overall deflected shapes are similar, however there is less rotation occurring at the top left corner, T1, of the test apparatus which is the main cause for the differences identified. The deflections in the prototype structure, however, are likely due to moments occurring at B1 and T1' which are not included in the deformations of the test apparatus. Overall, the test apparatus predicts the prototype structure to be within 1.9mm at SLS and 1.5mm at ULS, which is deemed to be adequate.

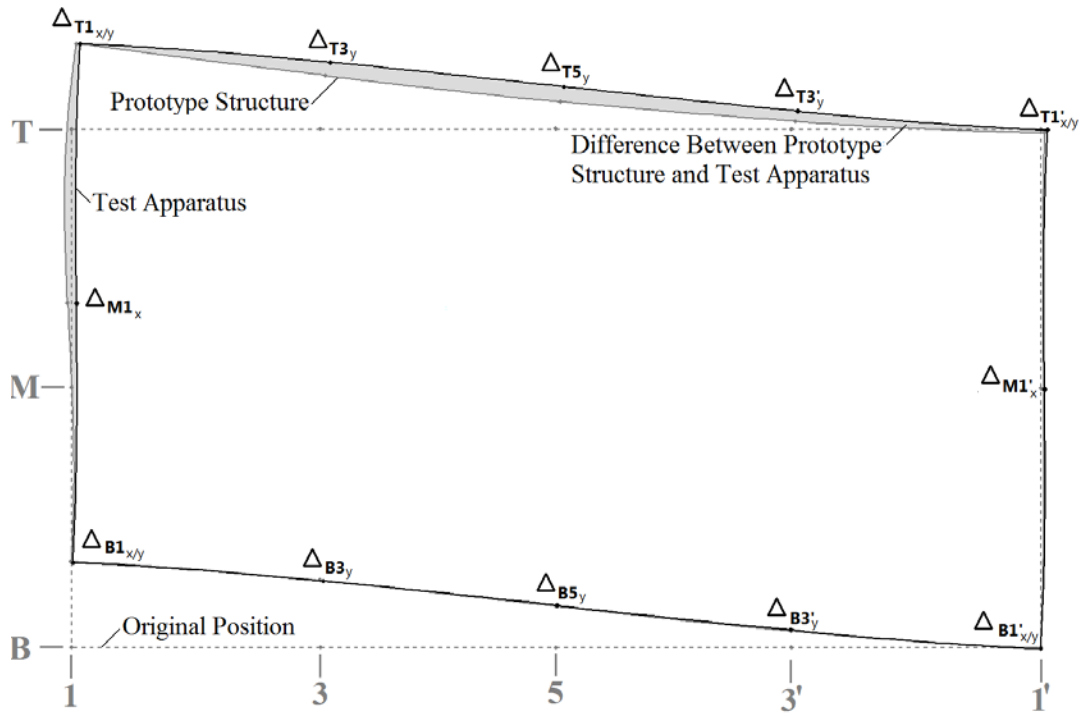


Figure 3-13 - Prototype Deflections vs. Test Apparatus Deflections for Vertical Racking

Table 3-4A - Deflection of Concrete Frame under Vertical Racking at SLS

Deflection (mm)	Top Beam							Middle of Columns		Bottom Beam						
	Δ_{T1x}	Δ_{T1y}	Δ_{T3y}	Δ_{T5y}	$\Delta_{T3'y}$	$\Delta_{T1'y}$	$\Delta_{T1'x}$	Δ_{M1x}	$\Delta_{M1'x}$	Δ_{B1x}	Δ_{B1y}	Δ_{B3y}	Δ_{B5y}	$\Delta_{B3'y}$	$\Delta_{B1'y}$	$\Delta_{B1'x}$
Prototype Structure	0.5	7.2	4.1	1.9	0.4	-0.5	0.3	-0.7	-0.2	0.0	7.5	6.3	3.8	1.4	0.0	0.0
Test Apparatus	0.7	7.5	5.8	3.8	1.7	0.1	0.7	-0.4	-0.4	0.0	7.5	5.8	3.8	1.7	0.1	0.0
Difference	0.2	0.3	1.7	1.9	1.3	0.6	0.4	(0.3)	0.2	-	-	(0.5)	-	0.3)	-	-

Table 3-4B - Deflection of Concrete Frame under Vertical Racking at ULS

Deflection (mm)	Top Beam							Middle of Columns		Bottom Beam						
	Δ_{T1x}	Δ_{T1y}	Δ_{T3y}	Δ_{T5y}	$\Delta_{T3'y}$	$\Delta_{T1'y}$	$\Delta_{T1'x}$	Δ_{M1x}	$\Delta_{M1'x}$	Δ_{B1x}	Δ_{B1y}	Δ_{B3y}	Δ_{B5y}	$\Delta_{B3'y}$	$\Delta_{B1'y}$	$\Delta_{B1'x}$
Prototype Structure	0.7	10.8	6.7	3.4	0.9	-0.5	0.5	0.4	0.3	0.0	11.0	8.6	5.3	2.1	0.0	0.0
Test Apparatus	0.7	11.0	8.2	4.9	1.9	0.0	0.7	0.2	0.5	0.0	11.0	7.7	4.2	1.5	0.0	0.0
Difference	-	0.2	1.5	1.5	1.0	(0.5)	(0.2)	(0.2)	0.2	-	-	(0.9)	(0.9)	(0.6)	-	-

Note: **bold** values represent noteworthy results and values in brackets represent test apparatus deflections that are lower than those predicted in the prototype structure

Uniform positive (or negative) out-of-plane pressures are applied to the ‘exterior’ side of the wall by a sealed pressurized air bag shown in Figure 3-14. Six out-of-plane reaction points, three along the top concrete beam and three along the bottom beam, restrain out-of-plane movement of the reinforced concrete frame during testing. Pressure Load Actuators (PLAs), attached to the back panel, generate positive and negative pressure inside the airbag using control protocols and calibrations previously developed (e.g. Nagy, 2008; Kopp, 2006).

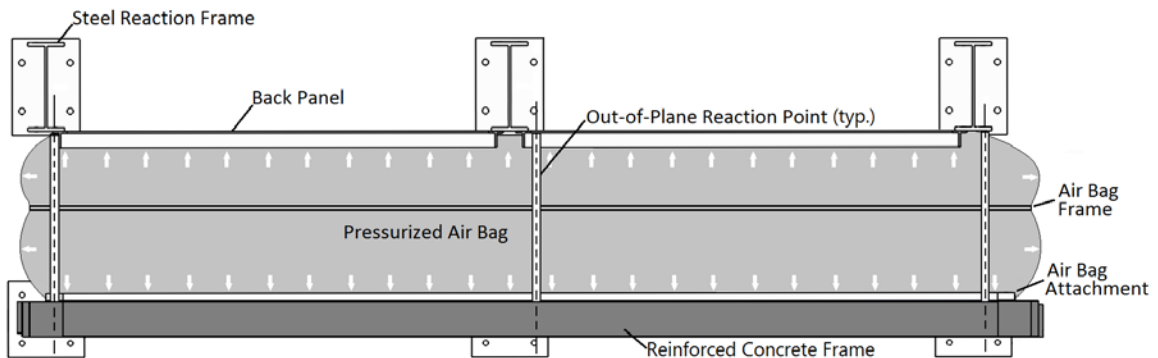


Figure 3-14 - Out-of-Plane Pressure Loading System

3.3.3 DESIGN AND CONSTRUCTION CHALLENGES

Figure 3-15 shows that the as-built dimensions are within typical construction tolerances of 12 to 19mm (1/2 to 3/4in) (CSA, 2010a). The out-of-plumbness of the columns required minor revisions to the connections to the steel frame, however the as-built tolerances were readily accommodated.

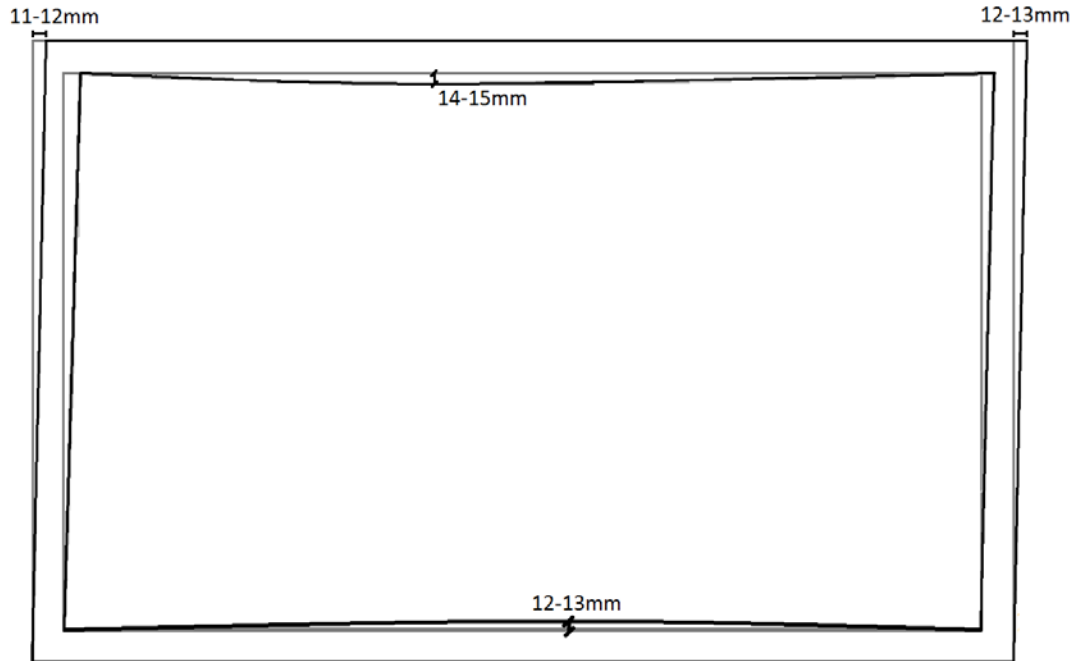


Figure 3-15 - As-built Variation from Designed Concrete Frame Dimensions

The development length required for the longitudinal reinforcement, as specified by CSA A23.3-04 (CSA, 2010a), and the geometric constraints at the corners of the frame posed a detailing challenge. Hooks are necessary to develop these bars, where the applied moments are greatest. However, hooking all the bars would have been impossible due to congestion within the corner joint. Thus, steel anchorage plates, shown in Figure 3-16, were welded to the ends bars in the outer faces of the columns. The plates bear against the concrete surface to prevent slippage of the reinforcement. The top of the column was also extended above the top of the beam to further ease congestion. Despite these modifications, the hook of the middle column bar, identified by the asterisk in Figure 3-16, needed to be cut to eliminate a geometric conflict.

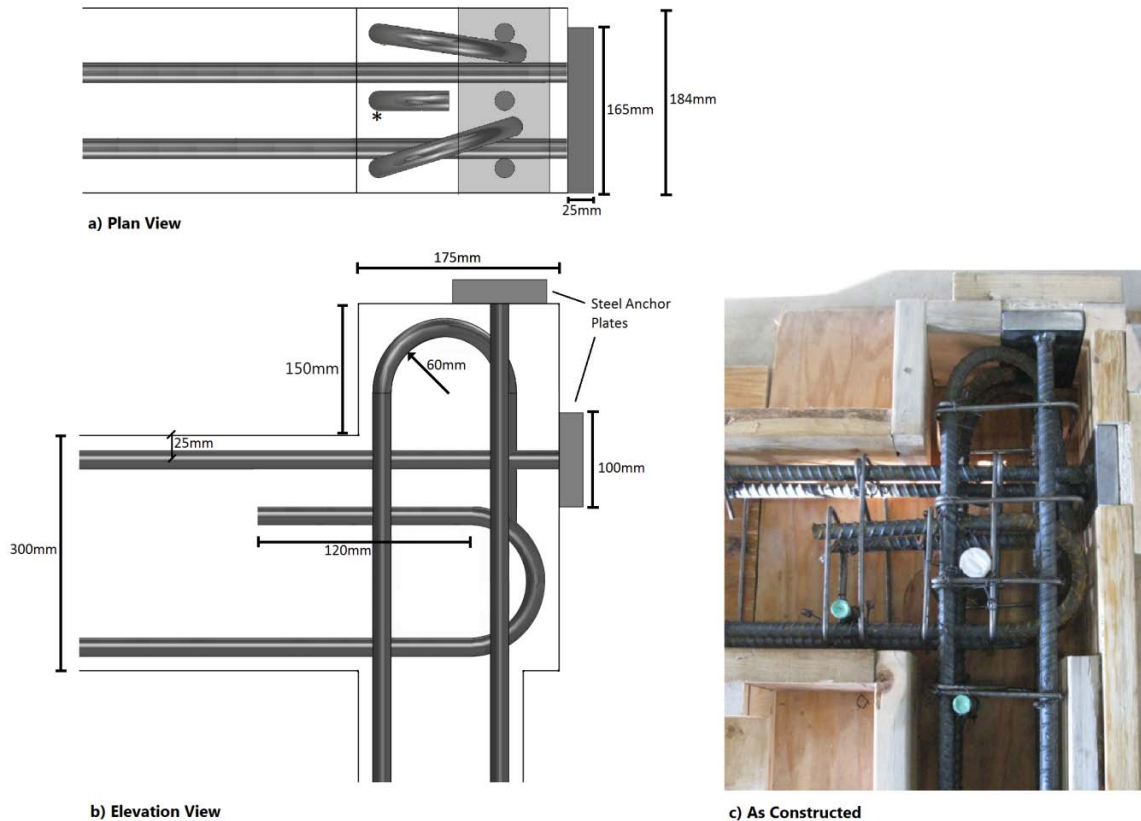


Figure 3-16 – Corner Reinforcement Detailing: a) Top View; b) Front View; c) As Constructed

Figure 3-17 shows the connection details at the bases of the concrete frame columns. The top W-shape enables full access to its bolted connection to the bottom W-shape. Longitudinal reinforcing bars, developed to yield at the base plate (CSA, 2010a), are welded to the top steel W-shape for effective load transfer from the concrete frame to the W-shape. For the vertical racking test, the bottom W-shape is replaced by a hydraulic jack and load cell, as shown in Figure 3-17c. The concrete frame requires bracing to ensure its out-of-plane stability. The steel W-shapes at the foot of each column, shown in Figure 3-17, are susceptible to bending at the web-top flange joint, which is unstiffened.

The load is applied at the top connection using a hydraulic jack, shown in Figure 3-18, located on one side of the W200 column for the Lateral Sway Push Test and on the other side for the Lateral Sway Pull Test. The bottom connection uses either a tension connection or wood blocking to ensure minimal movement when subjected to tension or compression, respectively, at this location.

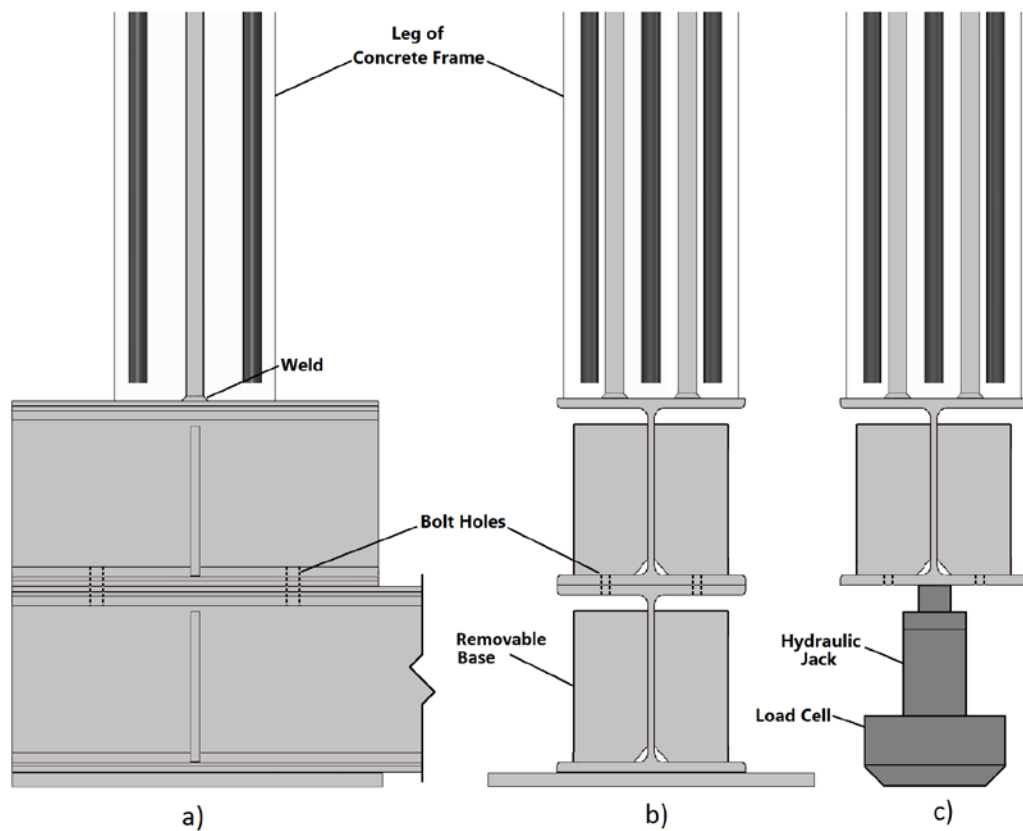


Figure 3-17 - Connection Detailing at Base of Concrete Frame: a) Front View; b) Side View During Lateral Sway Test; c) Side View During Vertical Racking Test

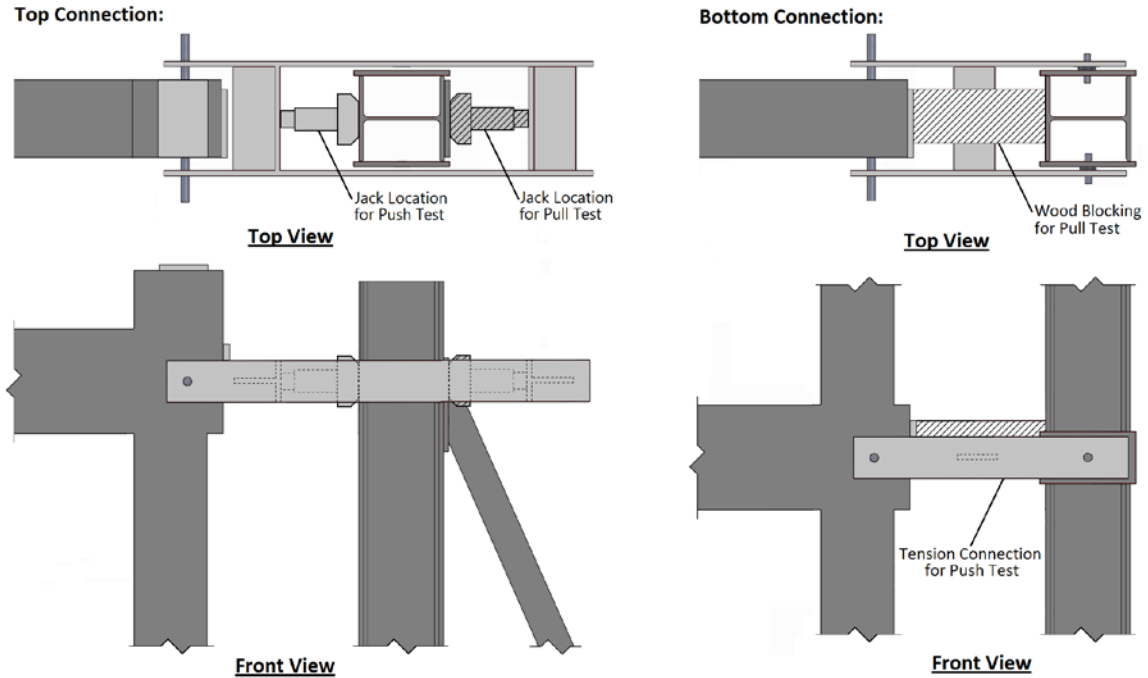


Figure 3-18 - Concrete Frame to Steel Frame Connection and Jack Locations

Figure 3-19 shows the air bag attached to the concrete frame before installation of the infill wall. The back panel, with round sleeves for the PLA hoses, is similar to that from past tests at IRLBH. White expansion foam sprayed on areas of potential air leakage is clearly visible. Threaded rods through metal sleeves in the reinforced concrete frame attach the air bag to the frame. The edges of the bag are connected to a continuous wood frame and the gap between the bag and the concrete surface is filled with expansion foam, ensuring a seal around the threaded rod but facilitating bag removal as necessary. An aluminum tubular frame was inserted in the middle of the air bag to reduce the deformations and stresses. The large volume of the bag (approximately 9.25 m^3) required the frame to be stiffened by additional internal wood bracing.



Figure 3-19 - As-built Concrete Frame with Airbag and Back Panel

3.4 WOOD INFILL WALL SPECIMEN

3.4.1 CRITERIA

The criteria used to determine the type of infill wall and connection that would be tested are: degree of inset, gap details and level of prefabrication.

Typical exterior wall systems, shown in Figure 3-20, involve various degrees of inset of the infill wall into the reinforced concrete frame. A fully inset infill wall is used in the present study for the following reasons:

- the concrete floor extension to the exterior wall face provides the most effective fire break between floors;

- the concrete floor extension is also the most effective in preventing water from contacting the wall top plate, enhancing the durability of the wood infill wall (Eriksson, 2005), and;
- the concrete floor extension also minimizes gaps at the connection points, reducing the moisture exposure (Eriksson, 2005).

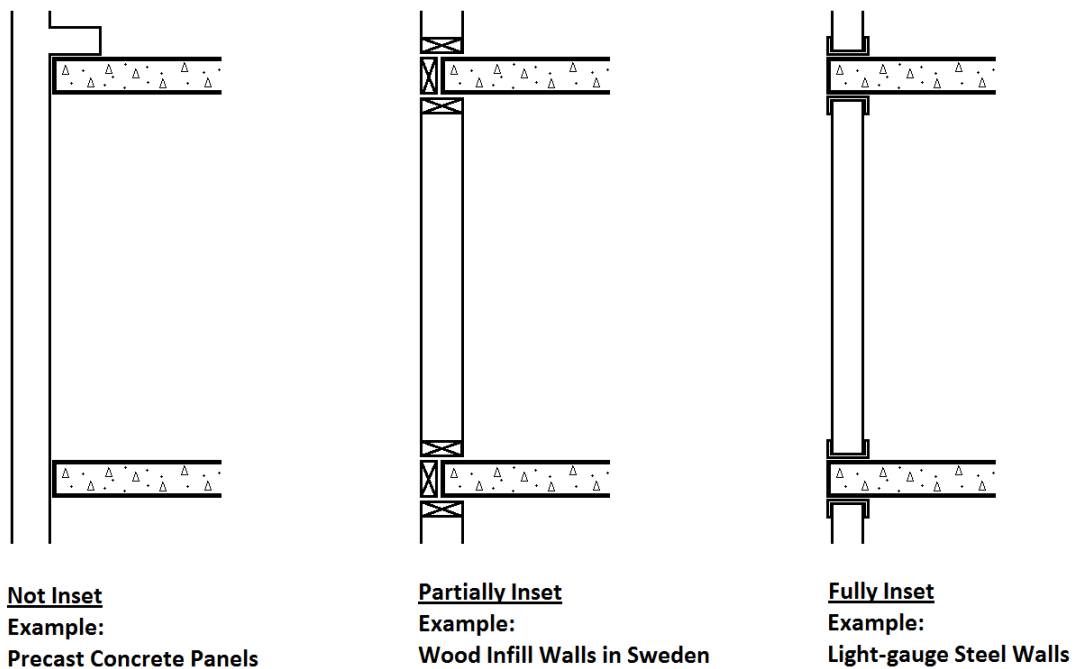


Figure 3-20 - Degrees of Inset of an Infill Wall: a) Not Inset; b) Partially Inset; c) Fully Inset

In general, exterior infill walls can be:

- fully assembled in-place;
- partially pre-fabricated with no exterior or interior sheathing, as 'open panels';
- partially pre-fabricated with only exterior sheathing, as 'closed panels', or;
- fully pre-fabricated, with both exterior and interior sheathing.

A fully pre-fabricated wall was selected for the present study because it is likely to exhibit the highest quality of construction. The fully enclosed wall panel is constructed in a controlled factory setting either on- or off-site (Eriksson, 2005). Typically all components of the wall panel are installed beforehand, including electrical conduits, windows and balcony doors. This option promises reliable quality control during wall pre-fabrication while minimizing on-site installation time, especially if the installation can be done from the interior of the building. However, maintaining low moisture levels in the wall during transportation and accommodating on-site concrete construction tolerances need to be considered.

A gap around the perimeter of the wall is required to account for movement of the reinforced concrete frame, as previously described in Table 3-1, to ensure that the infill wall remains non-loadbearing. The standard practice for existing wood infill walls is to allow a gap of 16 to 19mm (5/8" to 3/4") (Eriksson, 2005), although on-site geometric tolerances may be substantially less or substantially greater than these values. Other types of exterior cladding and wall systems, such as light-gauge steel framing and precast concrete panels, require a tolerance of +/- 1.5 in. (+/- 38.1mm) (e.g. CSSBI, 1991). Fortunately, significant expansion and contraction of wood only occurs normal to the

grain, with only minor dimensional changes parallel to the grain (Keenan, 1986). Therefore only the top and bottom plates of the infill walls contribute to gap change due to moisture changes, which are therefore small.

3.4.2 CONNECTION DESIGN CONCEPT

Different types of connections at various locations can accommodate the in-plane deflections of the frame surrounding the infill wall. The three cases shown in Figure 3-21 were investigated to find an appropriate type and location of connections for ULS horizontal deflection summarized in Table 3-1. All connections have adequate out-of-plane capacities (i.e., in the Y-direction) but allow rotation of the wall edges due to out-of-plane loading. Layout A requires the top connections to accommodate the positive and negative lateral (X-direction) displacements of the concrete frame but evenly distributes the out-of-plane loading between the four connections. Layout B requires the connections to accommodate less overall movement in the X-direction but increases the out-of-plane reaction at the top and bottom connections. Layout C, adopted in the present study, allows unrestricted movement of the top of the infill wall in the X-direction and evenly distributes the out-of-plane load to the top and bottom connections. This layout only requires the connections to restrict movement in the X-direction at the bottom of the wall while ensuring full out-of-plane support from the top and the bottom.

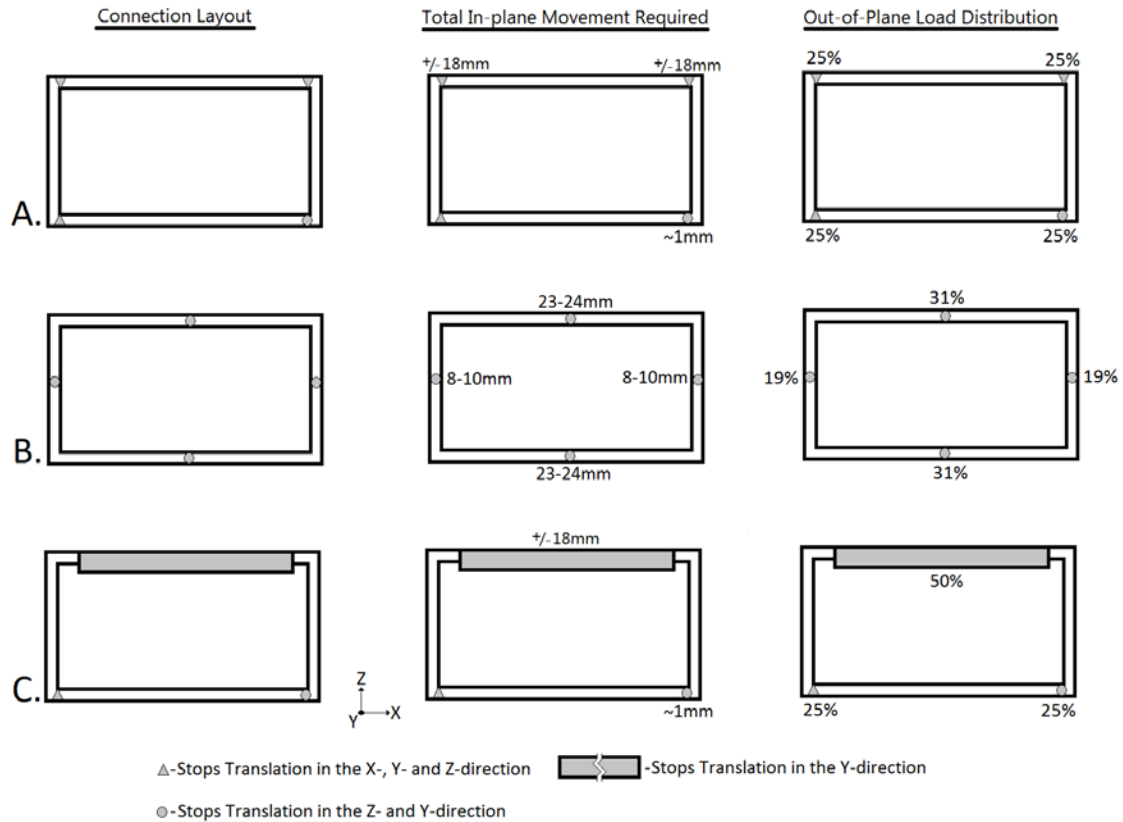


Figure 3-21 - Type and Location of Connections for Infill Wall System

A top connection capable of accommodating in-plane movement has been successfully used for partially pre-fabricated wood infill walls (BAPL, 2002) and light-gauge steel wall in the United States and Canada (CSSBI, 1991) as shown in Figure 3-22(a) and (b), respectively. Both connections use a light-gauge steel 'C'-channel, with its web oriented horizontally, attached to the concrete frame. This detail limits longitudinal and axial load transfer, while the flanges have sufficient flexural rigidity to transfer the out-of-plane wind loads. The top connection used for the present study is a wider 'C'-channel 1mm thick steel that accommodates the full width of the sheathed wall between the vertical flanges as shown in Figure 3-22(c). The two 2438mm (8 ft.) long channels are 5mm wider than the infill wall, to facilitate installation, and each flange is 35mm deep. The gap

between the top of the infill wall and the bottom of the concrete frame must exceed 5mm, to allow the frame to deflect, and be no more than 20mm, to ensure at least 15mm of bearing for the out-of-plane load transfer.

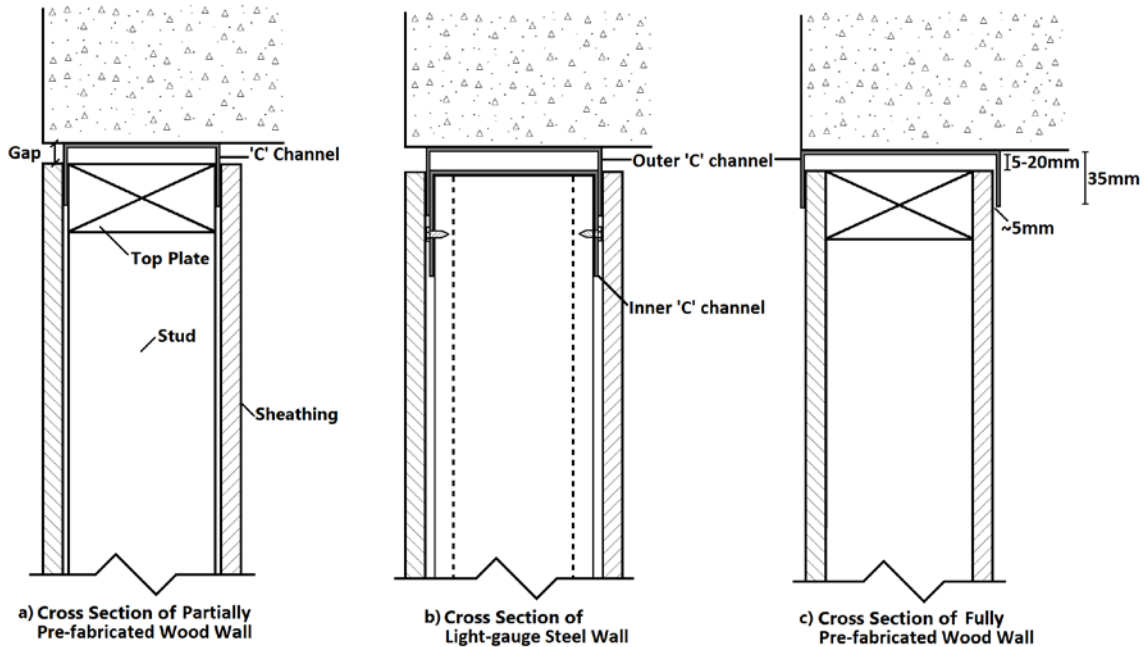


Figure 3-22 - Cross Sections of Top Connections: (a) Partially Prefabricated Wood Wall; (b) Light-gauge Steel Wall; (c) Fully Prefabricated Wood Wall.

The bottom connection required further detailing as it must also restrain the in-plane (X-direction) movement. Existing techniques used to connect partially pre-fabricated infill wall panels to concrete frames include expansion bolts, steel angles, concrete anchors and dowel pins (Eriksson, 2005; Wang, 2008; NSPRC, 2004). These connections accommodate any vertical deflection of the structure while maintaining out-of-plane load

transfer but typically require full access to the wall interior for installation. A fully pre-fabricated wall has sheathing installed on both sides making these connections unfeasible.

The connection shown in Figure 3-23(a) was therefore created with a strip of 1mm thick sheet metal beneath the sheathing, that is attached to the bottom plate using structural wood screws and to the concrete frame using standard concrete screws. Wood shims are placed below the wall to accommodate the required gap, at least 5mm, and to transfer the self-weight of the wall to the concrete through simple bearing. This option was selected because it uses readily available materials, can be installed simply from the interior side of the wall and can accommodate any number of connections. There is, however, potential for the sheet metal strip to deform as shown due to positive and negative wind pressures if the wood screw is installed horizontally. The eccentricity, e , between the bottom connection and the point of maximum horizontal deflection, Δ_H , is shown in Figure 3-23(b) and (c) assuming the concrete screw acts as a pin connection. Under positive wind pressure, the wall bottom plate bears against the sheet metal strip, minimizing e_1 , and so Δ_H . Negative pressure increases the eccentricity to the head of the structural wood screw, however, increasing e_2 and so Δ_H .

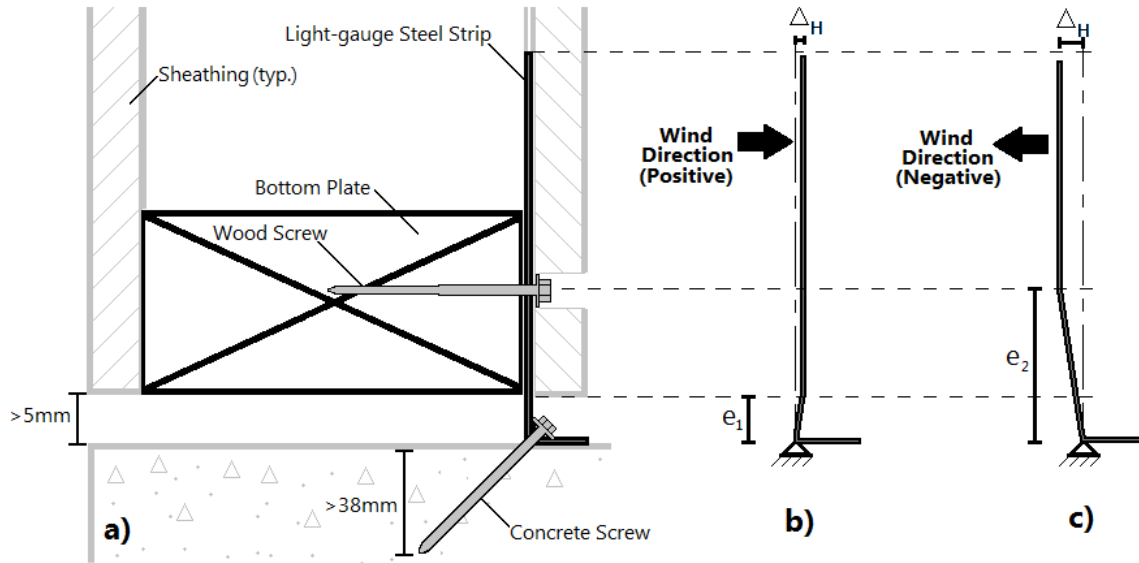


Figure 3-23 - Initial Bottom Connection Design: (a) Cross Section; (b) Deformed Shape for Positive Wind Pressure; (c) Deformed for Negative Wind Pressure.

Hence, an additional piece of light-gauge steel, shown in Figure 3-24, was added to the wood shim to reduce Δ_H . The light-gauge steel 'lip' fits under the light-gauge steel strip and the concrete screw attaches both to the concrete. The structural wood screw is rotated 45 degrees to attach the wood shim to the bottom plate. Under positive wind pressure, the structural wood screw is placed in tension, causing the wood shim to compress against the concrete screw and limit lateral deflection. Under negative pressure, the horizontal component of the compressive forces through the structural wood screw and bottom plate causes horizontal tension in the shim that is then transferred to the concrete by the concrete screw.

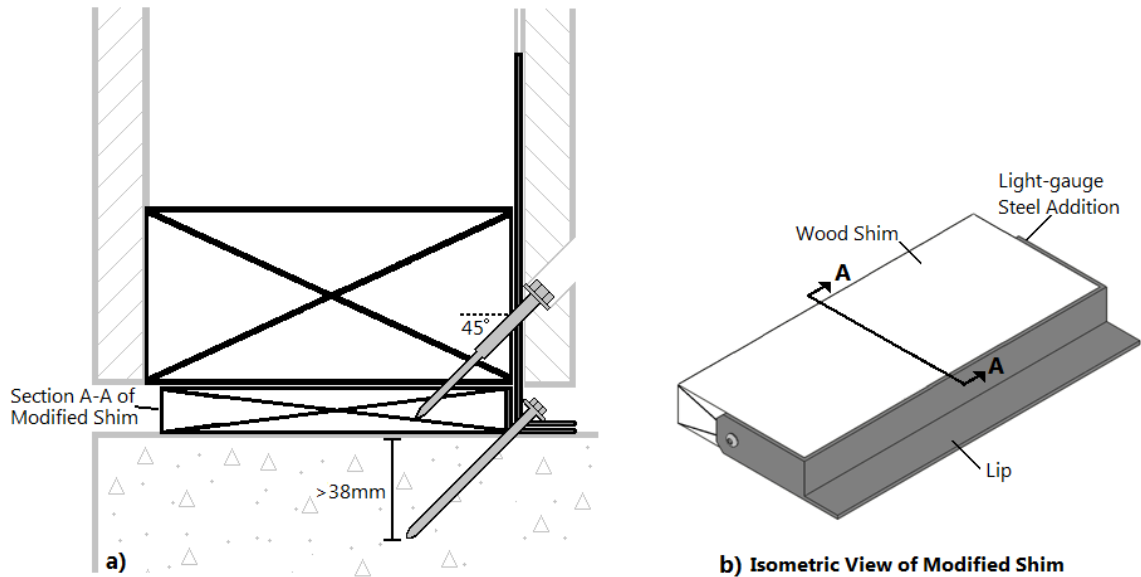


Figure 3-24 - Modified Bottom Connection with Shim: (a) Cross Section; (b) Shim.

The critical component of this connection is the tensile resistance of the concrete screw. The average ultimate capacity, according to the manufacturer, is 9.7 kN per fastener if the embedment length exceeds 38mm (1/2") (CFS, 2012). Assuming a resistance factor of 0.5, the factored resistance is 4.85 kN per fastener, so at least three connections are required to resist the ULS loads shown in Table 3-2.

The final connection design, shown in Figure 3-25, uses four wood shims with concrete screws to accommodate the symmetry of the wall and to cover any uncertainty in the assumed resistance factor. Five additional connections, without shims, are provided as secondary connections. It is anticipated, however, that these will only begin to resist load if large lateral deflections occur at the wood shim connections.

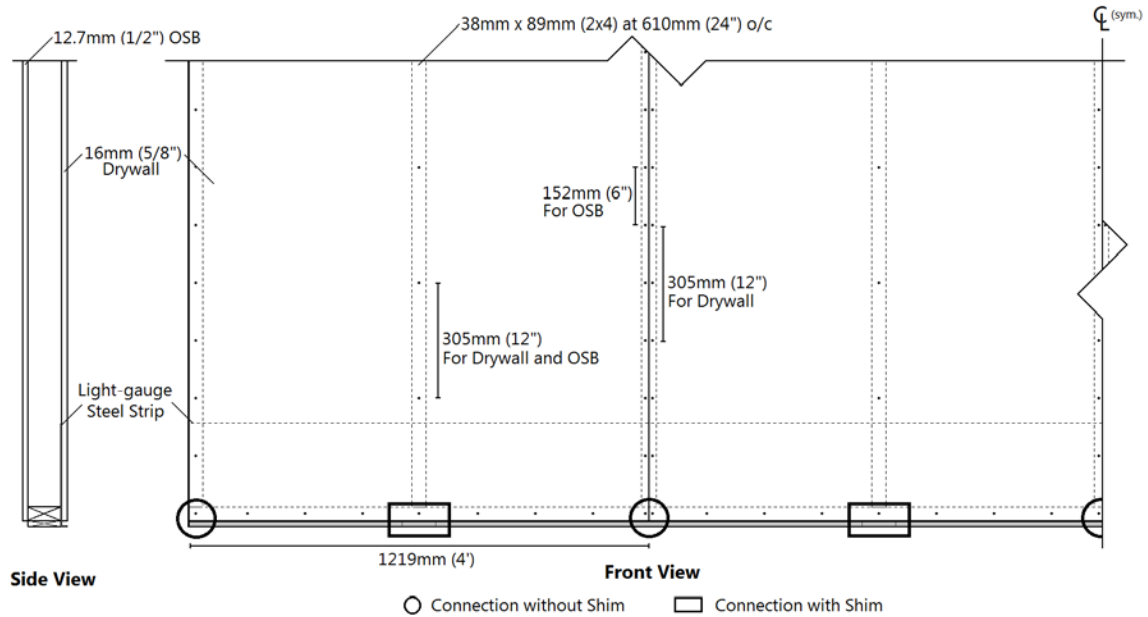


Figure 3-25 - Final Wall Design

The infill wall was designed to satisfy the CSA-O86-09 (CSA, 2010c) provisions for bending members with the following assumptions:

- the self-weight of the wall is the only axial load present and is assumed negligible,
- only the four main connections are in full bearing (i.e., span length of the bottom plate to resist lateral loads is 4ft.),
- sheathing thickness is greater than 3/8" (9.5mm), and
- the connections act as pins (i.e., do not restrain rotation about any axis).

The design uses 38mm x 89mm (2x4) No. 1/2 grade SPF studs spaced at 610mm (24") centers, with 1219mm x 2438mm (4'x8') sheets of 12.7mm (1/2") Oriented Strand Board (OSB) and 16mm (5/8") drywall sheathing placed vertically. The exterior sheathing is

connected to the studs by 6d nails spaced at 152mm (6") around the edge of the panel and 305mm (12") in the centre. The interior sheathing uses standard drywall screws spaced at 305mm (12").

3.4.3 CONSTRUCTION

The infill wall was constructed horizontally on the floor of the IRLBH. The studs were nailed to the top and bottom plates before attaching the drywall sheathing and then the OSB sheathing. A lifting harness was constructed and attached 1219mm (4') from each end of the wall using 15.9mm (5/8") lag screws. Full rotation of the wall was allowed during lifting, leaving it in an almost vertical position once off the ground. This slightly off-center position reduced the total height of the wall enabling it to fit between the bottom concrete beam and the flanges of the previously attached 'C'-channel. Further details of the lifting method are included in Appendix H. Once lifted into position beneath the 'C'-channel, the bottom of the infill wall was then pulled in towards the concrete frame to sit flat on the bottom beam. This allowed the top of the wall to pivot around the exterior flange of the 'C'-channel, rotating the top plate and sheathing between the two flanges. The entire wall was then lifted vertically to allow installation of the wood shims and placed in its final position, as shown in Figure 3-26. The top horizontal gap between the concrete beam and the infill wall is within the previously listed range of 5mm to 20mm, while the bottom horizontal gap meets the requirements of being greater than 5mm. The vertical gaps also meets the suggested range of 16mm to 38mm (5/8" to 1 1/2").

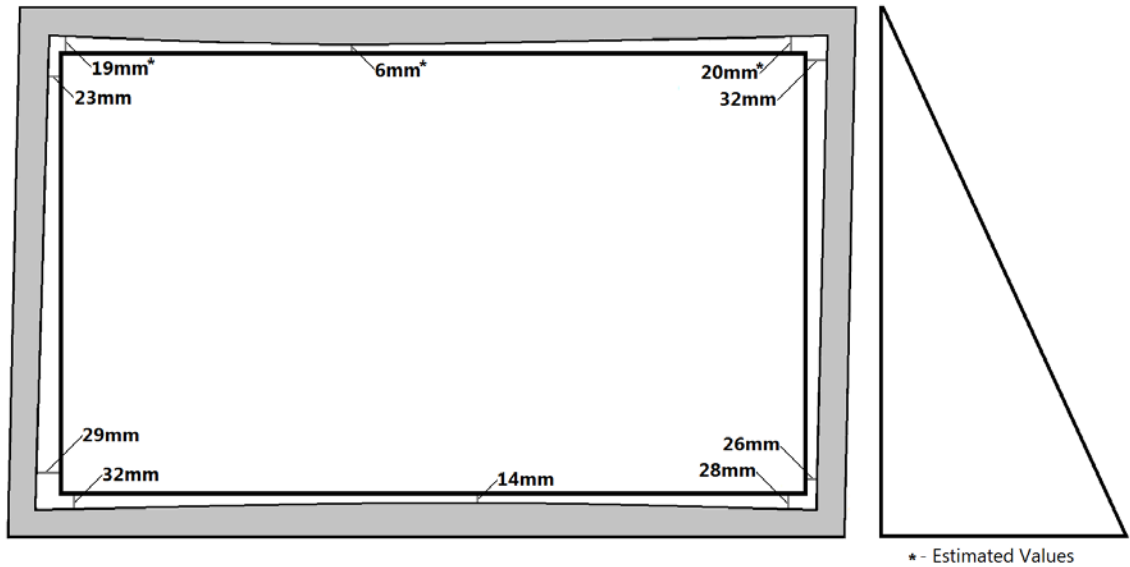


Figure 3-26 - Final Gap Dimensions

The thin strip of sheet metal, shown in Figure 3-23 and Figure 3-24, was slid downwards to bear against the concrete surface. Concrete screws and structural wood screws, as well as additional drywall screws, were then installed. Great Stuff™ insulation expansion foam was sprayed between the edge of the wall and the concrete frame. Blueskin, a non-permeable air barrier, was installed in sheets on the exterior side of the infill wall and concrete frame.

3.4.4 MODELLING

The infill wall was incorporated into the SAP2000 (2009) model for in-plane analysis only. Shell elements were used, with $E = 8900$ MPa and thicknesses of 12.7mm, to create a rigid body which was connected to the bottom concrete frame at the shim location, shown in Figure 3-25, with link elements that had infinite stiffness in compression and a stiffness of 150 N/mm in tension (Grenier, 2012).

3.5 SUMMARY AND CONCLUSIONS

This chapter described the design and construction of a full scale test apparatus and wall specimen used to investigate the chosen wood/concrete hybrid niche: "non-load-bearing light-frame wood infill walls in reinforced concrete frame structures".

A prototype structure taken from the 1984 Concrete Design Handbook was used to determine the critical in-plane boundary conditions placed on the infill wall by the deformed shape of the reinforced concrete frame structure. Two principal in-plane deformations were determined to have the potential to cause damage: lateral sway due to wind loads and vertical racking due to differential column shortening caused by the creep of the concrete. Critical ranges were established for each case at SLS and ULS and used to design the reinforced concrete frame test apparatus. A pressurized air bag system was also incorporated into the test apparatus apply realistic out-of-plane wind loading to the infill wall specimen.

The 8'x16' light-frame wood specimen was designed as a fully prefabricated wall and was inset into the concrete frame structure. A gap between the infill wall and the reinforced concrete frame structure of approximately 5-20mm was chosen to accommodate the in-plane deformations determined by the prototype structure and general concrete construction tolerances. The top connection of the infill wall uses a light-gauge steel 'C'-channel, similar to a light-gauge steel infill wall, which allows for unrestrained in-plane movement, while restraining out-of-plane movement. A novel bottom connection, using a light-gauge steel sheet and wood shims, was designed for use in a full sheathed pre-fabricated walls system.

The main conclusions that are determined from this chapter are:

1. The lateral sway deformation in a reinforced concrete frame structure due to wind loading is greatest at the second storey of an exterior frame, assuming the first storey is designed for a different purpose that would likely avoid the use of a wood infill wall (i.e., commercial use). The critical differential deflection range of the frame loaded at SLS is 6-7mm and at ULS, where wind is the principal load, is 16-18mm.
2. The vertical racking deformation in a reinforced concrete frame structure due to the differential shortening of columns is greatest at the top storey of an exterior frame. The critical differential range of the frame at SLS is 7-8mm and at ULS, where a factor of 1.4 is applied to the DL, is 10-12mm.
3. The predicted deflections of the test apparatus were within 3.3mm of the prototype deflections for the lateral sway test and 1.9mm for the vertical racking test. The test apparatus was therefore deemed to simulate accurately the critical deformations seen in the prototype structure.
4. The design of the test apparatus and wall specimen meet all of the listed objectives and constraints, including the gap limits.

4 EXPERIMENTAL PROGRAM AND RESULTS

4.1 OVERVIEW

The objectives of the research reported in this chapter are to:

- assess the performance of the test apparatus by comparing the observed in-plane and out-of-plane deflections, and associated applied loads, to those predicted using SAP2000;
- assess the performance of the wood infill wall by comparing the observed in-plane and out-of-plane deflections to those predicted using conventional calculations including code provisions;
- assess the performance of the top and bottom connections subjected to out-of-plane pressure at SLS, and the effect of in-plane racking on their performance;
- investigate the change in gap, accounting for any resistance of the non-structural insulation foam; and
- Formulate recommendations about testing methods and procedures.

Five sets of tests at SLS and two at ULS, shown in Table 4-1, were conducted as part of the present study. The test conducted by Jared Harnish will be reported in detail in a forthcoming CEE Undergraduate thesis, but data concerning the performance of the test apparatus are presented and discussed in the present study. The out-of-plane tests were used as control tests to investigate any behavioral changes of the wall or connections due to damage sustained during in-plane vertical and horizontal racking tests. The target values for each test were previously listed in Table 3-1 and a list of all the tests attempted is included in Appendix J.

Table 4-1 - Summary of Tests Performed

Test	Loading	Limit	No. of Tests	Target Value	Test Date	Performed By:
Out-of-Plane 1	Negative Pressure Positive Pressure	SLS	3	-0.9 kPa 1.44 kPa	April 4 th 2012	Jeff Blaylock
In-plane Vertical Racking	Vertical Displacement	SLS	1	7-8mm	May 25 th 2012	Jeff Blaylock
Out-of-Plane 2	Negative Pressure Positive Pressure	SLS	3	-0.9 kPa 1.44 kPa	May 29 th 2012	Jeff Blaylock
In-plane Horizontal Racking	Push Displacement	SLS	2	6-7mm	June 21 st 2012	Jeff Blaylock
	Pull Displacement					
Out-of-Plane 3	Negative Pressure Positive Pressure	SLS	3	-0.9 kPa 1.44 kPa	June 22 nd 2012	Jeff Blaylock
In-plane Vertical Racking	Vertical Displacement	ULS	1	10-12mm	July 19 th 2012	Jared Harnish
In-plane Horizontal Racking	Pull Displacement	ULS	1	16-18mm	July 23 rd 2012	Jared Harnish

4.2 OUT-OF-PLANE TEST 1

Details for the out-of-plane test apparatus has been previously described in Chapter 3.

The test pressures, both positive and negative, are presented in Table 3-2.

4.2.1 PROCEDURE

The volume of the bag is approximately 9.25 m³, much larger than used in previous tests (e.g Nagy, 2008), and was able to accommodate a practical amount of leakage. The pressure test trace used to control the pressure within the bag was, in general, in accordance with ASTM E330-02 "Standard Test Window Structural Performance by Static Pressure" (ASTM, 2010). A pre-test load, equaling half the test pressure, was

applied before each test, as shown in Figure 4-1. Each full test uses at least four increments of loading, not including the pre-pressure phase. The pre-pressure phase was necessary to improve the response of the PLAs to the initial change in bag volume before it became fully pressurized. A pressure of 0.2 kPa was found sufficient to stabilize the volume of the bag and ensure control of the PLAs.

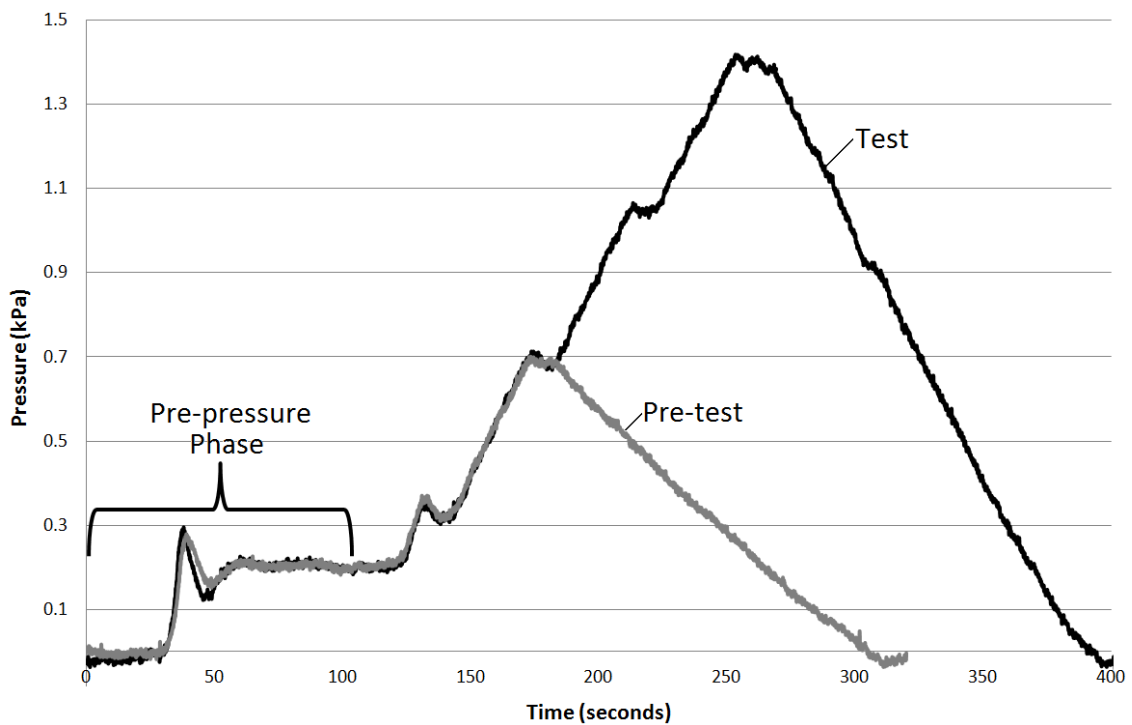


Figure 4-1 - Pressure Loading Trace

Figure 4-2 shows the original and modified pressure traces used for the ‘pre-pressure phase’ and the actual pressures generated by the PLAs. The original trace, which ramps uniformly to 0.2 kPa over 35 seconds, was grossly exceeded if only 2 PLAs were present. Increasing to 12 PLAs improved the control, but the target pressure was still greatly

exceeded at elapsed time of 25-40 and 60-100 seconds. Using a modified trace, ramping to 0.2 kPa in two steps starting 30 seconds after the PLAs were turned on, the 12 PLAs were able to generate accurately the target pressure after the initial 60 seconds.

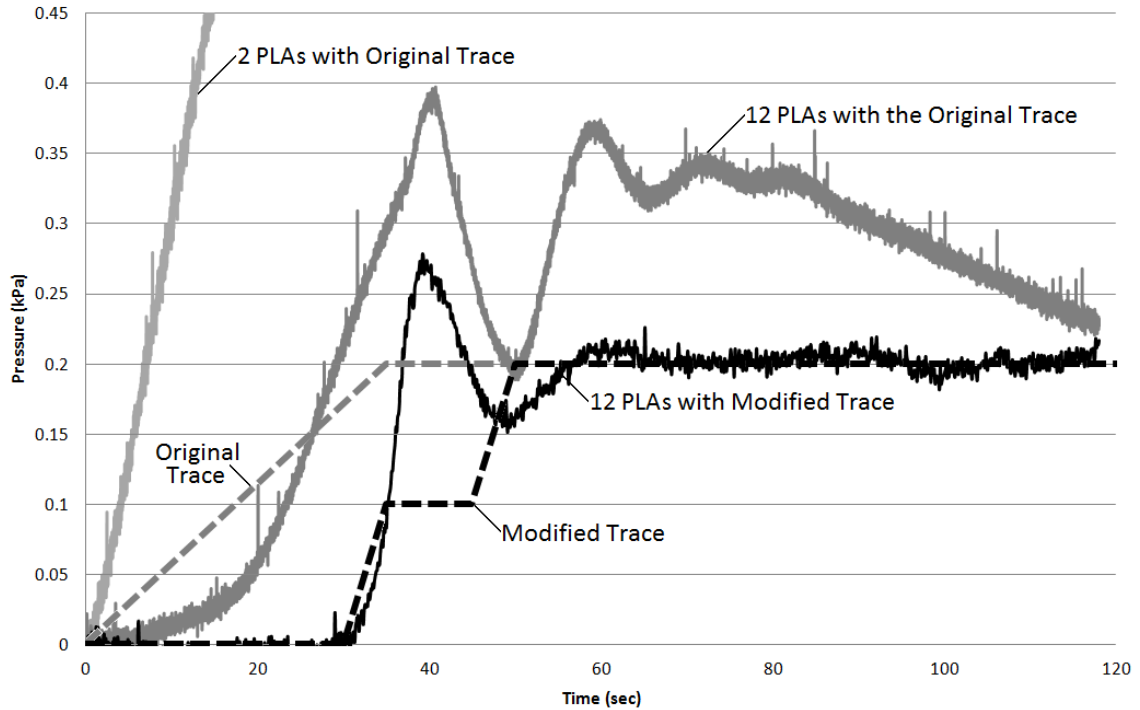


Figure 4-2 - Details of Pre-pressure Phase

4.2.2 INSTRUMENTATION

Linear Variable Displacement Transducer (LVDT's) were used to determine the deflections of the concrete frame, the steel reaction frame, and the infill wall. The deflection of half of the wall was measured, at the locations shown in Figure 4-3, as the wall was assumed to be symmetric about the center (Line 5). Both ends of the wall were

measured to check this assumption. The out-of-plane wall deflections near the top connection were recorded at the edges, T1 and T1', and at stud locations T3 and T5. Out-of-plane wall deflections near the bottom connections were measured at the edges, B1 and B1'; at two stud locations with shims, B2 and B4; and at two stud locations without shims, B3 and B5. Out-of-plane wall deflections at mid-height were measured at five consecutive stud locations over half of the wall, M1 to M5, as well as at the quarter points, QT5 and QB5, along the center. The out-of-plane displacements at each support, CT1, CT5, CT1', CB1, CB5 and CB1', and between supports, CT3, CB3, CM1 and CM1', were also measured to quantify the displacements of the concrete frame.

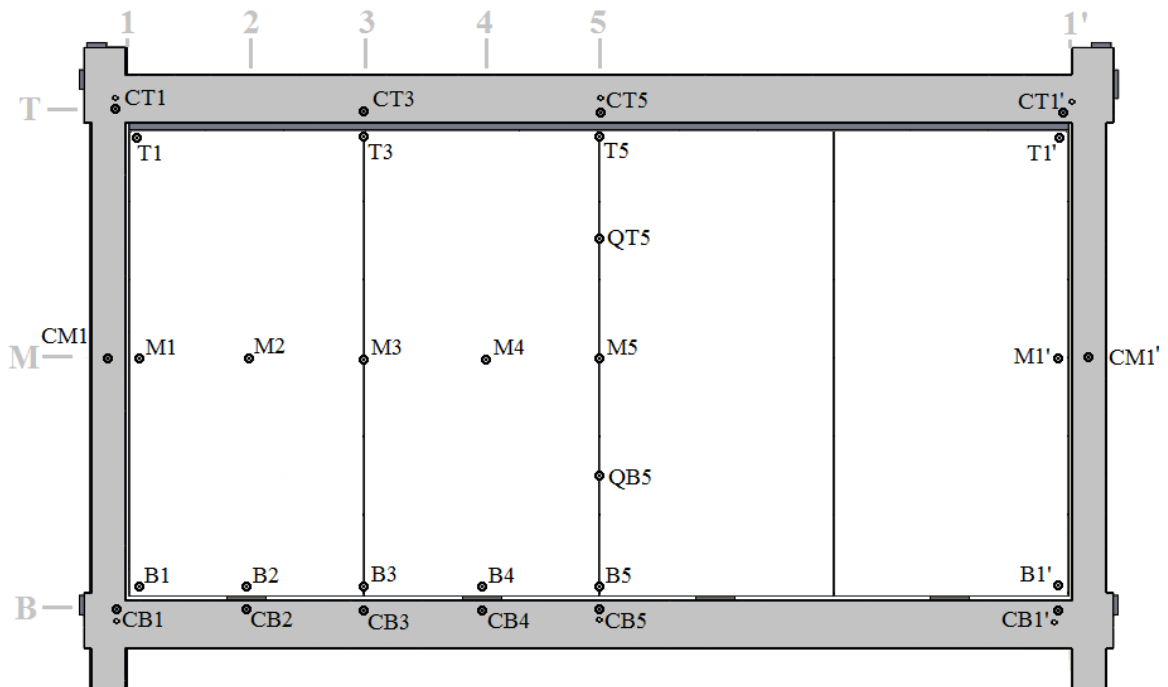


Figure 4-3 - Out-of-Plane LVDT Locations

4.2.3 PERFORMANCE OF SPECIMEN

Table 4-2 shows the out-of-plane displacements at the top and bottom of the infill wall, near the connections, with respect to the concrete frame at the locations shown in Figure 4-3. The exact displacement of the bottom and top connection cannot be properly determined because the LVDT's were placed approximately 70mm (2 ¾") from the surface of the concrete beam, as shown in Figure 4-4, and so captured deflections due to the end rotations of the wall. Further details can be determined for the data from the center line of the test apparatus, Line 5, since additional information is collected at points QT5 and QB5. These quarter point results, as well as a methodology for determining the displacements at the connections more accurately, are presented in Appendix K.

Table 4-2 - Out-of-plane Horizontal Deflections near the Top and Bottom Connections

Location on Wall	Test 1.1 Pressures	Deflection at Location (mm)					
		1	2	3	4	5	1'
Near Top Connection (T)	Negative (-0.9 kPa)	-0.2	-	-0.6	-	-0.9	-0.2
	Positive (1.44 kPa)	0.3	-	1.2	-	1.6	0.3
Near Bottom Connection (B)	Negative (-0.9 kPa)	-0.3	-0.8*	-0.9	-0.9*	-0.7	-0.2
	Positive (1.44 kPa)	0.4	2.4*	1.8	2.5*	1.8	0.3

* - Near Shim Location

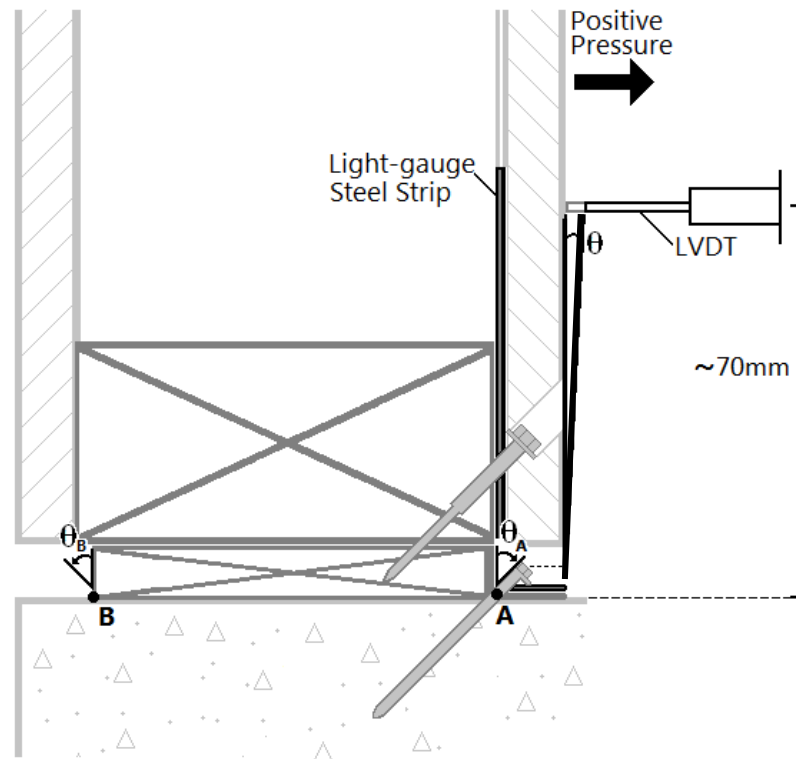


Figure 4-4 - LVDT Location and Points of Rotation at Bottom Connection

(For further details see Figure 3-23)

Table 4-2 shows that the displacements near the top of the wall at the center of the wall, Location 5, are consistently larger than those at Location 3, even though the wall at both locations has the same tributary area. This may be because the two 2438mm (96 in.) long halves of the 'C'-channel meet at Location 5 causing a minor reduction in stiffness at this location. The average stiffness of the top connection in the negative and positive directions are similar (i.e., $-0.9/-0.75 = 1.2$ kPa/mm and $1.44/1.4 = 1.03$ kPa/mm). This similarity is expected due to the symmetry of the connection about a vertical axis through the middle of the 'C'-channel web. Overall, the top connection had an out-of-plane deflection of less than 1.6mm and 0.9mm under positive and negative pressures, respectively.

The positive and negative displacements of the infill wall at the corners (i.e., T1, T1', B1 and B1') are approximately equal to each other, but are much smaller than expected. Similarly, the displacement of the wall near the bottom shim connections (i.e., Locations 2 and 4) are approximately the same, as expected. The average stiffness in the negative and positive directions, however, are not similar (i.e., $-0.9/-0.85 = 1.06$ kPa/mm and $1.44/2.45 = 0.59$ kPa/mm respectively). This extra flexibility in the positive direction may be due to the rotation of the wall which, as shown in Figure 4-4, will likely occur around Point A under positive pressure and Point B under negative pressure. The rotation around Point A, or more specifically the concrete screw, will not be restricted. The rotation around Point B will, however, be resisted by tension in the light-gauge steel strip, potentially reducing the displacement under negative pressure. Overall, the bottom connection had an out-of-plane deflection of less than 2.5mm and 0.9mm under positive and negative pressures, respectively.

The displacement of the wall near the shim connections, Locations 2 and 4, could not be predicted. The displacement at the bottom of the wall with respect to the shims (i.e., B1', B3, and B5), however, has been predicted and is compared to the observed results in Table 4-3. Almost all of the observed deflections are in the opposite direction to the predicted results, as clearly shown in Figure 4-5. This is especially evident at the corner of the wall (i.e., B1-B2) under positive pressure where a deflection of 3.5mm greater than the shim displacement at Line 2 was predicted. The observed displacement, however, is 2mm less than the displacement at the shim. It is likely that the observed lack of movement of the bottom of the wall is due to the shear stiffness of the insulation foam filling the horizontal and vertical gaps.

Table 4-3- Displacement of the Bottom of the Wall with Respect to the Shims

Test 1.1 Pressures	Results	Deflection (mm)		
		B1 - B2	B3 - (B2+B4)/2	B5 - B4
Negative (-0.9 kPa)	Observed	0.5	-0.1	0.2
	Predicted	-2.1	-0.1	-0.5
Positive (1.44 kPa)	Observed	-2.0	-0.6	-0.7
	Predicted	3.5	0.1	0.75

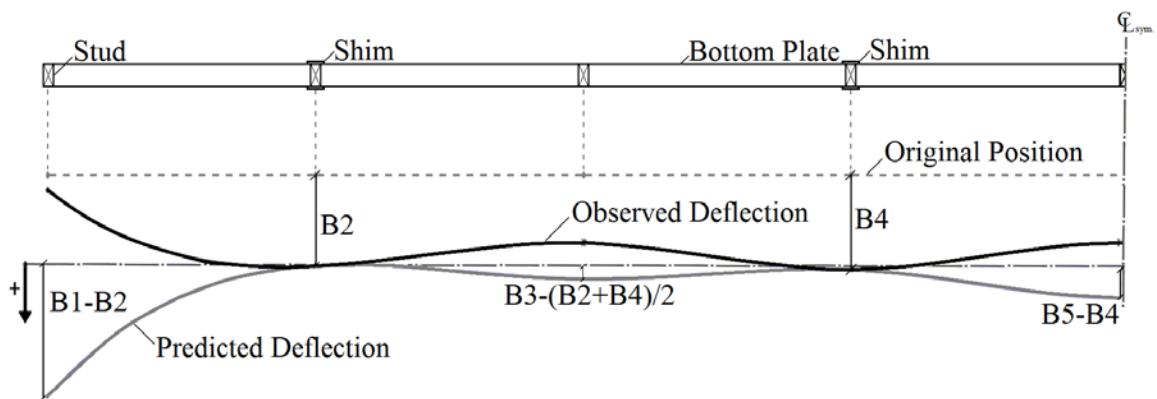


Figure 4-5 - Deformation of Bottom Plate With Respect to Shim Deflections

The wall deflection at midheight may be computed from the measured midspan displacements of the wall, Δ_M , and if the displacements at the top and bottom are accounted for as shown in Figure 4-6. Table 4-4 shows the approximate deflection at midheight of the wall, Δ_W , which was computed using the following equation:

$$[4.1] \quad \Delta_W = \Delta_M - \left(\frac{\Delta_T + \Delta_B}{2} \right)$$

where Δ_T is the deflection of the wall near the top connection and Δ_B is the deflection of the wall near the bottom connection.

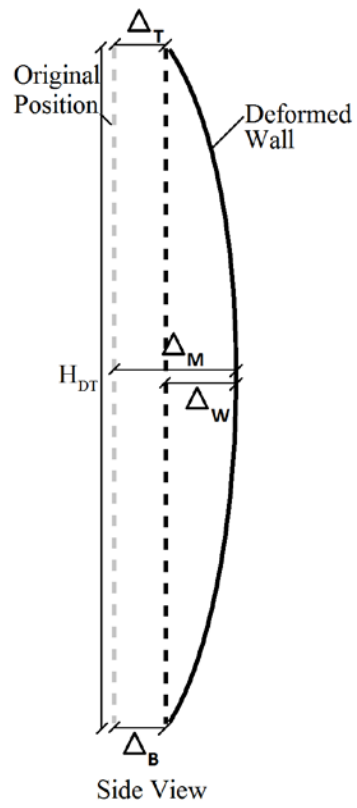


Figure 4-6 - Midheight Deflection of Infill Wall

Table 4-4 - Deflection of the Wall at Midheight

Test 1.1 Pressures	Observed Deflection (mm)						Predicted Deflection (mm)	
	W1	W2	W3	W4	W5	W1'	Bare stud	for $H_{DT}/360$
Negative (-0.9 kPa)	-1.0	-6.8	-7.5	-9.0	-6.8	-0.4	-11.9	-6.5
Positive (1.44 kPa)	1.7	12.5	13.6	16.6	13.8	1.0	19.1	6.5

The wall locations W2, W3, W4 and W5 have the same tributary area and should therefore have the same deflection. This is observed at W2 and W3. However at W4 and, to a lesser extent, W5, larger deflections were observed, possibly because the studs at these locations have a lower Young's Modulus. The observed deflections are less than those predicted for the bare stud, using the 5% (50%) fractile Young's Modulus values specified in CSA-086-09 (CSA, 2010c) indicating that these values may be conservative for the studs tested, as well as some additional stiffness contributed by the exterior and interior sheathing. All values exceed the SLS limit of $H_{DT}/360$, where H_{DT} is the distance between the top and bottom LVDT. Also, the observed deflections along the edge of the wall, at W1 and W1', are not equal. These deflections should be approximately half the deflection of the other deflections since the end studs have half the tributary areas of the interior studs. These deflections are likely dependant on the restraint provided by the foam insulation in the vertical gaps at the end of the wall, which is not necessarily the same.

The results from Test 1.2 under positive and negative pressure and Test 1.3 under negative pressure were all consistent with the Test 1.1 results. Test 1.3 under positive pressure, however, was slightly more variable. Table 4-5 shows the mean displacements, and their standard deviations, for Test 1.1 and 1.2 under positive pressure, as compared to Test 1.1, 1.2 and 1.3. The standard deviations increases consistently with the addition of the Test 1.3 data. This variability mainly occurs at the mid-height deflection and at the center top and bottom connections. Figure 4-7 shows the response at Points B5, T5 and M5. In Test 1.3, there is an increase of 0.2-0.4mm displacement at the bottom and top connection points, Figure 4-7(a) and (b) respectively, and 0.2-0.7mm displacement mid-

height of the wall, Figure 4-7(c). Subsequent use of the out-of-plane test to investigate any effect on in-plane racking will therefore be based on the Test 1.3 results.

Table 4-5 - Out-of-Plane Test 1.1/1.2 compared to Test 1.1/1.2/1.3 under Positive Pressure

Tests	Quantity	T5	W1	W2	W3	W4	W5	B5
1.1/1.2	Mean (mm)	1.6	1.3	12.6	13.8	16.7	13.9	1.8
	St. Dev. (mm)	0.0	0.0	0.1	0.1	0.1	0.1	0.0
1.1/1.2/1.3	Mean (mm)	1.8	1.8	12.9	14.0	17.2	14.4	1.9
	St. Dev. (mm)	0.2	0.2	0.4	0.4	0.6	0.5	0.2

Note: T1-T4, T1', W1', B1-B4 and B1' are not included because their standard deviations were <0.1

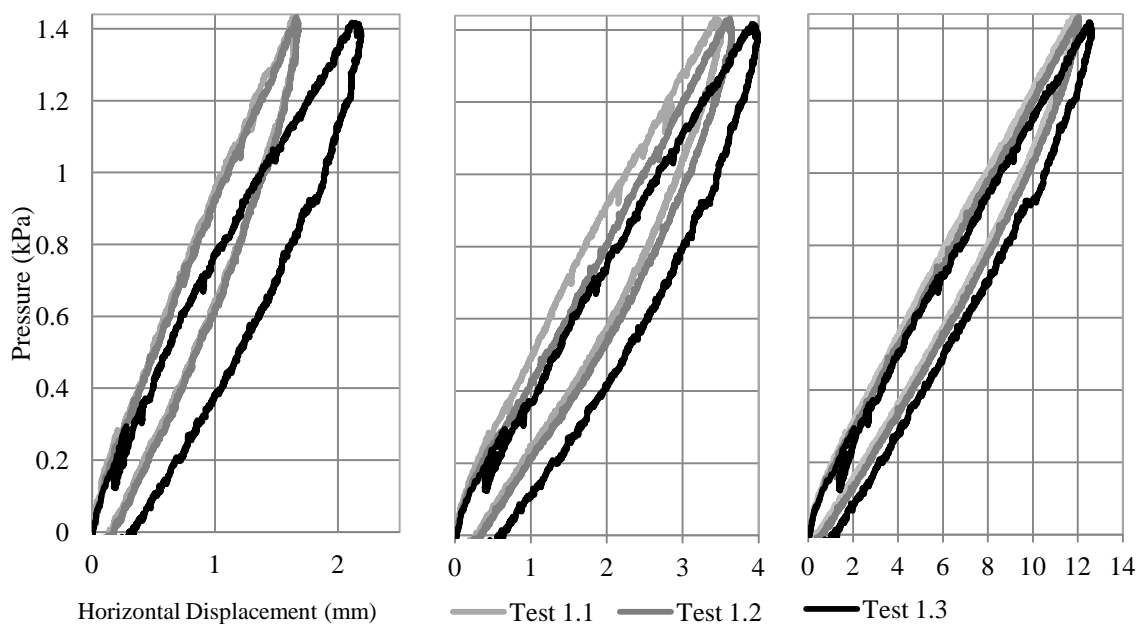


Figure 4-7 - Comparison of Tests 1.1, 1.2 and 1.3 at points a) T5; b) B5 and c) M5

4.2.4 PERFORMANCE OF TEST APPARATUS

The out-of-plane supports were designed to control out-of-plane movement of the concrete frame. The corner connections (i.e., CT1, CT1', CB1 and CB1'), shown in Table 4-6, had almost no displacement. The deflections of the beams at Location 5 are clearly larger, especially for the bottom connection, CB5. This is due to the flexibility of temporary connections that were constructed midspan of the beams.

Table 4-6 - Out-of-plane Support Deflections for Test 1.1

Pressure	Deflection (mm)					
	CT1	CT5	CT1'	CB1	CB5	CB1'
Negative (-0.9kPa)	0.0	-0.4	0.0	-0.1	-1.8	0.0.
Positive (1.44kPa)	0.0	0.8	0.0	0.1	1.7	0.1

The observed deflections of the concrete beams and columns between the out-of-plane support points is shown in Table 4-7. The predicted values shown are based on the following assumptions:

- the gross moment of inertia and the transformed moment of inertia, accounting for the reinforcement, were both considered;
- the elastic modulus of concrete, E_c , is 29900 MPa;
- the top connection applies a uniform distributed load along the top beam and the bottom connection applies two point loads, transferred by the shim connections, to the bottom beam;

- The beams are conservatively assumed to be simply supported, despite being continuous at Line 5;
- the contribution of the insulation foam in resisting the column midheight deflections is idealized as negligible or fully effective, leading to the ranges of predicted deflections shown.

The deflection at the column midheight between connections, as shown in Figure 4-8, was computed using the following equation:

$$[4.2] \quad \Delta_{CM*} = \Delta_{CM} - \left(\frac{\Delta_{CT} + \Delta_{CB}}{2} \right)$$

where Δ_{CT} , Δ_{CM} and Δ_{CB} are the recorded displacements at the top, mid-height and bottom, respectively, of the column and Δ_{CM*} is the deflection of the column with respect to the top and bottom displacements. Similarly, for the beams,

$$[4.3] \quad \Delta_{B3*} = \Delta_{B3} - \left(\frac{\Delta_{B1} + \Delta_{B5}}{2} \right)$$

where Δ_{B1} , Δ_{B3} and Δ_{B5} are the recorded displacements at the corner, quarter-span and mid-span, respectively, of the beam and Δ_{B3*} is the deflection of the beam with respect to the displacements at the out-of-plane supports.

Table 4-7 – Concrete Frame Deflections Between Supports

Pressure	Results	Deflection (mm)			
		Top Beam	Bottom Beam	Left Column	Right Column
Negative (-0.9kPa)	Observed (mm)	0.2	0.5	0.1	0.1
	Predicted (mm)	0.1 - 0.2	0.1 - 0.2	0.0 - 0.1	0.0 - 0.1
Positive (1.44kPa)	Observed (mm)	0.3	0.5	0.1	0.2
	Predicted (mm)	0.1 - 0.2	0.2 - 0.3	0.0 - 0.1	0.0 - 0.1

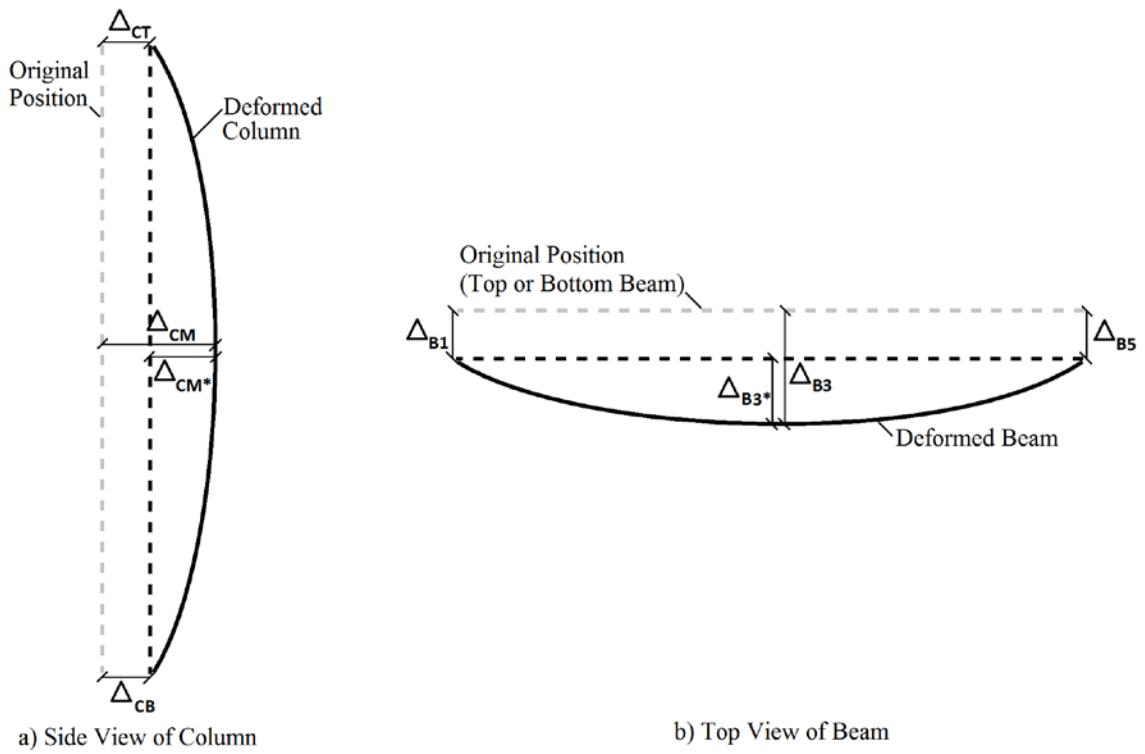


Figure 4-8 - Net Deflections at: a) Mid-height of Column; b) Midspan of Beam

The observed top and bottom beam deflections are larger than the predicted deflections for both positive and negative pressures, but since the largest deflection is $H_{DT}/4800$, this difference may not be significant. The observed range in columns is 0.1 - 0.2mm, close to the predicted values of 0.1mm which assumes full load transfer along the length of the column. This implies that there is out-of-plane load transfer occurring through the insulation foam.

4.3 LATERAL SWAY TESTS

The lateral sway tests use the test apparatus and the loading criteria described in Chapter 3 with goal of creating lateral displacements within the critical ranges stated in Table 3-1.

4.3.1 INSTRUMENTATION

The in-plane instrumentation, shown Figure 4-9, captures the deflection of the concrete frame (shown in black), the change in gap between the wood infill wall and the concrete frame (in grey) and the movement/deformation of the wood infill wall (in grey with diagonal hatching). The lateral loads were applied at the top right corner of the concrete frame. Both the horizontal displacement at height H , and the horizontal differential displacement over the storey height H' , were measured. For this study, a load moving the top of the concrete frame to the left will be referred to as a "Push Test" and a load moving the top of the concrete frame to the right will be referred to as a "Pull Test".

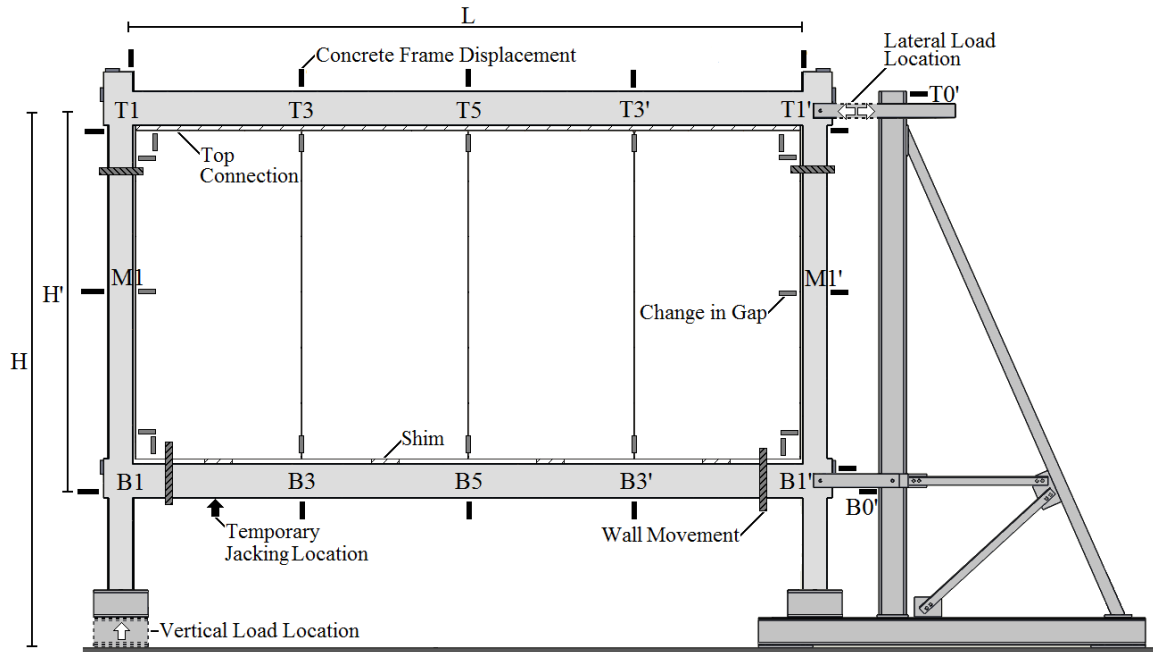


Figure 4-9 - In-plane Instrumentation Location and Test Apparatus Details

4.3.2 PERFORMANCE OF TEST APPARATUS

The lateral sway response of the concrete frame are shown in Figure 4-10 for Pull Tests 1 and 2, represented by positive load and displacement, and Push Tests 1 and 2, represented by negative load and displacement. The displacements shown are the differential displacements over the storeys height, H . Maximum displacements and the associated applied loads are also presented in Table 4-8. The predicted linear response is also shown, which assumes a measured elastic modulus of the concrete of 29900 MPa. The uncracked moments of inertia of the beams and columns in the SAP model are increased by factors of 1.3 and 1.56, respectively, to account for the relatively heavy reinforcement in the members.

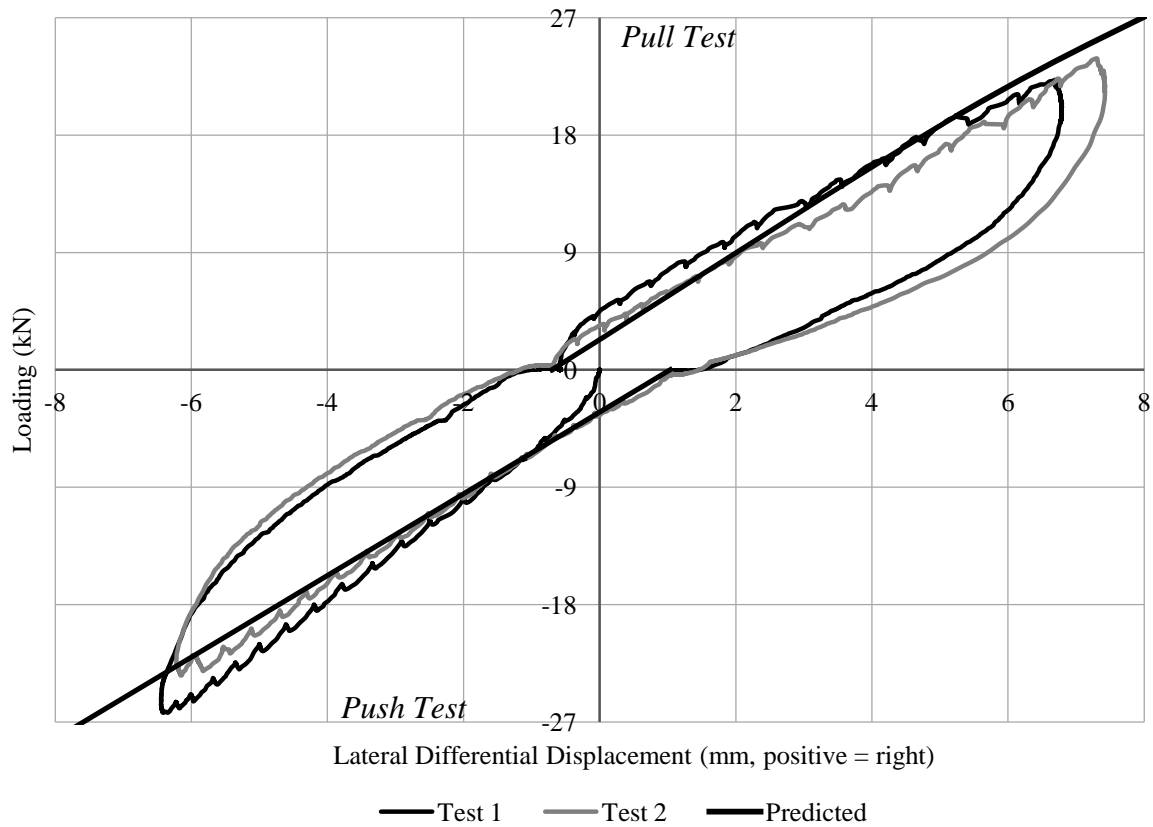


Figure 4-10 - Lateral Sway Response at SLS

Table 4-8 - Concrete Frame Response During Lateral Sway Test at SLS

(Associated with Figures 4-10 and 4-11)

Test		Stiffness (kN/mm)		Max. Observed Displacement	Load (kN)		Percent Error (%)
		Observed	Predicted		Observed	Predicted	
Pull SLS 1	H	3.1	3.2	6.6mm	22.1	23.4	6
Pull SLS 2		3.0		7.2mm	23.7	25.3	7
Push SLS 1	H	3.7	3.1	6.4mm	26.3	23.3	-13
Push SLS 2		3.3		6.2mm	23.4	22.7	-3
Pull ULS 1	H	3.1/2.1	3.2/2.6	17.6mm	46.8	51.5	9

Figure 4-10 shows the load-deflection response of the frame subjected to specified wind loads. The load was initially applied at a rate of 0.36 kN/sec, and the evident 'saw tooth' response is due to the manual pumping of the hydraulic jack. The unloading response is relatively smooth because the load was released continuously when the jack pressure was relieved. Residual displacements, of approximately +1mm and -0.5mm occurred after each Pull and Push Test, respectively. Accounting for these residual displacements, the stiffnesses predicted using the linear elastic SAP model are close to the observed values. Table 4-8 shows that there is a slight decrease in stiffness between Pull Test 1 and Pull Test 2, yet the results are fairly repeatable. There is a larger decrease in stiffness, however, between Push Test 1 and Push Test 2. The overall observed stiffnesses of the frame are larger during the Push Tests, especially Push Test 1, than the Pull Tests. The predicted stiffness is slightly greater than the observed value for the Pull Test and less than the observed value for the Push Test. The maximum observed lateral differential displacements between the top and bottom beams for the right side of the concrete frame are generally within the target range of 6-7mm. The predicted loads to reach the maximum SLS displacements are within 6% of the observed load, except for Push Test 1 which showed a stiffer response.

An ultimate pull test was also performed, shown in Figure 4-11, to a maximum observed lateral differential displacement of 17.6mm, within the target range of 16-18mm. There is clearly a reduction in stiffness, from 3.2 kN/mm to approximately 2.1 kN/mm, at an approximate lateral differential displacement of 10mm. It is likely that this response is due to cracking in the concrete, although no visible cracks were observed in the test frame. Despite this, a bi-linear response is assumed with a reduction of stiffness from the

original stiffness at SLS of 3.2 kN/mm to a predicted stiffness at ULS of 2.6 kN/mm. The predicted load to cause a 17.6mm deflection is therefore 51.5kN, which is within 9% of the observed value.

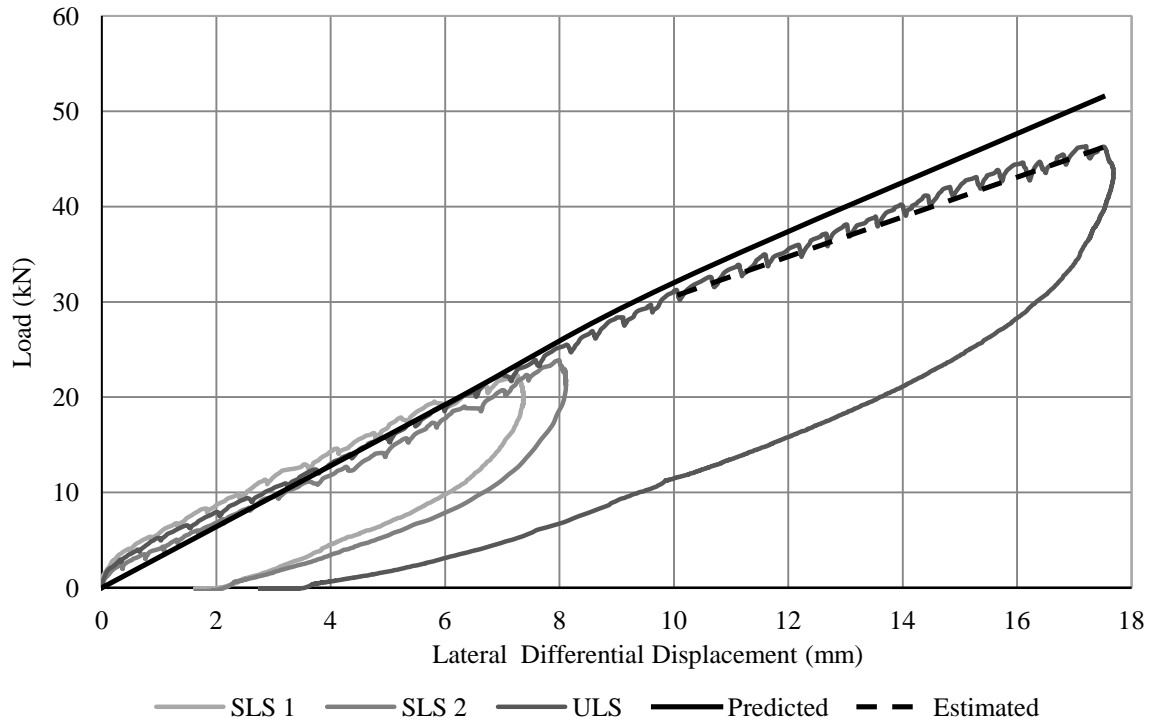


Figure 4-11 - Lateral Sway Pull Test Response at SLS and ULS

(Associated with Table 4-8)

The response of the steel frame is shown in Figure 4-12 and Figure 4-13, and summarized in Table 4-9. The stiffness of the steel frame during the push test at SLS for the full height of the test apparatus, H , was estimated by Line A to be 6.4 kN/mm and shows the predicted load to be 37% more than observed. The stiffness, of 8.4 kN/mm, for the difference between the bottom and top connection, H' , of the steel frame was, however, accurately predicted, where the predicted load was within 3% of the observed. The

variation between H and H' is due to the (e.g., 3.8-2.7mm \Rightarrow 0.9mm displacement which was observed at the bottom connection, as compared to the almost zero amount of difference that was predicted. Similarly, the observed stiffness for the pull test at SLS, estimated by Line B to be 6.9 kN/mm for a height H, was not accurately predicted, whereas the predicted results were again within 3% of the observed. The results for the pull test at ULS show that a displacement of 3mm occurs before the connections become consistently stiff which is estimated by Line C to be 9.6 kN/mm. The observed load for height H and H' are more comparable for this test, likely because there is smaller effect of the bottom connection under higher loads, and predicted within 6%. The predicted stiffness of 8.9 kN/mm, however, is more comparable to the observed stiffness for the full height, H, 9.6 kN/mm, than the differential height, H', of 13.4 kN/mm.

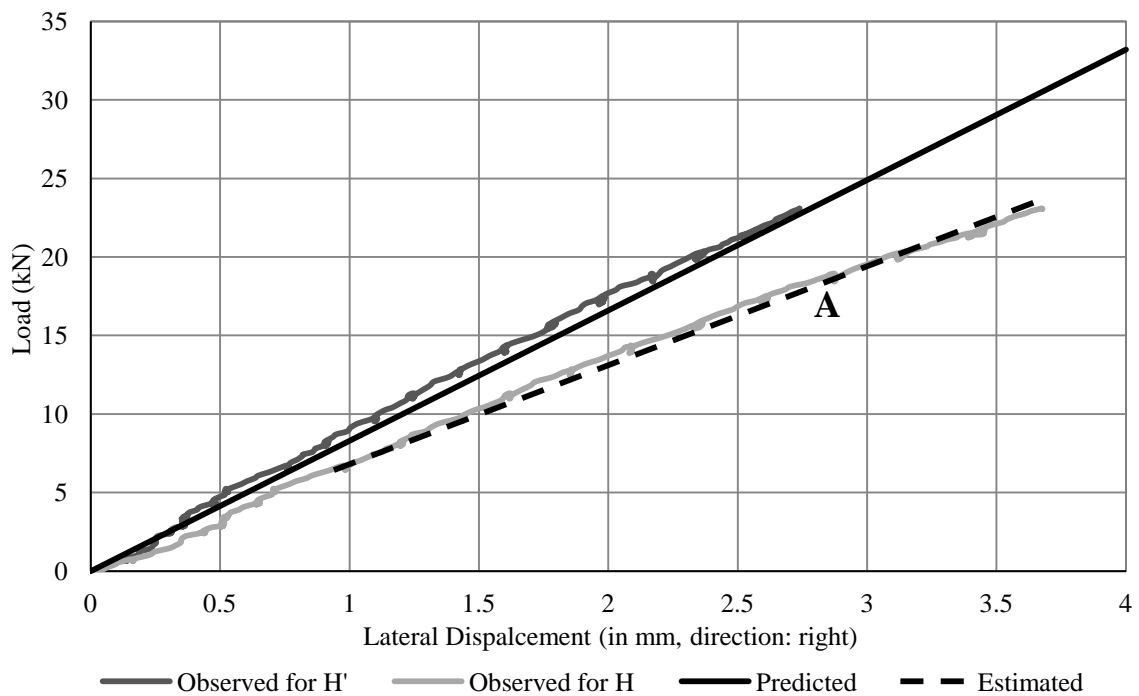


Figure 4-12 - Steel Frame Displacement for Average Push Test 1 and 2 Results at SLS

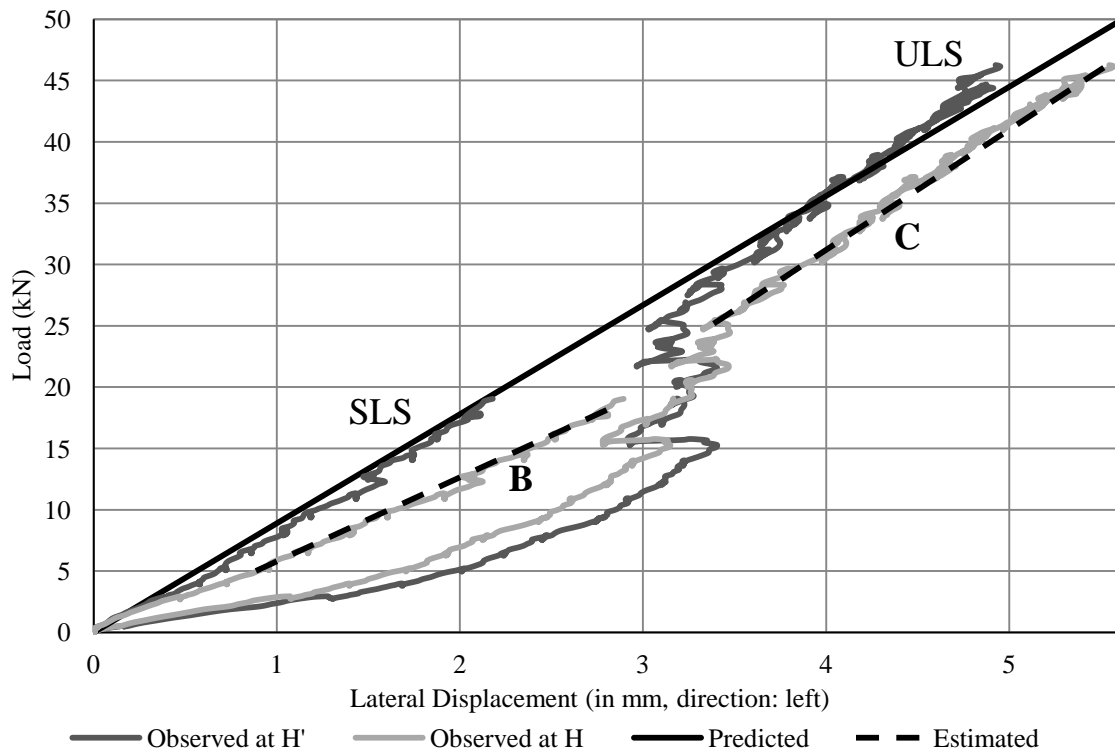


Figure 4-13 - Steel Frame Displacement for Avg. Pull Test 1/2 at SLS and Test at ULS

Table 4-9 - Steel Frame Response during Lateral Sway Tests

Test		Stiffness (kN/mm)		Max. Observed Displacement	Load (kN)		Percent Error %
		Observed	Predicted		Observed	Predicted	
SLS Push 1/2	H	(A) 6.3	8.3	3.8mm	23.0	31.5	37
	H'	8.4		2.7mm	23.0	22.4	-3
SLS Pull 1/2	H	(B) 6.9	8.9	2.9mm	19.0	25.8	36
	H'	8.8		2.2mm	19.0	19.6	3
ULS Pull	H	(C) 9.6	8.9	5.5mm	46.3	49.0	6
	H'	13.4		4.9mm	46.3	43.6	-6

Table 4-10A, B, and C shows the average observed and predicted displacements of the concrete frame for the push and pull test at SLS and ULS, where the displacement points are identified in Figure 4-14 and the horizontal displacement at Δ_{T1} is used as the control displacement. The differences between the predicted and observed values are also shown, where the values shown in brackets represent instances where the predicted deflection underestimates the observed response. Differences greater than 0.5mm are likely significant.

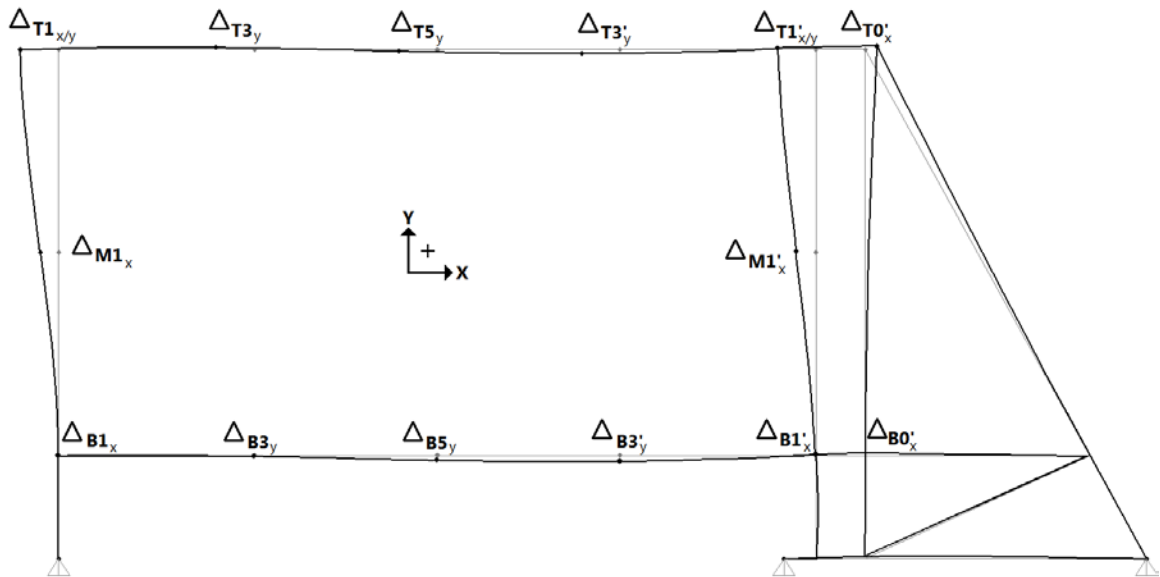


Figure 4-14 - Deflected Shape of Concrete Frame under Lateral Sway Loading

(Associated with Table 4-10A, B and C)

Table 4-10A - Concrete Frame Deformation for Lateral Sway (Push) Loading at SLS

Deflection (mm)	Top Beam							Middle of Columns		Bottom Beam				
	Δ_{T1x}	Δ_{T1y}	Δ_{T3y}	Δ_{T5y}	$\Delta_{T3'y}$	$\Delta_{T1'y}$	$\Delta_{T1'x}$	Δ_{M1x}	$\Delta_{M1'x}$	Δ_{B1x}	Δ_{B3y}	Δ_{B5y}	$\Delta_{B3'y}$	$\Delta_{B1'x}$
Avg. Observed	-7.9	0.1	0.6	-0.2	-0.1	0.1	-7.1	-4.5	-3.2	-1.4	0.5	0.4	0.1	-0.3
Predicted	-7.1	0.0	0.5	-0.2	-0.6	0.2	-7.1	-3.8	-3.3	-0.2	-0.3	-1.1	-1.2	0.0
Difference	(0.8)	-	-	-	0.5	-	-	(0.7)	-	(1.2)	0.8	1.5	1.3	(0.3)

Table 4-10B - Concrete Frame Deformation for Lateral Sway (Pull) Loading at SLS

Deflection (mm)	Top Beam							Middle of Columns		Bottom Beam				
	Δ_{T1x}	Δ_{T1y}	Δ_{T3y}	Δ_{T5y}	$\Delta_{T3'y}$	$\Delta_{T1'y}$	$\Delta_{T1'x}$	Δ_{M1x}	$\Delta_{M1'x}$	Δ_{B1x}	Δ_{B3y}	Δ_{B5y}	$\Delta_{B3'y}$	$\Delta_{B1'x}$
Avg. Observed	8.5	-0.2	-0.3	*	0.4	0.2	7.9	4.4	3.5	1.1	-0.3	-0.1	0.0	0.1
Predicted	7.8	0.0	-1.2	-0.8	-0.1	-0.4	7.9	3.6	4	0.2	-0.6	-0.3	0.2	0.1
Difference	(0.7)	(0.2)	0.9	-	(0.5)	(0.6)	-	(0.8)	0.5	(0.9)	0.3	0.2	0.2	-

Table 4-10C - Concrete Frame Deformation for Lateral Sway (Pull) Loading at ULS

Deflection (mm)	Top Beam							Middle of Columns		Bottom Beam				
	Δ_{T1x}	Δ_{T1y}	Δ_{T3y}	Δ_{T5y}	$\Delta_{T3'y}$	$\Delta_{T1'y}$	$\Delta_{T1'x}$	Δ_{M1x}	$\Delta_{M1'x}$	Δ_{B1x}	Δ_{B3y}	Δ_{B5y}	$\Delta_{B3'y}$	$\Delta_{B1'x}$
Avg. Observed	18.4	-0.1	-0.6	0.4	1.8	0.7	17.5	9.3	7.6	2.1	-0.6	-0.2	0.0	0.3
Predicted	17.5	0.0	-2.4	-1.3	0.3	-0.9	17.5	8.2	9.1	0.5	-0.8	0.2	1.1	0.8
Difference	(0.9)	-	1.8	(1.7)	(1.5)	(1.6)	-	(1.1)	1.5	(1.6)	0.2	(0.4)	1.1	0.5

Notes:

- Tables 10A, B and C are associated with Figure 4-4
- Differences ≤ 0.1 are not included, * is an error in recorded data, **bold** values represent noteworthy results and values in brackets represents a predicted deflection that is lower than the observed deflection.

Overall the deformed shape for the push test at SLS, presented in Table 4-10A, is accurately predicted. The horizontal displacements of the right column, Line 1', are accurately predicted, however the left column displacements, Line 1, are slightly underestimated. The predict response suggests that the left and right column should be similar, although the observed results show the left side displacing 0.7-1.2mm more than the right side where the load is applied. The observed vertical displacements of the top beam, Line T, are fairly close to the predicted values. The predicted displacements of bottom beam, Line B, are all larger than the observed displacements, indicating that the bottom beam maybe stiffer than expected.

Similarly, the observed deformed shape for the pull test at SLS, presented in Table 4-10B, is accurately predicted. The predicted horizontal displacements of the right column, Line 1', are again accurate, yet the left column, Line 1, displaced 0.7-0.9mm more than predicted, similar to the push test results. The predicted displacements of bottom beam, Line B, are much closer to the observed values, however the displacements of the top beam, Line T, show some inconsistencies. A similar, although larger, response was observed during the Pull Test at ULS, shown in Table 4-10C. All predicted displacements of the concrete frame are within 1.7mm of the observed values.

4.3.3 PERFORMANCE OF SPECIMEN

Table 4-11A and B compares the predicted and observed wall movement during the lateral test at SLS for both the push and pull test, respectively. The variables listed in the column heading are shown in Figure 4-15. There is very little predicted movement of the wall, i.e, no expected deformation, as shown by Δ_D , for both the push and pull tests. The observed results indicated that the top of the wall moving laterally with the deformation of the concrete frame with some smaller vertical displacements, and that this movement includes a change of the wall diagonal length of 3.2-4.5mm. The differences highlighted between the predicted and observed results are likely due to the insulation foam which again seems to be transferring load from the concrete frame to the wood infill wall, which is not accounted for in the predicted results.

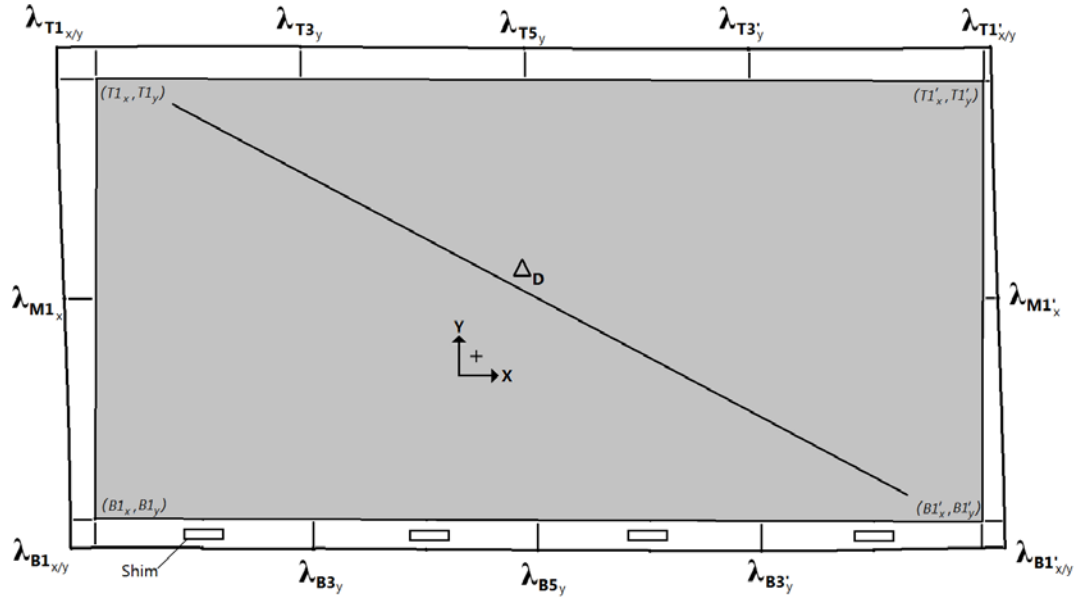


Figure 4-15 - Notation for Gap Change and Wall Movement

(Associated with Table 4-11A/B, Table 4-12A/B, Table 4-16 and Table 4-17)

Table 4-11A - Wall Rotation under Lateral Sway (Push) Loading at SLS

Deflection (mm)	TI_x	TI_y	TI'_x	TI'_y	BI_x	BI_y	BI'_x	BI'_y	Δ_D
Observed	-4.4	-0.9	-4.3	2.1	0.0*	-0.9	0.0*	2.1	3.2
Predicted	0.5	-0.3	0.5	-1.4	0.0	-0.3	0.0	-1.4	0.0
Difference	(4.9)	(0.6)	(4.8)	(3.5)	-	(0.6)	-	(3.5)	(3.2)

Table 4-11B- Wall Rotation under Lateral Sway (Pull) Loading at SLS

Deflection (mm)	TI_x	TI_y	TI'_x	TI'_y	BI_x	BI_y	BI'_x	BI'_y	Δ_D
Observed	4.5	1.5	5.2	-1.3	0.0*	1.5	0.0*	-1.3	-4.5
Predicted	-0.2	-0.9	-0.2	0	0.2	-0.9	0.3	0	0
Difference	(4.7)	(2.4)	(5.4)	(1.3)	(0.2)	(2.4)	(0.3)	(1.3)	(4.5)

Notes:

- Tables 11A and B are associated with Figure 4-15
- * is an estimated value, **bold** values represent noteworthy results and values in brackets represents a predicted displacement that is lower than the observed displacement.

Table 4-12A and B compare the predicted and observed change in gap during the lateral sway test at SLS for both the push and pull test, respectively, with positive values representing an increase in gap. The maximum predicted changes in gap 6.4 - 7.8mm occur at the top corners of the wall, λ_{T1x} and $\lambda_{T1'x}$ in Figure 4-15. As shown in Figure 4-16 for the top right corner, these correspond approximately to the predicted lateral displacements of the concrete frame. The observed gap changes at these locations, however, was only 1.6 - 1.8mm with a similar response in both an increase and decrease in gap. This further indicates that the infill wall is clearly moving with the lateral sway displacement of the concrete frame, again emphasizing the likelihood that the insulation foam is transferring load to the infill wall. Table 4-12A and B also show minor discrepancies between the observed and predicted gap changes along the bottom and top beams, especially at the corners of the infill wall as the wall starts to rotate.

Table 4-12A - Change in Gap under Lateral Sway (Push) Loading at SLS

Deflection	Top Beam					Middle of Columns		Bottom Beam								
	λ_{T1x}	λ_{T1y}	λ_{T3y}	λ_{T5y}	λ_{T3y}	λ_{T1x}	λ_{T1y}	λ_{M1x}	λ_{M1x}	λ_{B1x}	λ_{B1y}	λ_{B3y}	λ_{B5y}	λ_{B3y}	λ_{B1x}	λ_{B1y}
Observed	1.7	1.2	0.4	0.3	-1.0	-1.8	-2.1	-0.1	0.0	-1.7	-1.0	-0.8	1.0	0.7	1.4	2.1
Predicted	7.1	0.4	1.1	0.7	0.6	-6.4	1.4	3.5	-4.0	0.2	-0.3	-0.3	0.3	0.0	-0.4	-1.4
Difference	5.4	(0.8)	0.7	0.4	(1.6)	4.6	(3.5)	3.6	4.0	(1.9)	(0.7)	(0.5)	0.7	0.7	1.8	3.5

Table 4-12B - Change in Gap under Lateral Sway (Pull) Loading at SLS

Deflection	Top Beam					Middle of Columns		Bottom Beam								
	λ_{T1x}	λ_{T1y}	λ_{T3y}	λ_{T5y}	λ_{T3y}	λ_{T1x}	λ_{T1y}	λ_{M1x}	λ_{M1x}	λ_{B1x}	λ_{B1y}	λ_{B3y}	λ_{B5y}	λ_{B3y}	λ_{B1x}	λ_{B1y}
Observed	-1.6	-1.7	-1.1	-1.0	-0.4	1.7	1.3	0.3	-0.5	1.9	1.5	1.4	0.6	-0.1	-2.3	1.3
Predicted	-7.7	0.9	-0.5	-0.4	0.1	7.8	-0.3	4.0	-3.7	-0.2	-0.8	-0.1	-0.1	-0.4	-0.1	0.3
Difference	6.1	(2.6)	(0.6)	(0.6)	(0.5)	6.1	(1.6)	3.7	3.2	(2.1)	(2.3)	(1.5)	(0.7)	0.3	(2.2)	(1.0)

Notes:

- Tables 12A and B are associated with Figure 4-15
- Differences ≤ 0.1 are not included, **bold** values represent noteworthy results, positive deflection represents an increase in gap and a negative displacement represents a decrease in gap, and differences in brackets represents a predicted change in gap that is lower than the observed change in gap.

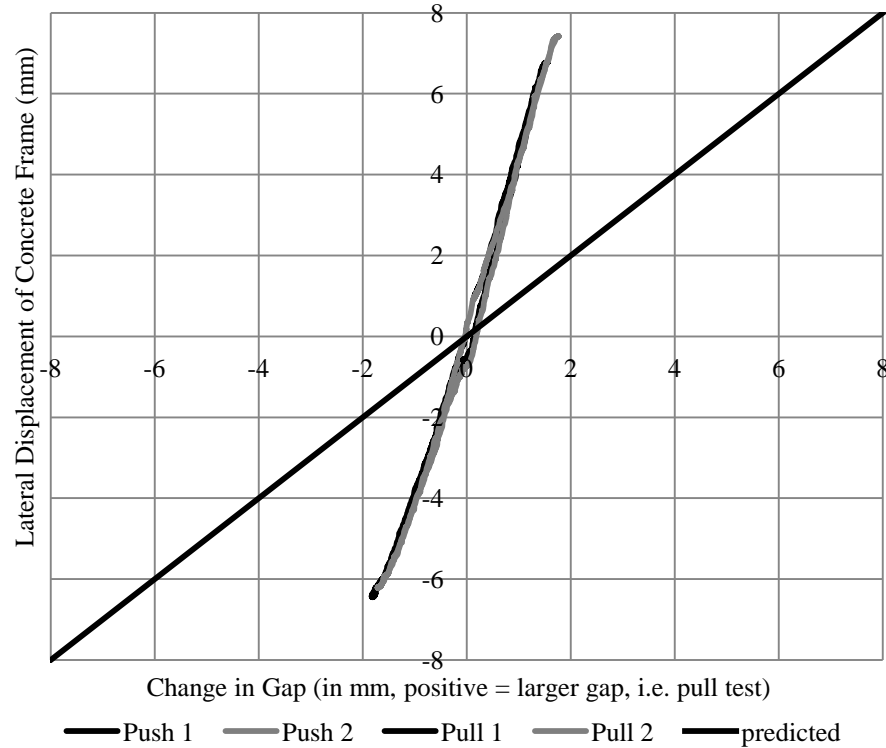


Figure 4-16 - Change in Gap at Top Right Corner for Lateral Sway Loading at SLS

4.4 VERTICAL RACKING TESTS

The vertical racking test uses the test apparatus and the loading criteria described in Chapter 3, with goal of creating vertical displacements within the critical ranges stated in Table 3-1. The in-plane instrumentation is the same as for the lateral racking tests shown in Figure 4-9. The vertical load is applied at the bottom left corner of the concrete frame to achieve the target vertical differential displacement between the two columns spaced a distance, L , apart. During the jack installation for the vertical load, a temporary jack was required, at the locations shown, to support the frame near the bottom left corner.

4.4.1 PERFORMANCE OF TEST APPARATUS

The combined response of the concrete frame under vertical loading at SLS and ULS is shown in Figure 4-17, and is also summarized in Table 4-13. The initial predicted response, as seen in Figure 4-17, shows no vertical deflection until the jacking load exceeded the vertical reaction due to the self-weight of the concrete frame and attachments, which was determined in a separate test to be 12.7kN. This was simulated in the SAP model as the self-weight of the concrete frame and reinforcement, including details such as the steel W-shape attached to the leg, the wood infill wall, and the wood bag attachment. The initial observed response at SLS at the frame lift-off (i.e., the point where the stiffness of the frame is engaged), say at a deflection of 0.6mm, was 16.2kN. The observed response at ULS at the frame lift-off, for this case say 4.2mm, was 18.3kN. The variation in initial response, or reduced initial stiffness, between the test at SLS and ULS is due to the added effect of the temporary loading device, shown in Figure 4-9, during the test at ULS which was accidentally left to support the weight of the frame during jacking. The extra $(16.2\text{kN}-12.7\text{kN})= 3.5\text{kN}$ at SLS and $(18.3-12.7)= 5.6\text{kN}$ at ULS, when compared to the predicted 12.7kN, may have been caused by wood blocking between the top right corner of the concrete frame and the steel frame, which preloaded the concrete frame before testing. The difference between these two values (i.e., 3.5kN vs. 5.5kN) could be attributed to the varied amount of preloading that occurred between tests.

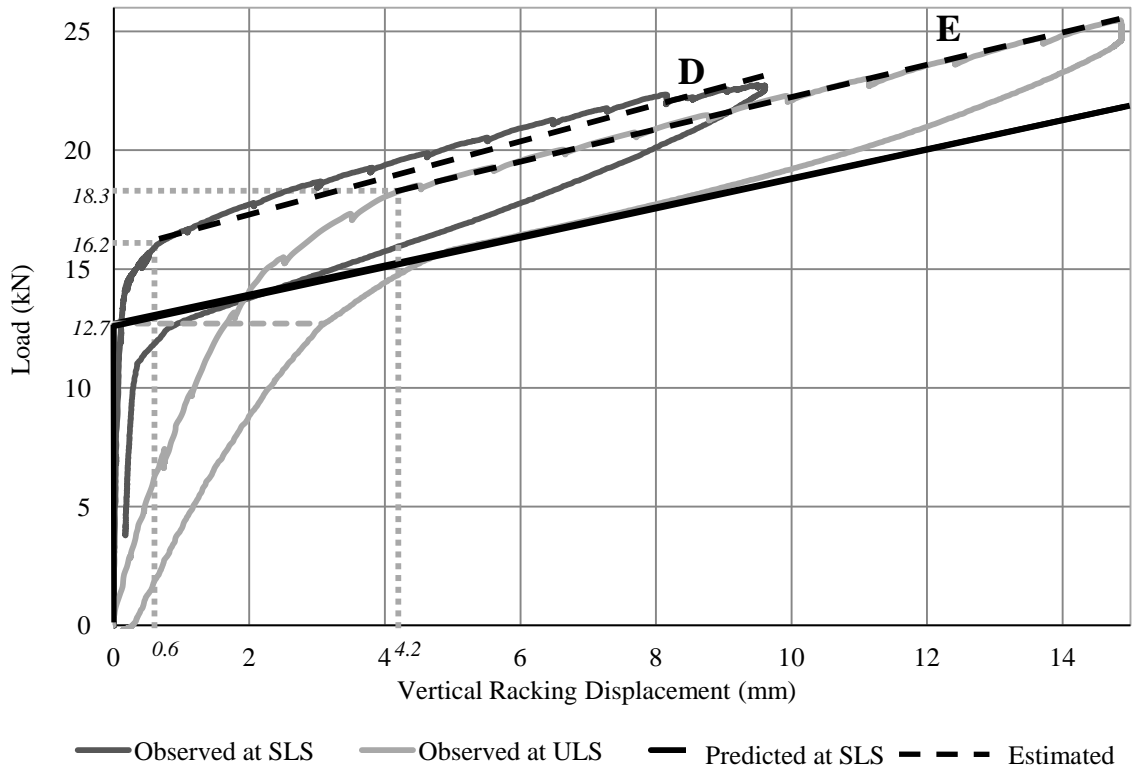


Figure 4-17- Observed and Predicted Response due to Vertical Racking at SLS and ULS

Table 4-13 - Test Apparatus Response During Vertical Racking Test

Test	Stiffness (kN/mm)		Max. Observed Displacement	Load (kN)		Percent Error (%)
	Observed	Predicted		Observed	Predicted	
Vertical at SLS	(D) 0.75	0.62	9.6mm	22.7	18.6	-18
Vertical at ULS	(E) 0.67	0.55	14.9mm	25.5	21.8	-14

The predicted stiffnesses of the test apparatus, shown Table 4-13 to be 0.62 kN/mm and 0.55 kN/mm, slightly underestimate the observed stiffnesses of 0.75 kN/mm and 0.67 kN/mm, shown in Figure 4-17 by lines A and B, which occurred during the test at SLS and ULS, respectively. The observed reduction in stiffness between tests, of 0.8 kN/mm, is likely due to minor cracking in the concrete frame and is similar to the predicted change in stiffnesses of 0.7 kN/mm. Despite this, the observed results at ULS show a consistently linear response after approximately 4.2mm with minimal residual displacement, which suggests that the overall response of the frame was essentially linear-elastic.

A vertical load of 22.7 kN was applied to reach a vertical racking deflection of 9.6mm for testing at SLS, which was 18% larger than the predicted load of 18.6kN. Including the extra load of 3.5kN increases the predicted load to 22.1kN, which is only 3% less than the observed response. A vertical load of 25.5 kN was applied to reach a vertical racking deflection of 14.9mm for testing at ULS, which was 14% larger than the predicted load of 21.8kN. Again including the extra load of 5.5kN increases the predicted load to 27.3kN, which is 7% more than the observed response. The stiffness during unloading is approximately 1.0-1.3 kN/mm and 0.6-1.2 kN/mm for the test at SLS and ULS, respectively. In, general, the response of the concrete frame during unloading was stiffer than during loading.

The response of the steel frame only is shown in Figure 4-18 for vertical racking tests at SLS and ULS, which is also summarized in Table 4-14. The lateral load that occurred at the top of the steel frame had to be estimated as this load was not measured during testing. To do this, the self-weight of 12.7kN was subtracted from the recorded vertical load

results, as load cause any lateral displacement, and was then multiplied by a factor of 1.9, a value that relates to the aspect ratio of the frame, which was then verified using the SAP model.

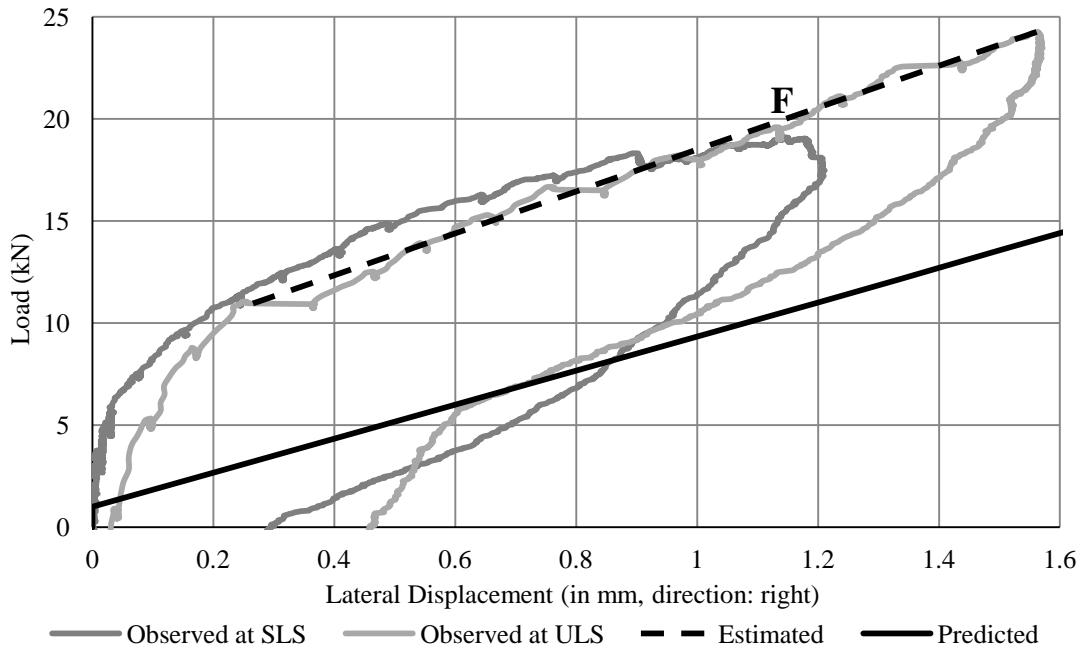


Figure 4-18 - Response of Steel Frame During Vertical Racking Test at ULS

Table 4-14 - Steel Frame Response During Vertical Racking Test

Test		Stiffness (kN/mm)		Max. Observed Displacement	Load (kN)		Percent Error (%)
		Observed	Predicted		Observed	Predicted	
Vertical at SLS	H	9.4	8.4	1.2mm	17.2	11.0	-36
Vertical at ULS	H	(F) 10.3	8.4	1.6mm	24.1	14.4	-40

The observed stiffness was 9.4 kN/mm and the applied load was 17.2kN at SLS, both larger than the predicted values of 8.4 kN/mm and 11.0 kN, respectively. A similar response occurred during loading at ULS with a larger variation between the observed and predicted stiffness and percent error for predicting the applied load. Figure 4-18 shows there was a nonlinear response that occurred for approximately the first 10kN which is not included within the predicted response. If included, the applied load is predicted within 12% and 3% of the observed load at SLS and ULS, respectively.

Table 4-15A and B show the predicted and observed responses for the vertical racking tests at SLS and ULS, respectively. The associated deflected shape and locations of the various measurements are shown in Figure 4-19. The differences between predicted and observed values are also shown in Table 4-15A and B, with positive values indicating a larger observed deflection than predicted.

The predicted lateral displacement at the top of the concrete frame and steel frame at SLS is 1.2mm. The frame is rotating about Point P, shown in Figure 4-19, where the displacement is zero, which leads to an associated vertical displacement at the top left side of the frame is 2.4mm. The differential vertical displacement between the columns is therefore 7.6mm (=10.0-2.4mm), which is within the target deflection range of 7-8mm. The observed deflections of the concrete frame are within 0.6mm of the predicted results. Slightly larger deflections occurred in the beams, Δ_{T5y} , $\Delta_{T3'y}$, Δ_{B5y} and Δ_{B5y} , and slightly smaller horizontal deflections occurred at mid-height of the columns, Δ_{M1x} and $\Delta_{M1'x}$. The lateral displacement at the top left corner of the concrete frame, Δ_{T1x} , and the steel frame, $\Delta_{T0'x}$, were both accurately predicted. The displacement of the right column (i.e., $\Delta_{T1'x}$, $\Delta_{M1'x}$ and $\Delta_{B1'x}$), however was overestimated. This change in displacement suggests that

the observed point of rotation is closer to mid-height of the column, i.e., Point Q. The predicted lateral displacement at the top of the concrete frame and steel frame at ULS is 1.9mm. Using the same reasoning as at SLS, the differential vertical displacement between the columns is therefore 11.1mm (=14.9-3.8mm), which is within the target deflection range of 10-12mm. The observed deflections of the concrete frame at ULS are within 1.0mm of the predicted results. Again, the observed and predicted beam deflections, Δ_{T5y} , $\Delta_{T3'y}$, Δ_{B5y} and $\Delta_{B5'y}$, varied slightly but the horizontal deflection mid-height of the right column, $\Delta_{M1'x}$, was accurately predicted.

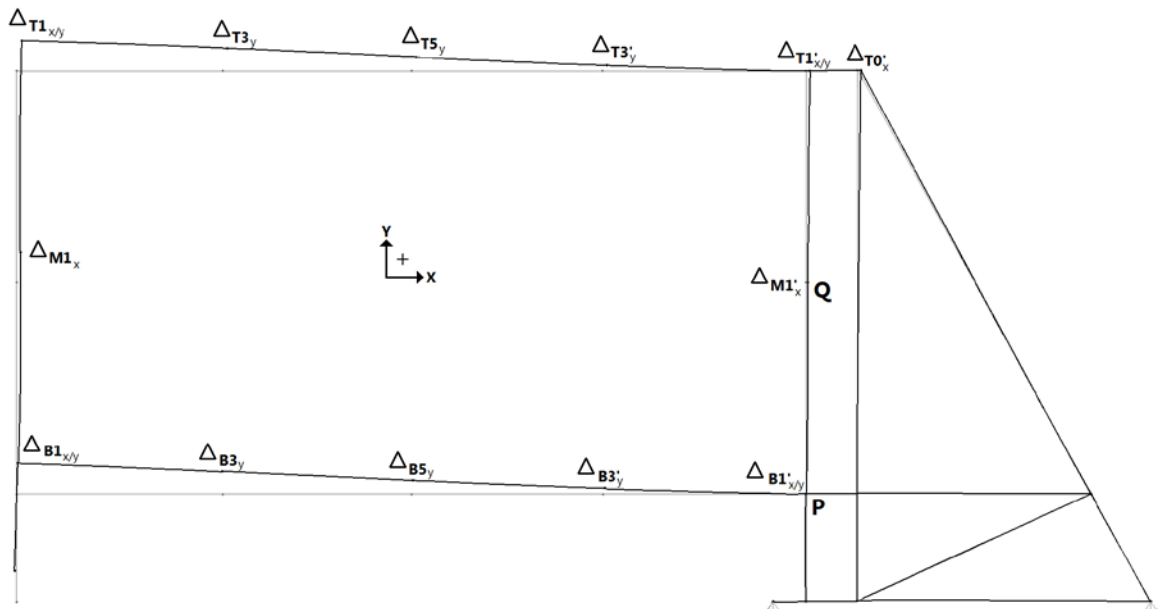


Figure 4-19- Deflected Shape of Concrete Frame under Vertical Racking

Table 4-15A - Displacement of Test Apparatus During Vertical Racking Tests at SLS

	Top Beam						Middle of Columns		Bottom Beam					
Deflection (mm)	Δ_{T1x}	Δ_{T1y}	Δ_{T3y}	Δ_{T5y}	Δ_{T3y}	$\Delta_{T1'x}$	$\Delta_{T1'y}$	Δ_{M1x}	$\Delta_{M1'x}$	Δ_{B1x}	Δ_{B3y}	Δ_{B5y}	$\Delta_{B3'y}$	$\Delta_{B1'x}$
Observed	1.2	10.0	7.4	5.2	2.4	0.5	0.4	0.4	-0.1	0.1	7.3	4.6	2.1	-0.5
Predicted	1.2	10.0	7.6	4.7	2.1	1.2	0.0	0.7	0.5	0.0	7.2	4.2	1.7	0.0
Difference	-	-	0.2	(0.5)	(0.3)	0.7	(0.4)	0.3	(0.6)	-	-	(0.4)	(0.4)	(0.5)

Table 4-15B - Displacement of Test Apparatus During Vertical Racking Tests at ULS

	Top Beam						Middle of Columns		Bottom Beam					
Deflection (mm)	Δ_{T1x}	Δ_{T1y}	Δ_{T3y}	Δ_{T5y}	Δ_{T3y}	$\Delta_{T1'x}$	$\Delta_{T1'y}$	Δ_{M1x}	$\Delta_{M1'x}$	Δ_{B1x}	Δ_{B3y}	Δ_{B5y}	$\Delta_{B3'y}$	$\Delta_{B1'x}$
Observed	2.0	14.9	11.2	8.0	3.6	1.8	0.5	1.4	0.8	0.8	10.2	6.4	3.0	0.2
Predicted	1.9	14.9	11.5	7.3	3.3	1.9	0.2	1.0	0.8	0.0	11.2	6.8	2.9	-0.2
Difference	-	-	0.3	(0.7)	(0.3)	-	(0.3)	(0.4)	-	(0.8)	1.0	0.4	-	(0.4)

Notes:

- Tables 4-15A and B are associated with Figure 4-19
- Differences ≤ 0.1 are not included, * is an error in recorded data, **bold** values represent noteworthy results and values in brackets represents a predicted deflection that is lower than the observed deflection.

4.4.2 PERFORMANCE OF SPECIMEN

Table 4-16 compares the predicted and observed wall movement during the vertical racking test at SLS, where the variables are shown in Figure 4-15. Table 4-17 compares the predicted and observed change in gaps during the vertical racking test at SLS, where positive values represent an increase in gap. The predicted movement of the upper left corner of the infill wall is 9.5mm upwards. At the bottom right corner, the wall displaces downwards 0.9mm, rotating around the closest shim, so that the gap at the bottom of the wall decreases 1.1mm while the gap at the top of the wall increases 1.1mm. The shims preserved the gap between the bottom of the wall and the lower beam so that as the beam rotates, the wall rotates with it, causing a lateral displacement of 5.5mm at the top of the wall. The largest change in gap, 4.5mm, therefore occurs at the top corners. Throughout the test the infill wall is predicted to stay square. Overall, the observed rotation of the infill wall is very slight and the observed gaps do not significantly change. This implies that the wall is moving with the concrete frame, not independently at the top of the wall as predicted. It is likely that any gap changes have been restrained by the insulation foam. The observed corner displacements show that the wall is deforming slightly (i.e., the wall is no longer square) and that the increase in the diagonal length which was not measured experimentally should be approximately 3.4mm.

Table 4-16 - Wall Rotation During Vertical Racking Tests at SLS

Deflection (mm)	TI_x	TI_y	TI'_x	TI'_y	BI_x	BI_y	BI'_x	BI'_y	Δ_D
Predicted	5.5	9.5	5.5	0.9	0.0	9.5	0.0	-0.9	0.0
Observed	0.8	9.5	0.5	0.8	0.0	9.5	0.0	0.8	1.1
Difference	-4.7	0.0	-5.0	-0.1	0.0	0.0	0.0	1.7	1.1

Table 4-17 - Change in Gap During Vertical Racking Tests at SLS

Deflection	Top Beam							Middle of Columns		Bottom Beam						
	λ_{T1x}	λ_{T1y}	λ_{T3y}	λ_{T5y}	λ_{T3y}	λ_{T1y}	λ_{T1x}	λ_{M1x}	λ_{M1x}	λ_{B1x}	λ_{B1y}	λ_{B3y}	λ_{B5y}	λ_{B3y}	λ_{B1y}	λ_{B1x}
Observed	0.6	0.4	0.2	-0.3	-0.3	-0.5	-0.5	-0.2	-0.1	-0.8	-0.6	-0.4	0.3	0.6	0.5	0.1
Predicted	4.5	0.3	0.7	0.4	0.4	-4.5	1.1	2.3	-2.4	0.2	-0.3	-0.2	0.0	0.0	-1.1	0.3
Difference	3.9	-	0.5	(0.7)	(0.7)	4.0	(1.6)	(2.5)	2.3	(1.0)	(0.3)	(0.2)	(0.3)	(0.6)	(1.6)	0.2

Notes:

- Tables 4-16 and 4-17 are associated with Figure 4-15
- For Table 4-17: differences ≤ 0.1 are not included, bold values represent noteworthy results, positive deflection represents an increase in gap and a negative displacement represents a decrease in gap, and differences in brackets represents a predicted change in gap that is lower than the observed change in gap.

4.5 OUT-OF-PLANE TEST 2 AND 3

4.5.1 EFFECT OF VERTICAL RACKING TEST

The effect of the vertical racking test is assessed by comparing Out-of-plane Test 1.3 and Test 2, as shown in Table 4-18, where a positive difference indicates an increase in deflection after the vertical racking test. The vertical racking has caused a reduction in stiffness near the top middle of the connection at T5, midspan of the wall at W4 and W5, and near the bottom connections B3, B4 and B5, especially under negative pressure. Overall these are very minor changes in displacement which shows that the vertical racking test at SLS had very little effect on wall specimen.

4.5.2 EFFECT OF LATERAL SWAY TEST

The effect of the lateral sway test is assessed by comparing Out-of-plane Test 2 and Test 3, as shown in Table 4-19, where a positive difference indicates an increase in deflection after the lateral sway test. There was a consistent reduction in stiffness under both positive and negative pressures at the top connection. This change is to be expected, however, as there was movement of the infill wall during the lateral test at the top of the wall which may have potentially weakened the restraint created by the insulation in the top gap. Similarly, the reduction in stiffness at midspan of the infill is likely due to the deformations experienced by the infill which caused the connections throughout the wall loosen slightly. Overall, the effects of the lateral racking test at SLS were fairly small, but may be cumulative if the lateral sway is due to repeated loading.

Table 4-18 - Comparison of Out-of-Plane Test 1.3 and 2

		T1	T3	T5	T1'	W1	W2	W3	W4	W5	W1'	B1	B2	B3	B4	B5	B1'
Negative Pressure:																	
Test 1.3	Observed	0.3	0.8	1.0	0.3	0.7	6.1	6.1	8.1	6.4	0.4	0.3	1.0	1.1	1.1	0.9	0.3
Test 2	Mean	0.3	0.8	1.3	0.3	0.7	6.0	6.2	7.9	6.1	0.4	0.4	1.0	1.4	1.4	1.3	0.3
	St. Dev.	-	-	-	-	-	-	-	-	-	-	-	-	-	-	-	-
Test 2 - Test 1.3		-	-	0.3	-	-	-	-	-0.2	-0.3	-	-	-	0.3	0.3	0.4	-
	% Difference	-	-	27	-	-	-	-	-3	-5	-	-	-	23	25	39	-
Positive Pressure:																	
Test 1.3	Observed	0.3	1.4	2.1	0.4	1.2	11.0	11.3	15.0	13.0	1.0	0.6	2.6	2.0	2.9	2.1	0.4
Test 2	Mean	0.4	1.5	2.4	0.5	1.4	11.0	11.3	14.8	12.9	0.9	0.8	2.7	2.1	3.1	2.2	0.4
	St. Dev.	-	-	0.2	-	-	-	-	0.2	-	-	-	-	-	-	-	-
Test 2 - Test 1.3		-	-	0.3	-	0.2	-	-	-0.3	-	-	-	-	-	0.2	-	-
	% Difference	-	-	14	-	16	-	-	-2	-	-	-	-	-	7	-	-

Table 4-19 - Comparison of Out-of-Plane Test 2 and 3

		T1	T3	T5	T1'	W1	W2	W3	W4	W5	W1'	B1	B2	B3	B4	B5	B1'
Negative Pressure:																	
Test 2	Mean	0.3	0.8	1.3	0.3	0.7	6.0	6.2	7.9	6.1	0.4	0.4	1.0	1.4	1.4	1.3	0.3
Test 3	Mean	0.5	1.3	1.7	0.4	0.7	N/A	6.7	8.0	7.2	0.4	0.4	1.1	1.5	1.5	1.4	0.5
	St. Dev.	-	-	-	-	-	-	-	-	-	-	-	-	-	-	-	-
Test 3 - Test 2		0.2	0.5	0.4	-	-	-	0.5	0.2	1.1	-	-	-	-	0.2	0.2	0.2
	% Difference	-	57	32	-	-	-	8	2	19	-	-	-	-	11	14	-
Positive Pressure:																	
Test 2	Mean	0.4	1.5	2.4	0.5	1.4	11.0	11.3	14.8	12.9	0.9	0.8	2.7	2.1	3.1	2.2	0.4
Test 3	Mean	0.7	2.0	3.2	0.7	1.5	N/A	12.0	15.0	13.7	1.0	0.8	2.6	2.0	3.3	2.4	0.6
	St. Dev.	-	-	-	-	-	-	-	-	-	-	-	-	-	-	-	-
Test 3 - Test 2		0.3	0.6	0.8	-	-	-	0.6	0.2	0.8	-	-	-	-	0.2	-	-
	% Difference	-	40	34	-	-	-	6	2	6	-	-	-	-	5	-	-

Note: differences ≤ 0.1 are not included, **bold** values represent noteworthy results, and % Difference does not include Mean values under 1.0mm

4.6 SUMMARY AND CONCLUSIONS

The 2.4m x 4.8m (8 ft. x 16 ft.) infill wall specimen was subjected to an initial out-of-plane pressure test at SLS, followed by lateral sway and vertical racking tests at both SLS and ULS. Between these racking tests, the out-of-plane pressure test at SLS was repeated to investigate the effect of the in-plane tests on the infill wall specimen. Conclusions associated with each test will be presented separately.

4.6.1 OUT-OF-PLANE PRESSURE TEST 1

A pressurized airbag, using a method similar to ASTM E330-02 Standard Test Window Structural Performance by Static Pressure (ASTM, 2010), was used to apply realistic out-of-plane pressures at SLS. The following conclusions can be made concerning the procedure and results:

1. A pre-pressure phase must be included in the pressure trace for large airbags to create an initial state of constant pressure, i.e., 0.2 kPa for this specific airbag, before loading to the test pressures begins. This enables a more accurate response from the PLAs before the pressure is increased. Increasing the number of PLAs from 2 to 12 also helped increase the accuracy of the overall response.
2. The overall midspan deflections of the infill wall exceeded the SLS limit of $H_{DT}/360$. These deflections were slightly less than the predicted results for a bare stud, likely due to the variability in the Young's Modulus values and the contribution of the sheathing.
3. The observed out-of-plane deflections around edges of the wall were much smaller than predicted, likely due to restraint from the expansion foam. This is

especially apparent along the edges at midspan of the wall where the deflections were predicted to be in the order of 10-15mm. The maximum out-of-plane deflection that occurred along the edge of the wall was no more than 1mm at the top and bottom and 2mm at midspan.

4. The overall repeatability for the results within Tests 1.1, 1.2 and 1.3 was good, except for Test 1.3 under positive pressure which showed a slight reduction in the stiffness of the wall.
5. The concrete frame performed well with little out-of-plane movement at the corner connection points of the concrete frame. Slightly larger deflections did occur at midspan of the beams due to the 'modified' support.

4.6.2 LATERAL SWAY TEST

A lateral load was applied to the concrete frame to create a sway displacement between the top and bottom beams that was within the pre-established critical range for SLS and ULS. The following conclusions can be concerning from the procedure and results:

1. The predicted response of the test apparatus at SLS was fairly closely the observed response, with the predicted loads being within 3 to 13% of the observed loads. The predicted response of the test apparatus at ULS was also fairly close to the observed response, with the predicted load being within 9% of the observed.
2. The predicted response of the steel frame for the push and pull test at SLS was very close, within 3%, to the observed results when considering the differential height, H' . There was larger variability when considering the full height, H , due to the minor displacements, between 0.7-0.9mm, that occurred at the bottom

connection. The predicted applied load for the pull test at ULS was predicted within 6% for both height H and H', however, the observed stiffness was larger than predicted.

3. The predicted deformed shape of the concrete frame is within 1.7mm of the observed shape for all observed tests, including deflections at ULS, which is deemed to be adequate.
4. It was predicted that there would be no in-plane movement of the infill wall as an adequate gap had been provided between the wall and the concrete frame. The observed results, however, show that the infill wall moved up to 4.5mm laterally, causing the wall to deform diagonally by +3.2mm and -4.5mm for the push and pull test, respectively, at SLS. This is consistent with the changes observed during the push tests, where the maximum predicted gap change was 7.8mm and the maximum observed gap change is 2.3mm. This indicates that there is in-plane load transfer through the insulation foam, even for gaps as large as 32mm, which is not accounted for in the current predictions.

4.6.3 VERTICAL RACKING TEST

A vertical load was applied to the concrete frame to create a racking displacement between the left and right columns within the pre-established critical range for SLS and ULS. The following conclusions can be concerning from the procedure and results:

1. The predicted stiffnesses of the test apparatus at SLS and ULS are reasonably close to the observed stiffnesses. The predicted loads, however, are 18% and 14% less than the observed loads at SLS and ULS, respectively. This may be due to

pretensioning of the concrete frame before testing which created a larger observed load.

2. The observed response of the steel frame was not accurately predicted, within 40%, as there was an initial non-linear response that was not accounted for in the model.
3. The racking displacement of the concrete frame at ULS was predicted to be 7.6mm to stay within the target deflection range of 7-8mm. The observed results are within 0.6mm of the predicted results.
4. The observed displacement of the infill wall was not as predicted. The observed maximum gap change was 0.8mm, whereas the maximum predicted change in gap was up to 4.5mm. This is again attributed to restraint provided by the insulation foam.

4.6.4 OUT-OF-PLANE PRESSURE TESTS 2 AND 3

Out-of-plane pressure tests were performed after the lateral sway test at SLS and vertical racking test at SLS. These responses were compared to Out-of-plane Pressure Test 1 to determine if the sway or racking deflections had any effects on the infill wall specimen.

The following conclusions can be made:

1. Out-of-plane Pressure Test 2 and 3 were almost completely repeatable.
2. There was generally no effect on the infill wall specimen from the vertical racking test at SLS.
3. There was minor reduction in stiffness at the top connection and a midspan of the wall due to the lateral sway test at SLS.

5 SUMMARY AND CONCLUSIONS

5.1 SUMMARY

The focus of this study was to improve the use of wood/concrete hybrid systems in mid- to high-rise structures. There are a number of methods to do this, although some of these niche areas have more potential than other. Current research has focused on using heavy timber methods for these larger structures, however there is little literature that addresses the use of light-frame timber. This study has therefore been carried out, by the support of the NEWBuildS Network, to identify and pursue avenues that may enhance the use of light-frame lumber in a mid- to high-rise market.

Chapter 2 reviewed spectrum of potential wood/concrete hybrid systems and identified three niche areas that are potentially feasible for mid- to high-rise structures. The potential maximum number of storeys of light-frame wood structures with wood/concrete hybrid flooring was investigated, and the investigation was repeated for structures with concrete lateral-load-resisting systems. The third niche area, wood infill walls in reinforced concrete structures, was explored by considering whether such wall should be load-bearing and identifying other factors that currently restrict their use in Canada.

Chapter 3 describes the basis of an experimental investigation of the structural aspects of light-frame wood infill walls in reinforced concrete frame structures. Analysis of a prototype reinforced concrete frame established the critical deflection ranges for lateral sway and vertical racking displacements in a single storey at Serviceability and Ultimate limit states. These in-plane racking limits were then adopted as design criteria for a full-scale, reinforced concrete frame test apparatus. An out-of-plane pressure system, applied

pressures to the exposed wall surface that were consistent with the wind loads specified in the NBCC (2010). Details of the 2.4m x 4.8m (8 ft. x 16 ft.) infill wall specimen are presented, and the basis of the design of the top and bottom connections to the concrete frame. These connections were intended to isolate the infill wall from the in-plane sway and racking deflections but transfer horizontal reactions due to out-of-plane wind loading from the wall to the frame.

Chapter 4 compares the experimental response of the test apparatus and wall specimen with predicted responses from linear-elastic analytical modeling. This assessment of the test specimen and test apparatus was performed for each of the following tests: Out-of-plane Pressure at SLS, In-plane Lateral Sway at SLS and ULS and In-plane Vertical Racking at SLS and ULS. Out-of-plane tests were also performed before and after each in-plane test to investigate its effect on the response of the infill wall specimen.

5.2 CONCLUSIONS

The conclusions that concerning feasible niches of light-frame wood/concrete hybrid construction (Chapter 2) are:

1. The use of light-frame wood structures with wood/concrete floor systems is infeasible for structures with 7 or more storeys due to the limited axial capacity of wood stud walls.
2. The use of light-frame wood structures with wood/concrete floor systems and a concrete lateral-load-resisting system is potentially feasible for structures up to 9 storeys.

3. Light-frame wood infill walls in reinforced concrete structures are feasible in mid- to high-rise structures if sufficient gap is provided around the perimeter of the wall to ensure that the wall remains non-load-bearing and prevents material incompatibility issues.

The conclusions concerning the design of a test apparatus to subject a wood infill wall to realistic concrete frame racking deformations (Chapter 3) are:

1. The critical in-plane racking deformations of a typical 8-storey reinforced concrete frame structure that must be accommodated by infill wall are:
 - a lateral sway deflection due to wind loading, which is largest at the base of the structure in an exterior frame with a maximum storey sway deflection range of 7-8mm at SLS and 16-18mm at ULS and;
 - a vertical racking deflection due to differential creep shortening, which is largest at the top of the structure at an exterior frame with a maximum storey racking deflection range of 7-8mm at SLS and 10-12mm at ULS.
2. The full-scale reinforced concrete frame test apparatus, which was designed to achieve the specified lateral sway and vertical racking displacements, accurately replicates the overall deformed shape of the critical frames.
3. Connections at the top and bottom of the wall were designed and implemented that allow a fully sheathed pre-fabricated infill wall to be used.

The conclusions concerning the performance of the test apparatus and wall test specimen (Chapter 4) are:

1. Due to the large (9.25m^3) volume of the airbag, the out-of-plane pressure loading system required 12 PLAs and a modified trace to generate positive and negative pressures of +1.44 and -0.9kPa, corresponding to the SLS wind loads specified in the NBCC (2010).
2. The wall specimen with 2x4 (38mm x 89mm) studs did not satisfy the SLS deflection limit of $L/360$, but the top and bottom connections performed adequately with out-of-plane deflections less than 2.5mm and 0.9mm, respectively.
3. The predicted displacements for the edges of the infill wall were approximately 10 times larger than the observed values, likely due to the expansion foam acting as a structural link between the wood infill wall and the concrete frame.
4. The concrete frame successfully withstood the out-of-plane pressures with almost no displacements at the corners and minor displacements, less than 2mm, at the middle supports.
5. The observed results for the deformed shape of the concrete frame during the lateral sway and vertical racking tests were within 1.7mm and 0.6mm, respectively, of the predicted results. The racking deformations in a typical sway frame structure at SLS and ULS were therefore adequately simulated by the test apparatus.
6. The predicted loads applied to the concrete frame during the lateral sway and vertical racking tests were within 8% and 18%, respectively, of the observed loads. This indicates that the linear-elastic analysis using SAP2000 (2009) was reasonably accurate.

7. The observed response of the infill wall during the in-plane tests at SLS was not well predicted. The observed change in gap was no more than 2.3mm, instead of the maximum predicted change of 7.8mm, again likely due to load being transferred from the concrete frame to the infill wall by the expansion foam.
8. The lateral in-plane test caused a minor reduction in out-of-plane stiffness of the infill wall and the top connection, where as the vertical in-plane tests had almost no effect.

Conclusions 3 and 7 pertain to the type of foam used (i.e. Great Stuff™) and may change if a different product is applied.

5.3 SUGGESTIONS FOR FUTURE WORK

The following future work is recommended:

1. Further out-of-plane pressure tests should be performed under loading at ULS to determine adequate performance, and mode of failure, of the infill wall and connections.
2. The infill wall should be redesigned to satisfy SLS limits. This should include using 2x6 (38mm x 140mm) lumber, instead of reducing the stud spacings the deeper stud allows more insulation in the wall cavity and so provides additional thermal benefits.
3. Repeat horizontal sway and vertical racking tests without an infill wall specimen to quantify the in-plane stiffness contributions of the infill wall.

4. The LVDTs should be placed closer to the connection points to minimize lateral measurements from the rotation of the wall.
5. During preparation for a vertical racking test, care should be taken when installing the top wood blocking to avoid pretensioning of the test apparatus.
6. Initial tests at ULS showed that minor cracking may be occurring, which may need to be accounted for in further predictions using an elastic-cracked analysis.
7. Repeated in-plane tests at SLS may cumulatively impact the out-of-plane stiffness of the infill wall, although only minor stiffness reductions were observed in the present study. Further tests should therefore include repetition of SLS in-plane sway deformations.

REFERENCES

ASTM (American Society for Testing and Material). (2010) "ASTM E330-02 Standard Test Method for Structural Performance of Exterior Windows, Doors, Skylights and Curtain Walls by Uniform Static Air Pressure Difference". Annual Book of ASTM Standards, Vol. 04.11.

BCBC (British Columbia Building Code). (2009) "BC Building Code Provisions". Victoria, British Columbia.

BAPL (Boral Australian Plasterboard Limited). (2002) "Plasterboard Exterior Wall Systems - Commercial Construction, Issue 3". Technical Product Information. Accessible at: http://www.boral.com.au/brochures/ordering/html_version/extwall/extwall_1.htm.

Crocetti, R.; Sartori, T.; and Flansbjerg, M. (2010) "Timber-Concrete Composite Structures with Prefabricated FRC Slab". *Proceedings for the World Conference on Timber Engineering 2010*. Trentino, Italy.

CSSBI (Canadian Sheet Steel Building Institute). (1991). "*Lightweight Steel Framing Design Manual*". Willowdale, Ontario.

CAC (Cement Association of Canada). (1984) "*Concrete Design Handbook, 2nd Edition, Part of National Standard of Canada CAN/CSA-A23.3-84 Design of Concrete Structures*". Canadian Standards Association, Mississauga.

CFS (Concrete Fastening Systems). (2012) "Tapcon[®] Concrete Screws Technical Information". Cleveland, Ohio. Website: <http://www.concretescrews.com/technical-info/tapcon-concretescrew.aspx>

Chuan, D.; Fragiaco, M.; Buchanan, A.; Crews, K.; Haskell, J.; and Deam, B. (2009) "Development of Semi-Prefabricated Timber-Concrete Composite Floors in Australasia". *New Zealand Timber Engineering Design Journal*. Vol. 17, Issue 1.

Chui, Ying Hei. (2009) "NEWBuildS Proposal Plan - NSERC Strategic Network on Innovative Wood Products and Building Systems". Draft Copy.

Cheung, Kevin. (2000) "Multi-storey Wood-frame Construction." Western Wood Products Association, USA.

Cheung, Kevin. (2008). "Multi-storey Timber and Mixed Timber-RC/Steel Construction in USA." *Structural Engineering International*. 18(2). Pg. 122-125.

CISC (Canadian Institute of Steel Construction). (2006) "Steel-framed Commercial Building Design Notes". Willowdale, Ontario.

Clouston, P.; Bathon, L.; and Schreyer, A. (2005) "Shear and Bending Performance of a Novel Wood-concrete Composite System". *Journal of Structural Engineering*. Pg. 1404 – 1412.

Clouston, Peggi and Schreyer, Alexander. (2008) "Design and use of Wood-Concrete Composites." *Practice Periodical on Structural Design and Construction*. ASCE. Pg. 167 – 174.

CMHC (Central Mortgage and Housing Corporation). (1970) "*Canadian Wood-Frame House Construction*". Ottawa, Ontario.

Cook, John. (1977) "Composite Construction Methods". John Wiley and Sons Inc.

CSA (Canadian Standards Association). (2010a) "National Standard of Canada CAN/CSA-A23.3-09 (R2010) Design of Concrete Structures". Canadian Standards Association, Mississauga, Ontario.

CSA (Canadian Standards Association). (2010b) "National Standard of Canada CAN/CSA-S16-09, Update No. 2 (2010), Design of Steel Structures". Canadian Standards Association, Mississauga, Ontario.

CSA (Canadian Standards Association). (2010c) "National Standard of Canada CAN/CSA-086-09, Update No. 1 (2010), Engineering Design in Wood". Canadian Standards Association, Mississauga, Ontario.

CWC (Canadian Wood Council). (2010) "Wood Design Manual 2010". Canadian Wood Council, Ottawa.

Dolan, D. (2005) "Handbook of Structural Engineering, Second Edition: Chapter 10 – Timber Structures." Editors: Chen, W.; Lui, E. CRC Press. Florida, United States of America.

Elliot, K. (2003) "Mixed Options for Precast Concrete Construction." *Concrete*. 37, pp. 18-23. Nottingham, United Kingdom.

Enjily, Vahik. (2006) "The TF2000 Project and its Impact on Medium-rise Timber Frame Construction in UK". *Time for Timber in Europe Conference*. Gdansk, Poland

Eriksson, Per-Erik. (2005) "Wood Components in Steel and Concrete Buildings – In-fill Exterior Wall Panels". Nordic Industrial Fund Project 02077.

EWC (European Wood China). (2010) "Strategies for Sustainable Construction: Building with wood in China." Technical Literature. Accessible at: http://www.canadawood.cn/english/downloads/tech_lit.php

Fragiacomo, M.; Schänzlin, J. (2010) "The Effect of Moisture and Temperature Variations on Timber-Concrete Composite Beams." *Proceedings for the World Conference on Timber Engineering*. Trentino, Italy.

Frangi, Andrea. (2011) 'Keynote Address'. *Presentation at the Theme 2 (Hybrid Building Systems) Research Exchange*. Ottawa, Ontario, Canada.

Gagnon, S., and O'Connor, J. (2006) "Hybrid Building Systems Problem Analysis Background and Literature Review." Project No. 4614, FPInnovations-Forintek Eastern Region, Quebec, Canada.

Gagnon, S. March, (2007) "Hybrid Building Systems: Now Opportunities for the Wood Products Industry." Forintek Canada Corporation - General Revenue Report Project No. 5318. FPInnovations-Forintek Eastern Region, Quebec, Canada.

Grenier, Daniel. 2012. Personal Communication. London, Ontario, Canada.

Gutkowski, R.; Balogh, J.; To, L. (2010) "Finite-Element Modeling of Short-Term Field Response of Composite Wood-Concrete Floors/Decks." *Journal for Structural Engineering*. Pg. 707-714.

Hibbler, R. C. (2006) "*Structural Analysis - Sixth Edition*". New Jersey. Published by Pearson Prentice Hall.

Holmes, Mike. (2006) "*Make It Right – Inside Home Renovation with Canada's Most Trusted Contractor*." Harper Collins.

Isoda, H., Okada, H., Kawai, N., and Yamaguchi N. (2000) "Research and development programs on timber structures in Japan." *Proceedings on World Conference of Timber Engineering 2000*. pp. 8.4.1-1—8.4.1-7. Whistler, Canada.

Johal, S. (2009) "History and Use of Midrise Buildings in Other Jurisdictions". Wood WORKS! Project. Technical Advisor.

Keenan, F. J. (1986) "*Limit States Design of Wood Structures - First Edition*". Morrison Hershfield Limited.

Kopp, G.A., Bartlett, F.M., Galsworthy, J., Henderson, D., Hong, H.P., Inculet, D.R., Savory, E., St. Pierre, L.M., & Surrey, D. (2006) "The Three Little Pigs full-scale Testing Facility". *Proc. 1st CSCE Specialty Conference on Disaster Mitigation*, Calgary, AB, 8-page paper on CD-ROM.

Krisciunas, R. (2010) "Wood-Concrete Composite Deck Questions UWO". Personal Communication.

Kuhlmann, U.; and Schänzlin, J. (2008) "A Timber-Concrete Composite Slab System for use in Tall Buildings." *Structural Engineering International*. 18(2). Pg. 174-178.

Lukaszewska, E.; Johnsson, H.; and Fragiacom, M. (2008) "Performance of Connections for Prefabricated Timber-concrete Composite Floors." *Material and Structures*. Vol. 41, pg. 1533-1550.

Lukaszewska, E.; Fragiacom, M.; and Johnsson, H. (2010) "Laboratory Tests and Numerical Analyses of Prefabricated Timber-Concrete Composite Floors." *Journal of Structural Engineering*. Pg. 46 – 55.

MacGregor, J., Bartlett, F.M. (2000) "*Reinforced Concrete: Mechanics and Design - First Edition*." Pearson. Toronto, Ontario, Canada.

Mehaffey, Jim R. (2010) "Exterior Infill Walls Fire Safety Requirements in Canada". Personal Communication.

Nagy, S., Bartlett, F.M., (2008) "Simulated Wind Load Tests of Large FRP/Foam Sandwich Panels". *Proceedings for the CSCE 2008 Annual Conference*. Quebec City, Quebec.

NBCC (National Building Code of Canada). (2010) "National Building Code of Canada 2010". National Research Council of Canada.

NSPRC (National Standard of the Peoples Republic of China). (2004) "Technical Code for Partitions with Timber Framework." Standard Classification: GBT 50361-2005.

Piazza, Maurizio, Ballerini, Marco. (2000) "Experimental and Numerical Results on Timber-concrete Composite Floors with Different Connection Systems". *Proceedings on World Conference of Timber Engineering 2000*. Whistler, Canada.

Rautenstrauch, K.; Mueller, J.; and Simon, A. (2010) "The First Timber-Concrete Composite Road Bridge in Germany." *Proceedings for the World Conference on Timber Engineering 2010*. Trentino, Italy.

Sakamoto, I.; Kawai, N.; Okada, H. and Isoda, H. (2002) "A Report of a Research and Development project on Timber-based Hybrid Building Structures". *Proceedings for the World Conference on Timber Engineering 2002*. Shah Alam, Malaysia.

Sakamoto, Isao. (2004) "Final Report of a Research and Development Project on Timber-based Hybrid Building Structures". *Proceedings for the World Conference on Timber Engineering 2004*. Lahti, Finland.

Sakamoto, I.; Kawai, N.; Okada, H.; Yanaguchi, N.; Isoda, H, and Yusa, S. (2004) "Final Report of a Research and Development Project on Timber-based Hybrid Building Structures". *Proceedings for the World Conference on Timber Engineering 2004*. Lahti, Finland.

SAP (Structural Analysis Program) (2009) "SAP 2000 Version 12 – Structural Analysis Program". Computers and Structures Inc. Berkeley, California.

Shackelford, Randy and Pryor, Steve. (2007) "Design Solutions for Wood-Frame Multi-Storey Buildings – Resisting Uplift and Lateral Forces". *Construction Specifier Magazine*. Simpson Strong-Tie.

Smith, Ian; and Frangi, Andrea. (2008a) "Tall Timber Buildings: Introduction." *Structural Engineering International*. 18(2). Pg. 114.

Smith, Ian; and Frangi, Andrea. (2008b) "Overview of Design Issues for Tall Timber Buildings." *Structural Engineering International*. 18(2). Pg. 141-147.

Stead, M. and Bartlett, F. M. (2010) "*Comparison of Sway Moment Magnifiers for Plane Concrete Frames Using CSA Standard A23.3*". Masters in Engineering Project Course Submission (ES 9500).

Surprenant, D. (2010) "The National Building Code of Canada: A Tool for Recovery in the Forest Industry?". Industry, Infrastructure and Resources Division. Parliamentary Information and Research Service. Background Paper. Library of Parliament. Publication No. 2010-27-E.

van de Lindt, J.; Pei, S.; Pryor, S.; Shimizu, H. and Isoda, H. (2010) "Experimental Seismic Response of a Full-Scale Six-Storey Light-frame Wood Building." *Journal of Structural Engineering*, Vol. 136 Pg. 1262-1273.

Wallace, D.; Cheung, K.; and Williamson, T. (1998). "Multi-Storey Wood Frame Construction in the United States." *New Zealand Timber Design Journal*. Vol. 7, Pg.11-23.

Wang, Jieying. (2008). "Non-Load-Bearing Wood-Framed Exterior Wall in Concrete, Steel and Masonry Structures". FPInnovations Forintek Presentation.

Wang, Jieying. (2011) Personal Communication.

Yeoh, D.; Fragiaco, M.; Buchanan, A.; Deam, B. (2010) "Experimental Performance of LVL-Concrete Composite Floor Beams." *Proceedings for the World Conference on Timber Engineering 2010*. Trentino, Italy.

Zhou, Lina. (2009) "Structural Response of Mid-rise Hybrid Building System Consisting of a Light Wood Frame Structure and Concrete Core – Thesis Proposal." University of New Brunswick.

APPENDIX A
FEASIBILITY STUDY RESULTS FOR CASES 2, 4-7

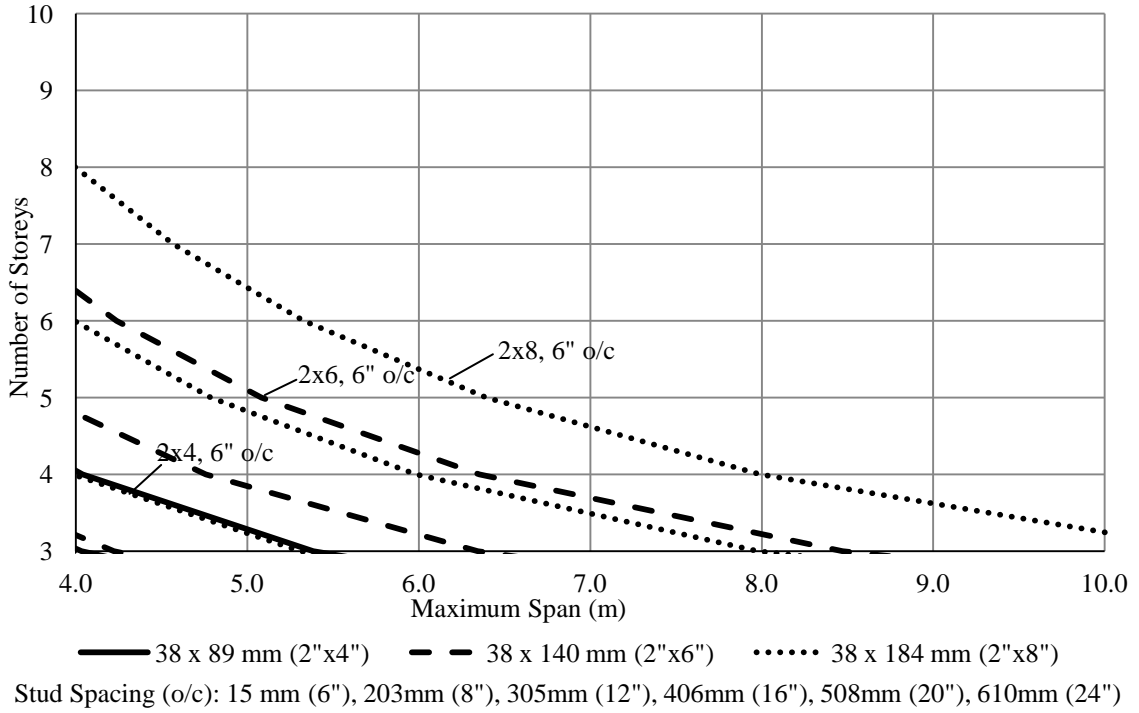


Figure A-1- Results for Case 2: Wood Structure with Light-weight Concrete Topping under Residential Loading

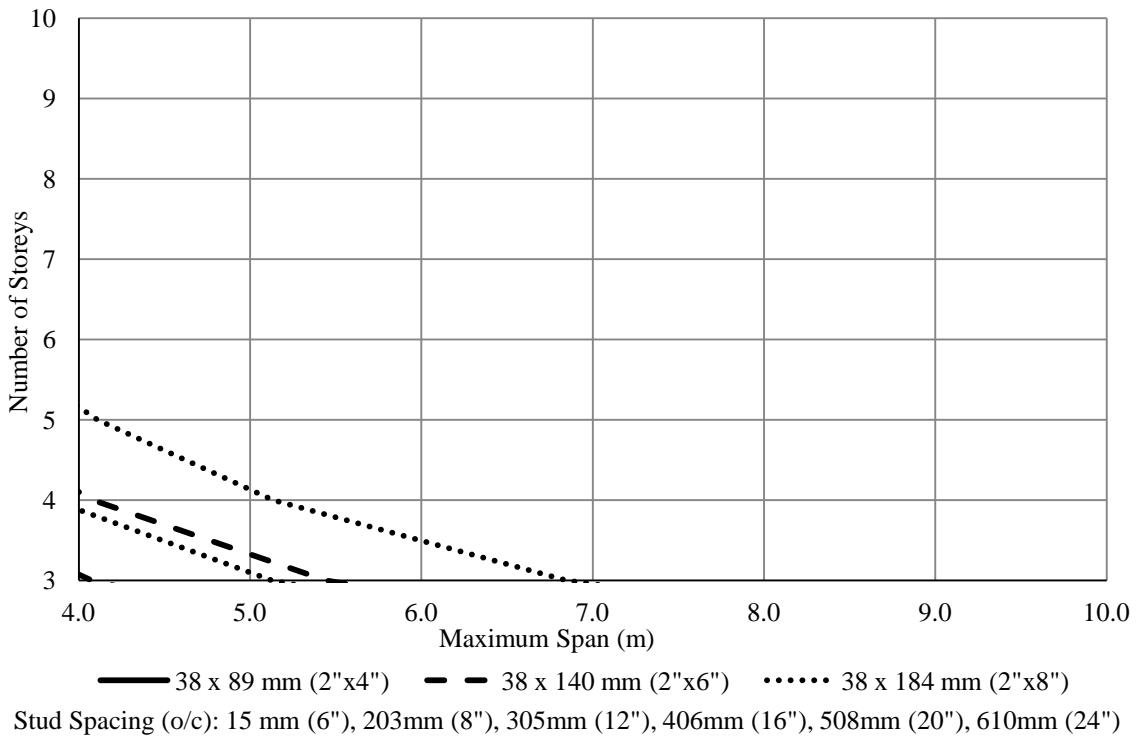


Figure A-2 - Results for Case 4: Wood Structure with Light-weight Concrete Slab under Residential Loading

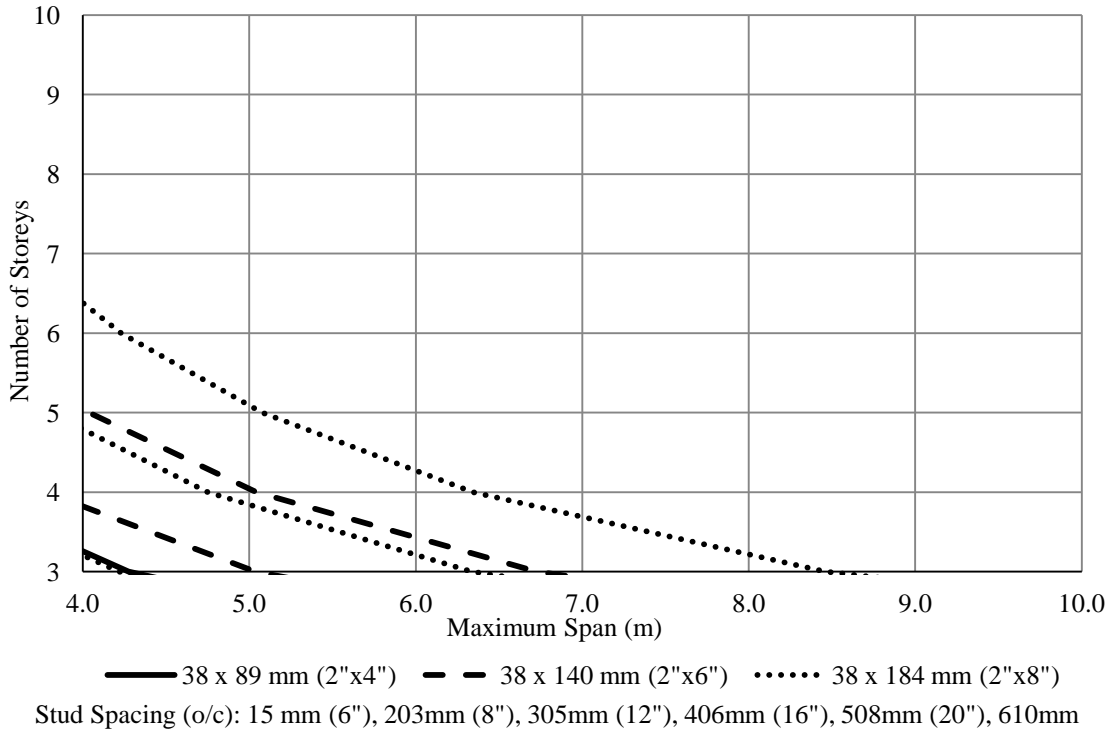


Figure A-3 - Results for Case 5: Wood Structure with Normal-weight Concrete and Wood Composite Flooring under Residential Loading

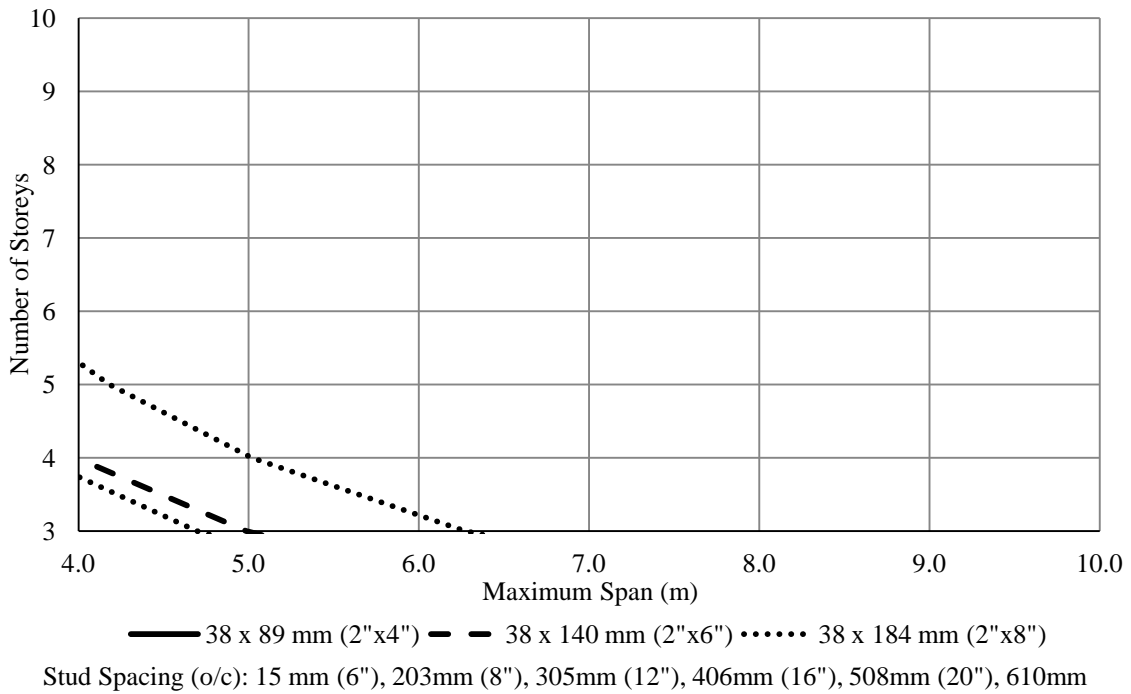


Figure A-4 - Results for Case 6: Wood Structure with Light-weight Concrete and Wood Composite Flooring under Business Loading

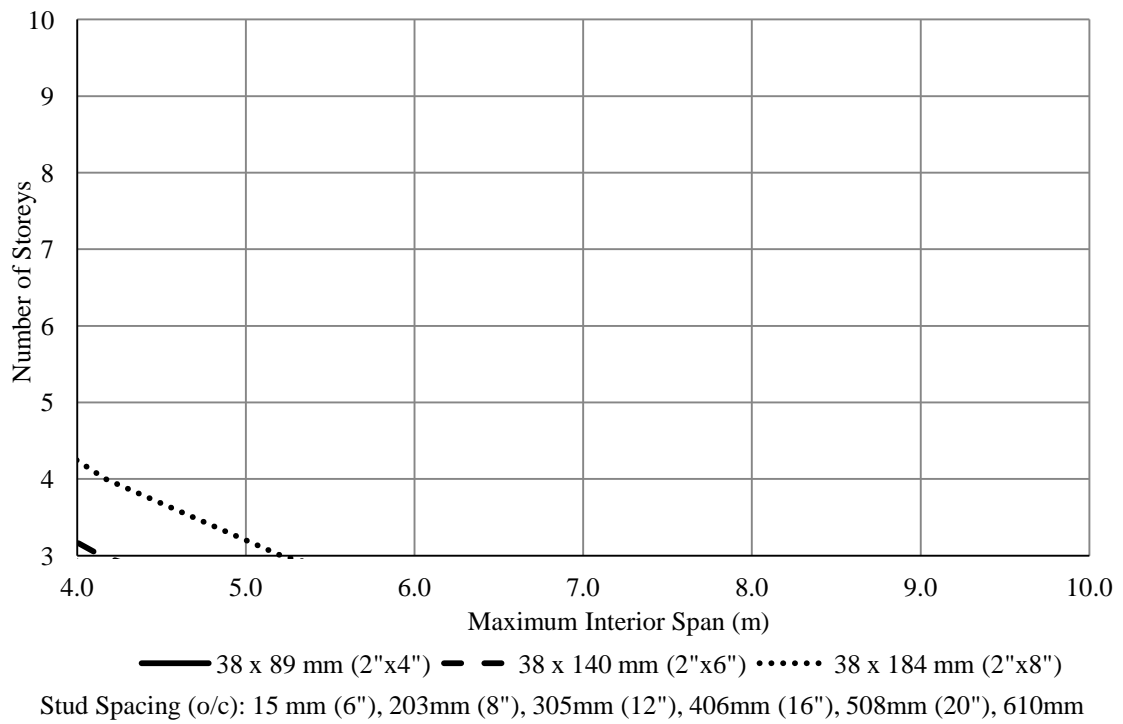


Figure A-5 - Results for Case 7: Wood Structure with Normal-weight Concrete and Wood Composite Flooring under Business Loading

**APPENDIX B
WIND LOADING**

B.2 TEST APPARATUS

For the out-of-plane testing, the test apparatus must be able to accommodate the realistic localized wind load on the infill wall. Details of the parameters are listed in Table B-3, with the pressures summarized in Table 3-2. The pressures for an infill wall account for both external and internal pressures, which results in the two cases shown in Figure B-1.

Table B-3 - Wind Loading Factors for the Exterior Cladding Elements

Variable		Value		Notes
		External	Internal	
I_w	SLS	0.75	0.75	---
	ULS	1.0	1.0	Normal Importance
q (kN/m ²)		0.53	0.53	50-yr. Return Period
C_e		1.34	1.11	Exposure A - Open level terrain
C_g/C_{gi}		2.5	2.0	Small Elements, including cladding
C_p/C_{pi} :	Positive	0.78	0.3	External: $H/D = 0.88$ and $H > 20m$ Internal: Category 2
	Negative	-0.48	-0.45	

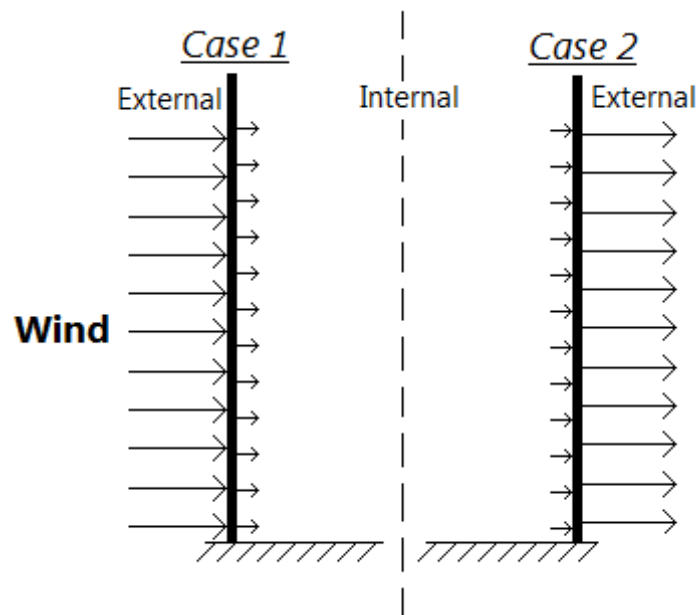


Figure B-1 - Pressure Cases for the Loading on Exterior Cladding

APPENDIX C
VERTICAL CREEP CALCULATIONS

C.1 LOADING DETAILS

The axial forces, P_c , in the columns of the prototype structure, determined using the SAP model with 1.0D at SLS and 1.4D at ULS, are shown in Table C-1.

Table C-1 - Axial Load in Columns at SLS and ULS

Storey	P_c (kN) at SLS		P_c (kN) at ULS	
	Exterior	Interior	Exterior	Interior
8	159	318	222	445
7	330	636	462	890
6	499	953	699	1334
5	667	1270	934	1778
4	833	1587	1166	2222
3	997	1904	1396	2666
2	1159	2222	1623	3111
1	1318	2539	1845	3555
0	1473	2855	2062	3997

C.2 SUMMARY OF RESULTS

Table C-2 shows the column shortening results at SLS and ULS after 25 years. The interior columns at the top of the structure will shorten by 20.1mm and the exterior columns will shorten 11.9mm after 25 years. The difference between these two columns leads to a differential shortening of 8.2mm. This is the critical vertical deflection SLS case for a wood infill wall located at the top exterior frame. This table also shows that as the interior columns at the top of the structure will shorten by 28.1mm at ULS and the exterior columns will shorten 16.6mm after 25 years. The difference between these two columns leads to a differential shortening of 11.4mm. This is the critical vertical deflection ULS case for a wood infill wall located at the top exterior frame. Therefore the final ranges are 7-8mm for SLS and 10-12mm for ULS.

Table C-2 - Vertical Shortening Results

Storey	Shortening, Δ , at SLS (mm)					Shortening, Δ , at ULS (mm)				
	Exterior, e		Interior, i		Differential ($\Sigma\Delta_i - \Sigma\Delta_e$)	Exterior, e		Interior, i		Differential ($\Sigma\Delta_i - \Sigma\Delta_e$)
	Δ_e	$\Sigma\Delta_e$	Δ_i	$\Sigma\Delta_i$		Δ	$\Sigma\Delta$	Δ	$\Sigma\Delta$	
8	0.2	11.9	0.4	20.1	8.2	0.3	16.6	0.6	28.1	11.4
7	0.5	11.6	0.8	19.6	8	0.7	16.3	1.2	27.5	11.2
6	0.8	11.2	1.3	18.8	7.6	1.1	15.6	1.8	26.3	10.7
5	1	10.4	1.7	17.5	7.1	1.4	14.6	2.4	24.5	10
4	1.3	9.4	2.1	15.8	6.4	1.8	13.1	3	22.2	9
3	1.5	8.1	2.5	13.7	5.6	2.1	11.4	3.6	19.2	7.8
2	1.8	6.6	3	11.2	4.6	2.5	9.3	4.1	15.7	6.4
1	2.6	4.9	4.3	8.2	3.3	3.6	6.8	6	11.5	4.7
0	2.3	2.3	3.9	3.9	1.6	3.2	3.2	5.5	5.5	2.2

APPENDIX D
OVERVIEW OF BEAM DEFLECTION CALCULATIONS

The total midspan beam deformation calculated from the instantaneous dead load deflection over a 5-year or longer period (CSA, 2010a) is computed as:

$$[D.1] \quad \Delta_{SD} + \Delta_{iL} + \Delta_{SL} + \Delta_W$$

or similarly,

$$[D.2] \quad \lambda_{5 \text{ year}} \Delta_{SD} + \Delta_{iL} + \lambda \Delta_{SL} + \Delta_W$$

where Δ_{SD} is the deflection due to sustained dead load, Δ_{SL} is the deflection due to sustained live load, an assumed 1/3 of the total live load, Δ_{iL} is the deflection due to immediate live load and Δ_W is the deflection due to specified wind load. For the long-term deflection multiplier, $\lambda_{5 \text{ year}}$, of 2.0 applied to the dead load and long-term deflection multiplier, $\lambda = \lambda_{5 \text{ year}} - \lambda_{10}$, of 3.0 (CSA, 2010a), this yields

$$[D.3] \quad 2\Delta_D + 2\Delta_L + \Delta_W$$

where Δ_L is the deflection due to the specified live load and Δ_D is the deflection due to the specified dead load.

APPENDIX E
EFFECTIVE MOMENT OF INTERIA CALCULATIONS

E.1 LOADING DETAILS

The effective moment of inertia, I_e , was calculated using the following equation (MacGregor and Bartlett, 2000):

$$[E-1] \quad I_e = I_{cr} + (I_g - I_{cr}) \left(\frac{M_{cr}}{M_a} \right)^3$$

where I_{cr} is the cracked moment of inertia, I_g is the gross moment of inertia, M_{cr} is the cracked moment and M_a is the applied moment. Further details for calculating I_{cr} , I_g and M_{cr} are shown by MacGregor and Bartlett (2000). The applied moments, shown in Figure E-1 for each frame element for a pull test at ULS, were simplified. This was done by assuming the maximum moment was consistent throughout each frame element as shown.

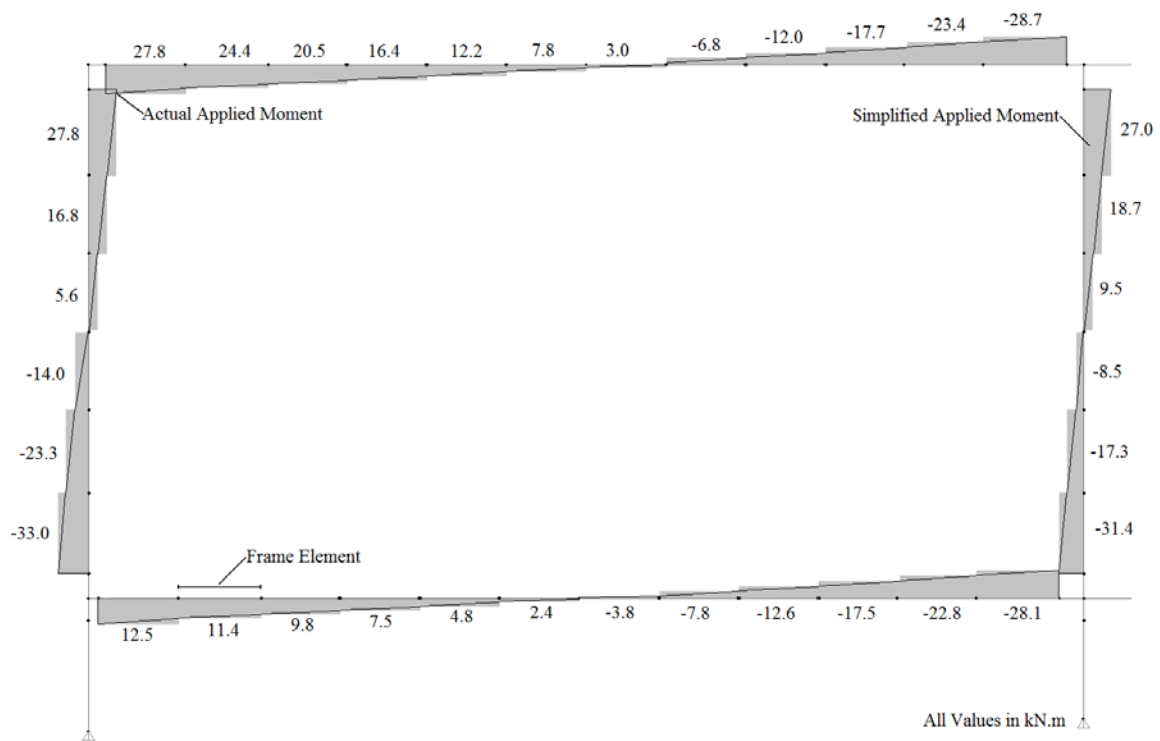
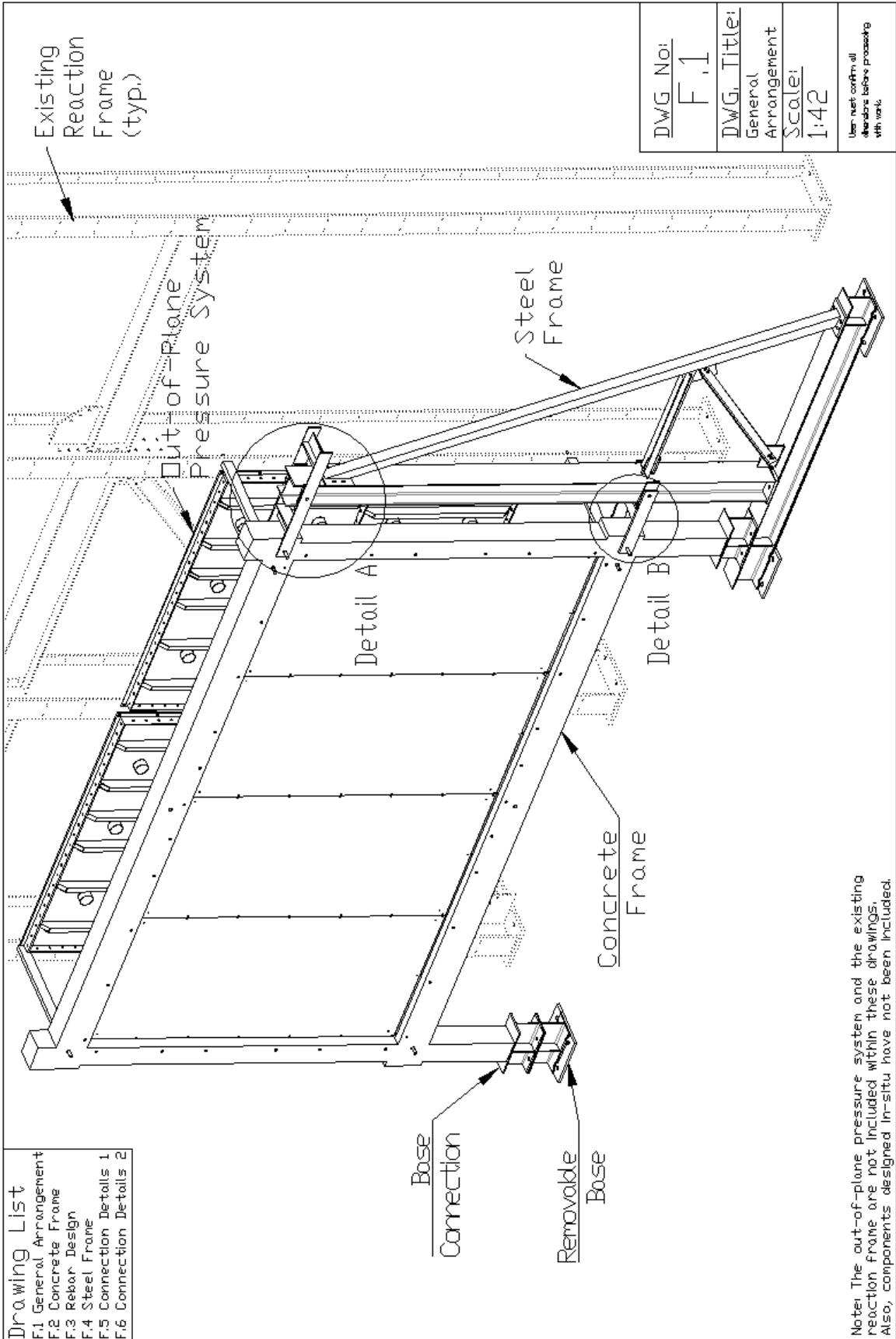


Figure E-1 - Predicted Applied Moments under Loading at ULS

APPENDIX F
ENGINEERING DRAWINGS FOR TEST APPARATUS

Dimensions in mm [inches]



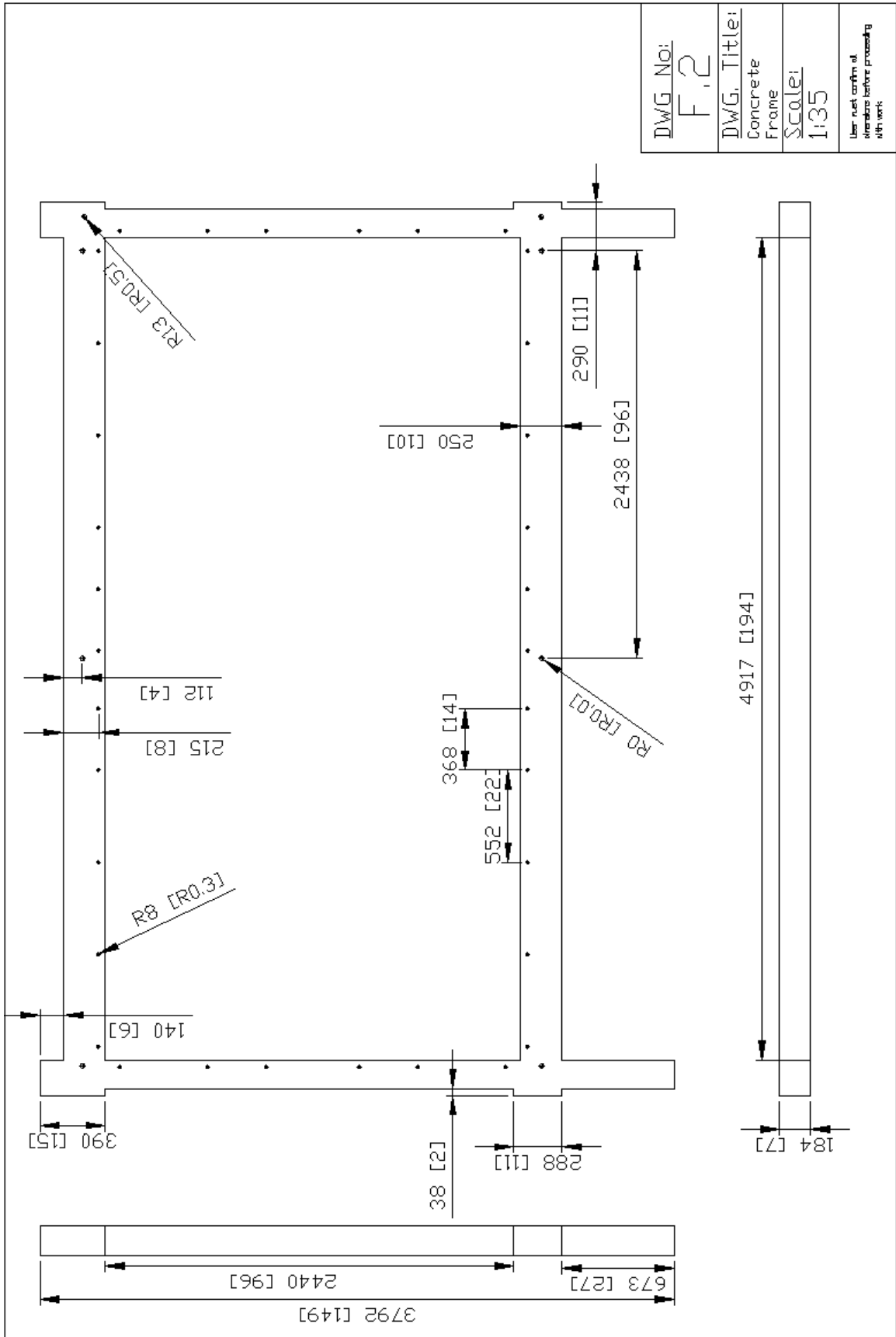
Drawing List

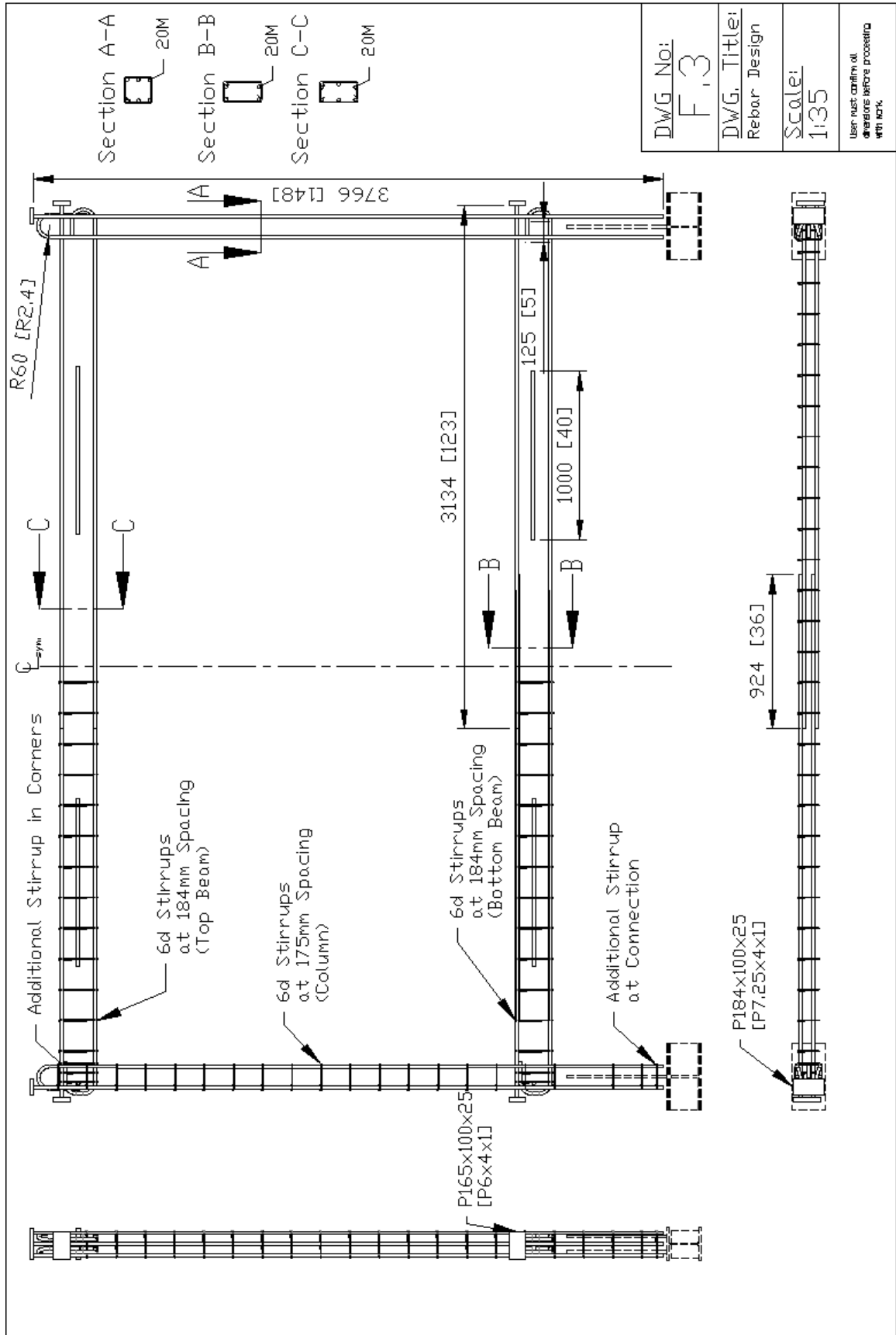
F.1	General Arrangement
F.2	Concrete Frame
F.3	Rebar Design
F.4	Steel Frame
F.5	Connection Details 1
F.6	Connection Details 2

DWG No:	F.1
DWG Title:	General Arrangement
Scale:	1:42

User must confirm all alterations before proceeding with work.

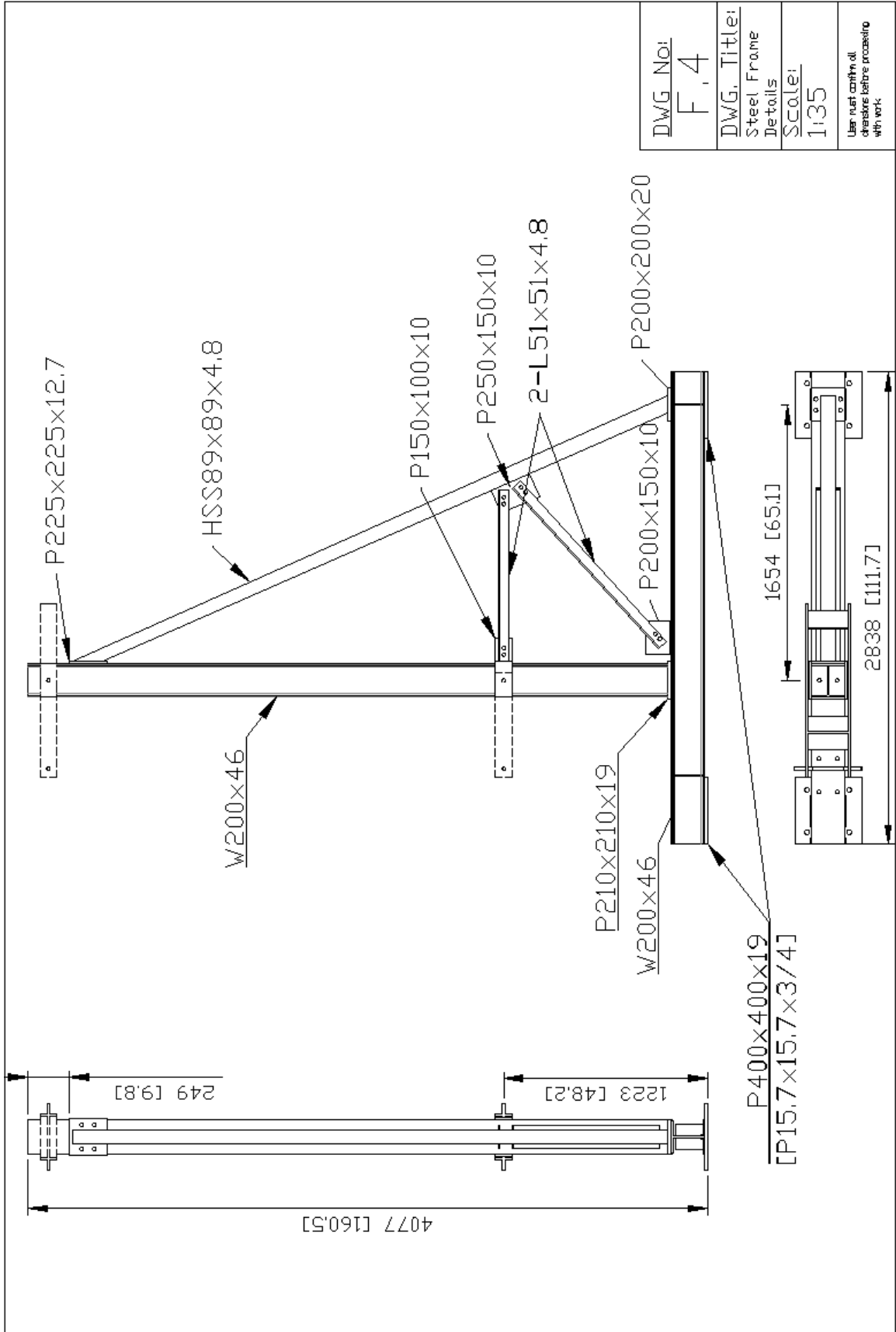
Notes: The out-of-plane pressure system and the existing reaction frame are not included within these drawings. Also, components designed in-situ have not been included.

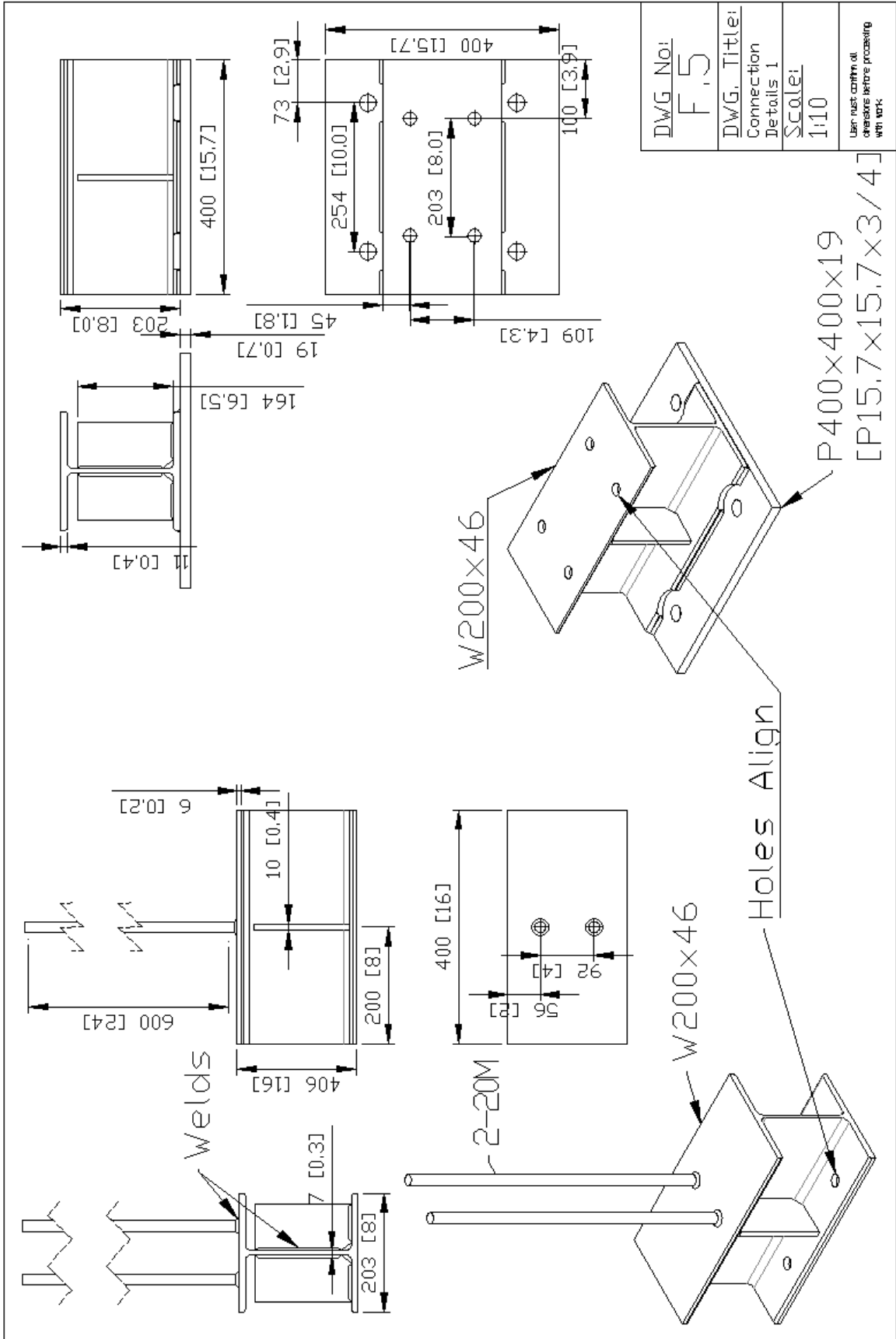


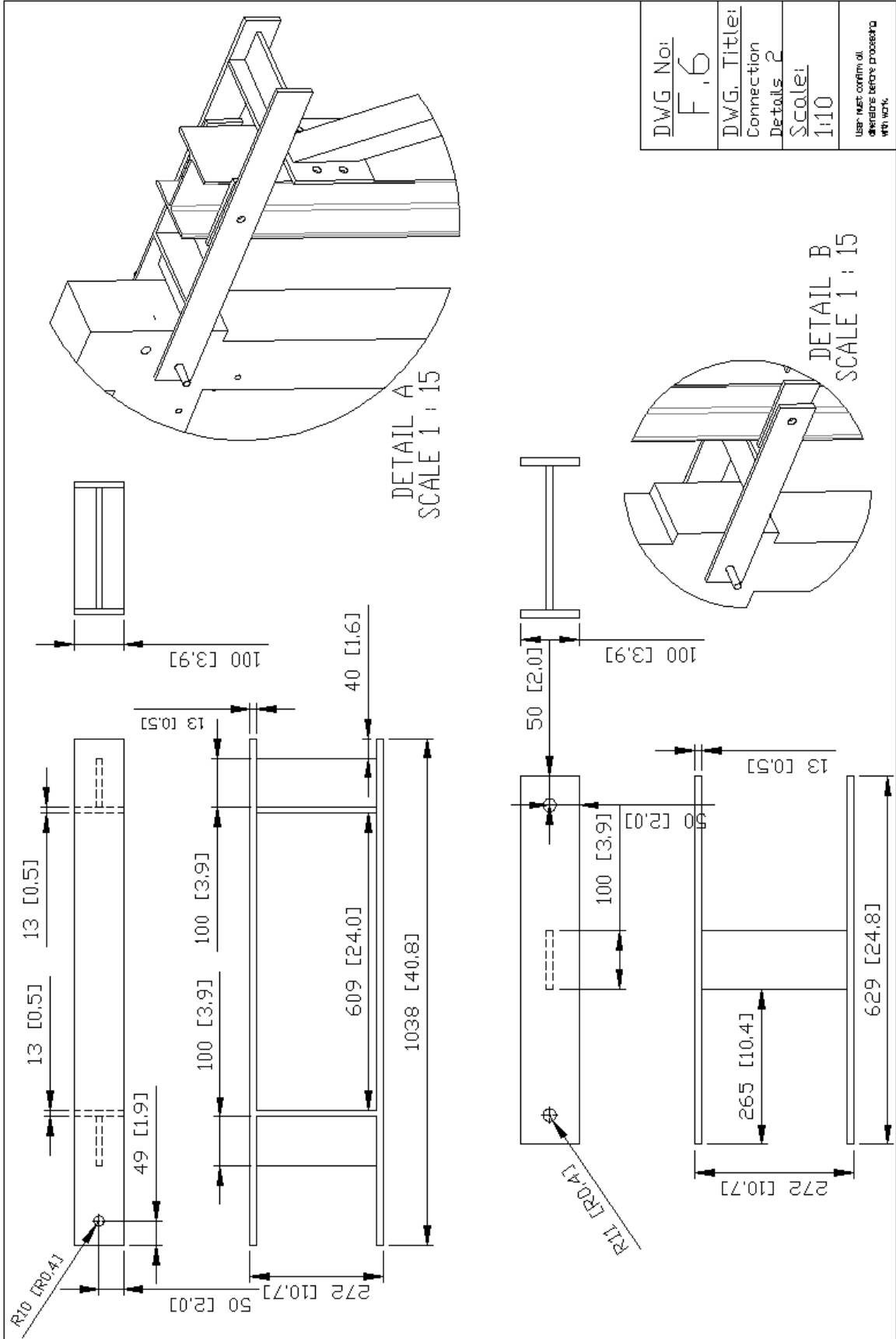


DWG No:	F.3
DWG Title:	Rebar Design
Scale:	1:35

User must confirm all operations before proceeding with work.







APPENDIX G
DESIGN LIMITS OF TEST APPARATUS

The values shown in Figure G-1 are the limits that were used during the design of the test apparatus. The steel frame was designed to withstand a factored +/-57kN and the concrete frame, both beams and columns, were designed to resist a moment of 33.0kN.m and a shear of 25.4kN. The ultimate capacity of the frame is likely much larger than this, however independent calculations will need to be done to properly determine these limits.

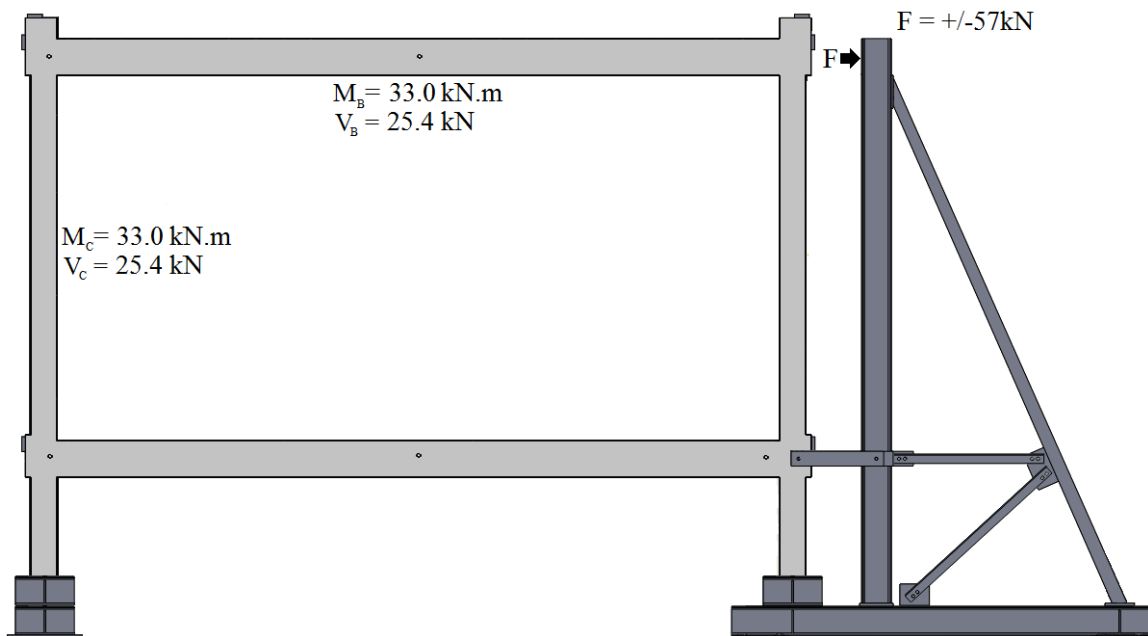


Figure G-1 - In-plane Design Forces for Test Apparatus

**APPENDIX H
WALL LIFT DETAILS**

H.1 CONCEPTUAL DESIGN

The design for lifting the infill wall involved two built-up 8ft long 2x8 lumber which was designed in accordance with CAN/CSA-O86-01 (CSA, 2010c) and used as the spreader beam, as shown in Figure H-1. Straps were then attached around each end of the beam and attached to an overhead crane. The connection to the infill wall uses a steel 'C'-channel and angle. The angle was screwed to the infill wall with 2 5/8" dia. lag screws at stud locations. The angle was placed in between the flanges of the 'C'-channel and a bolt was inserted to connect them together. This allows the infill wall to be constructed horizontally and then lifted vertically, as shown in Figure H-2, pivoting about the connection point to a nearly vertical position. This allows for simple installation when fitting the infill wall into the concrete frame.

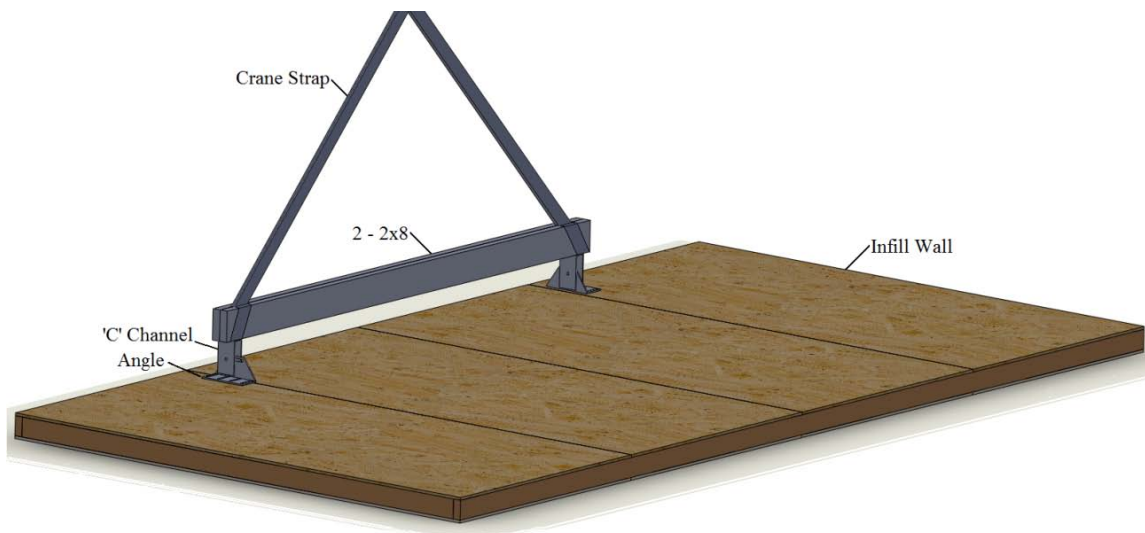


Figure H-1 - Lifting Connection Attached to Infill Wall

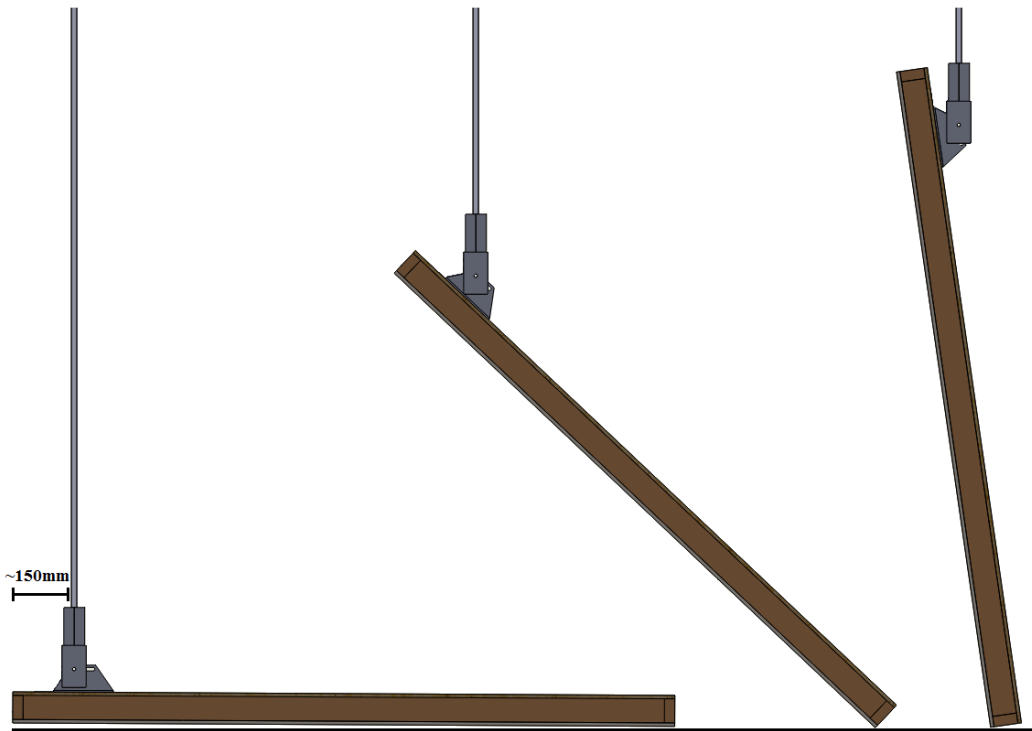


Figure H-2 - Lifting of the Infill Wall

APPENDIX I
WALL DEFORMATION CALCULATIONS

I.1 OVERVIEW

Figure I-1a) shows the original position of the infill wall and the approximate location of LVDTs T5, QT5, W5, QB5 and B5. As previously mentioned, the displacement of the top and bottom connections cannot be accurately determined by the displacements at T5 and B5 as an unknown amount of wall rotation is also being measured. Figure I-1b) shows the displacement of the wall, and the connections, under negative pressure. For Case 1, the original position at midheight of the infill wall is used as the center axis, where the results are shown in Table I-1. The goal is to determine an equation which represents the deformed shape of the infill wall, using a fifth-degree polynomial, and use it to solve for the predicted displacements at the top and bottom connection. To simplify the equation, Case 2 is introduced which changes the location of the axis to midheight of the deformed shape and switches the x and y axis, leading to the results shown in Table I-1. Using this data, the polynomial for the deformed shape is:

$$[I.1] \quad y = 2.4 \times 10^{-9} x^4 + 5.0 \times 10^{-6} x^3 - 4.6 \times 10 x^2 - 5.8 x$$

where y is the displacement of the infill wall and x is the vertical position along the wall. With this, the displacements at the top and bottom connections can be determined, as shown in Table I-1.

Similarly, the equations for the deformed shape under positive pressure is :

$$[I.2] \quad y = 8.2 \times 10^{-9} x^4 + 6.8 \times 10^{-6} x^3 - 9.6 \times 10 x^2 - 8.7 x$$

where the results are shown in Table I-2.

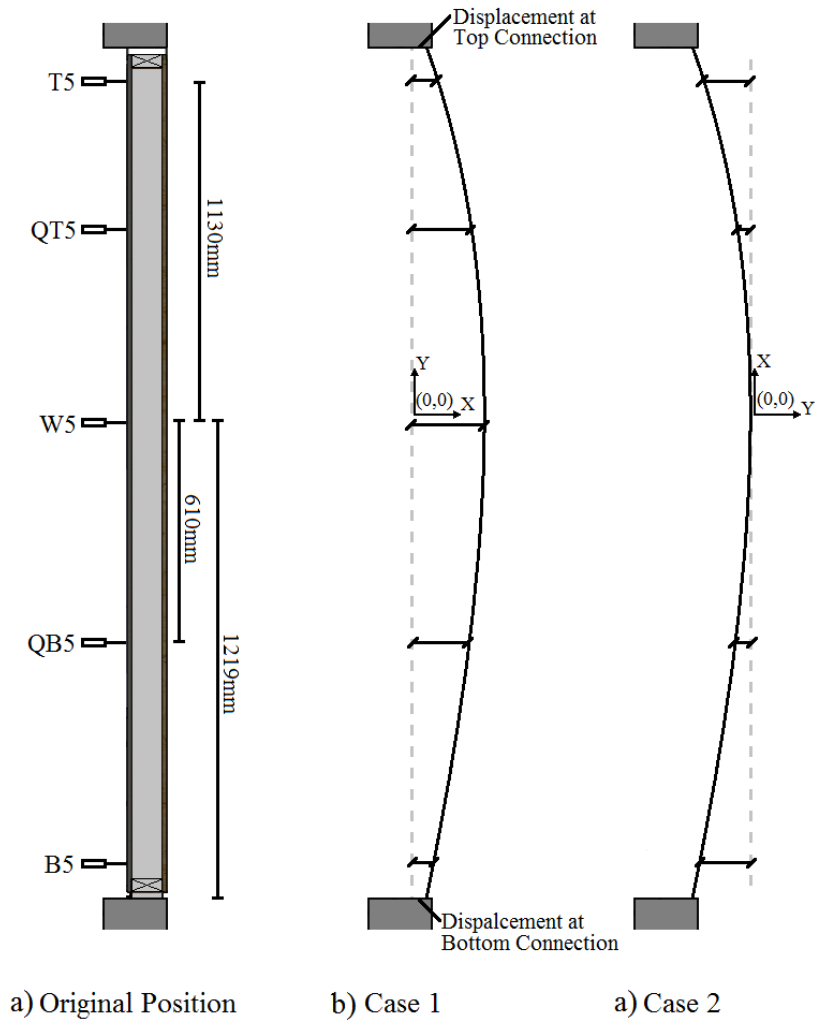


Figure I-1 - Out-of-plane Infill Wall Deflection: a) Original Position; b) Case 1; c) Case 2

Table I-1 - Displacement of Infill wall under Negative Pressure

Location	Case 1 (mm)		Case 2 (mm)		Case 1 (mm) - Updated	
	Y	X	Y	X	Y	X
Top Connection	1219	-	-6.1	1219	1219	0.3
T5	1130	1.0	-5.4	1130	1130	1.0
QT5	610	4.5	-1.9	610	610	4.5
W5	0	6.4	0	0	0	6.4
QB5	-610	5.0	-1.4	-610	-610	5.0
B5	-1130	0.9	-5.5	-1130	-1130	0.9
Bottom Connection	-1219	-	-6.5	-1219	-1219	0.0

Table I-2 - Displacement of Infill wall under Positive Pressure

Location	Case 1 (mm)		Case 2 (mm)		Case 1 (mm) - Updated	
	Y	X	Y	X	Y	X
Top Connection	1219	-	12	1219	1219	-0.8
T5	1130	-2.1	11	1130	1130	-2.1
QT5	610	-9.2	3.8	610	610	-9.2
W5	0	-13.0	0	0	0	-13.0
QB5	-610	-9.9	3.1	-610	-610	-9.9
B5	-1130	-2.1	11	-1130	-1130	-2.1
Bottom Connection	-1219	-	13	-1219	-1219	-0.4

I.2 CONCLUSIONS

The final results for the top and bottom connection predicts that there is no more than 1mm displacement occurring during loading at SLS. These results are almost half the displacements initially measured at point T5 and B5 which suggests that this issue requires further consideration in future studies.

APPENDIX J
TESTING DETAILS

J.1 LOGBOOK SUMMARY

Date(s)	No. of Tests	Notes
<i>Out-of-Plane Test 1</i>		
March 15th-23rd 2012	46	2 -12 PLAs were used
April 4th 2012	5	Test 1.1 Negative Pressure (-0.9kPa)
April 5th 2012	7	Test 1.1 Positive Pressure (1.44kPa)
April 11th 2012	10	Test 1.2 (-0.9kPa and 1.44kPa)
April 16th 2012	5	Test 1.3 (-0.9kPa and 1.44kPa)
<i>Vertical Racking Test at SLS</i>		
May 11th 2012	3	Displacement Range: 12 - 28mm, DT06. Larger tolerance in top corner connection
May 24th 2012	2	Displacement Range: 12 - 20mm, DT06. Bushing used to reduce tolerance.
May 25th 2012	1	Displacement of 10mm, DT06. Blocking was used in top connection
<i>Out-of-Plane Test 2</i>		
May 29th 2012	12	Tests 2.1 - 2.3 (-0.9kPa and 1.44kPa)
<i>Lateral Sway Test at SLS</i>		
June 1st 2012	3	Lateral Push Test - Displacement: up to 9.0mm, DT05
June 5th 2012	1	Lateral Push Test - Displacement: up to 9.6mm, DT05
June 6th 2012	1	Lateral Push Test - Displacement: up to 9.0mm, DT05. Modified bottom connection.
June 7th 2012	3	Lateral Push Test - Displacement: up to 7.0mm, DT05. Pretensioned bottom connection.
June 14th 2012	1	Lateral Push Test - Displacement: up to 7.0mm, DT05. Extended bottom connection blocking into steel frame.
June 20th 2012	1	Lateral Push Test - Displacement: up to 7.0mm, DT05. Movement of DT frame was fixed.
June 21st 2012	4	Lateral Push and Pull Tests - Displacements: 7.5-8.8mm
<i>Out-of-Plane Test 3</i>		
June 22nd 2012	16	Tests 3.1 - 3.3 (-0.9kPa and 1.44kPa). Frame inside bag came loose. Temporary repair preformed.

J.2 LVDT LOCATIONS

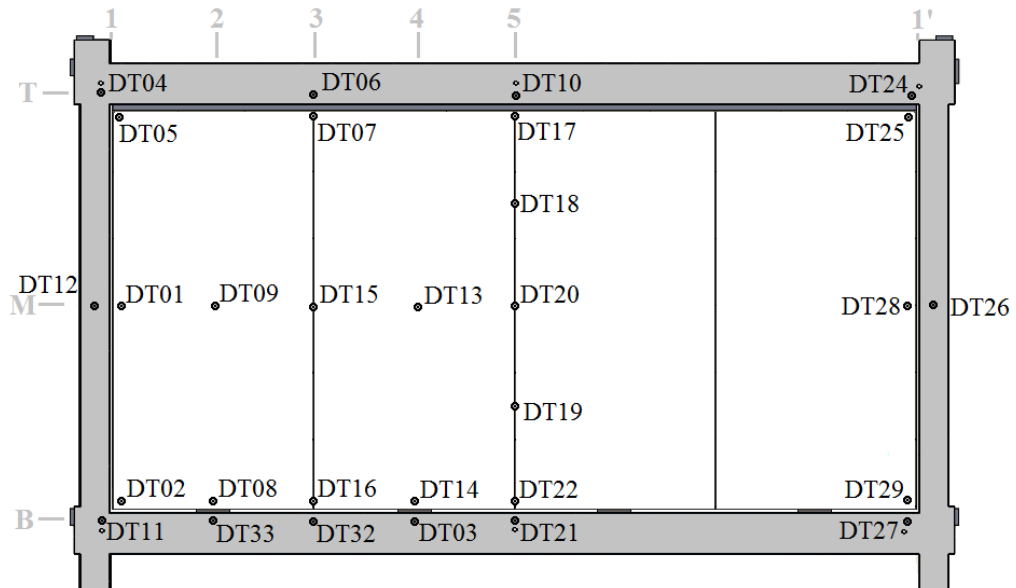


Figure J-1 - Out-of-Plane Test LVDT

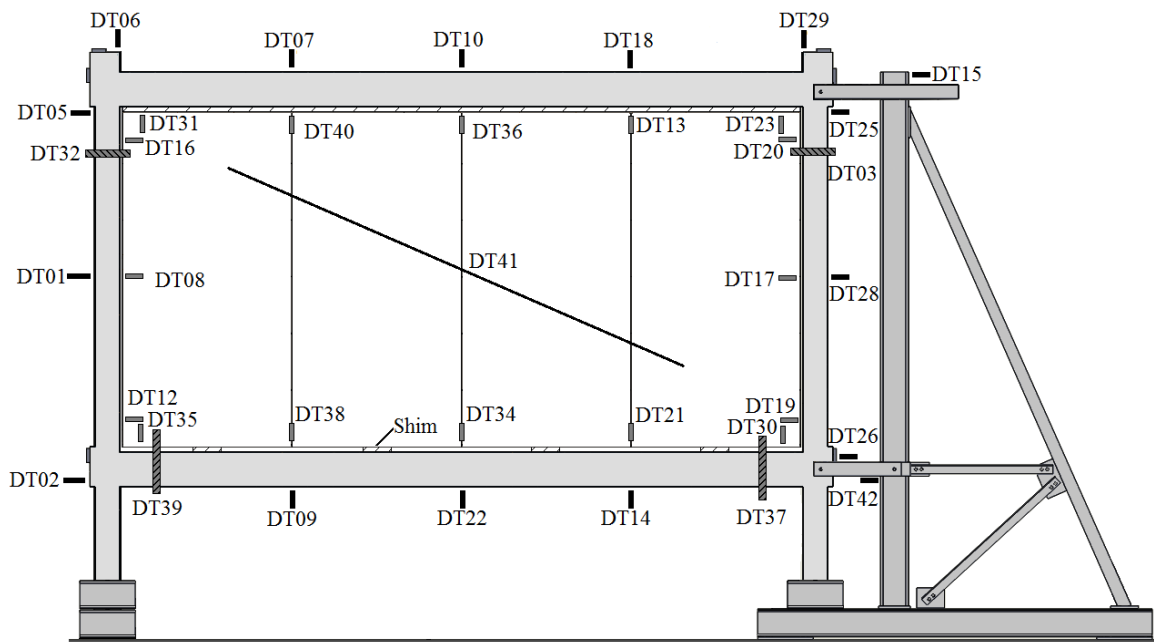


Figure J-2 - In-Plane Test LVDT

CURRICULUM VITAE

Identification Jeffrey R. L. Blaylock, b. Brampton, Ontario, Canada, 1986

Post-Secondary Education and Degrees

2009 - 2012 Master of Engineering Science, Structural
Western University, London Canada

2005 - 2009 Bachelor of Engineering Science, Structural
Western University, London Canada

Honors and Awards

- 2011 Graduate Teaching Assistant Union Scholarship Award for
Community Involvement.
- 2010 Graduate Teaching Assistant Union Scholarship Award for
Community Involvement.
- 2009 Canadian Society for Civil Engineering (CSCE) Best Student Award
for Class of 2009.
- 2009 Dean's List, Faculty of Engineering, Western University.
- 2008 Dean's List, Faculty of Engineering, Western University.

Related Employment

- 2009 - 2011 Teaching Assistant
Western University
London, Canada
- May - July 2009 Employee, Assisted Facility Manager
Insurance Research Lab for Better Homes
London, Canada
- May - Aug. 2008 Junior Project Coordinator
NAC (North America Construction) Constructors Ltd.
Morrison, Ontario, Canada

Related Presentations

- May 2012 2nd NEWBuildS Workshop, Vancouver, British Columbia
- February 2012 NEWBuildS Mid-rise Building Project: Highly Qualified Personnel
Workshop, Ottawa, Ontario
- January 2011 1st NEWBuildS Workshop, Vancouver, British Columbia

Publications

- Blaylock, J. and Bartlett, M. 2011. " *Niche Areas for Mid-rise Light-frame Wood-Concrete Hybrid Construction*", Proceedings of the CSCE 2011 General Conference, Ottawa, ON, GC-136, 10-page paper in CD-ROM Proceedings